SANDIA REPORT
SAND2020-11959
Printed October 2020

Sandia National Laboratories

Shear Behavior of Artificial Clay Seams within Bedded Salt Structures

Steven R. Sobolik, Sandia National Laboratories, Albuquerque, New Mexico

Evan Keffeler and Stuart Buchholz RESPEC Inc., Rapid City, South Dakota

Prepared by
Sandia National Laboratories
Albuquerque, New Mexico
87185 and Livermore,
California 94550

Issued by Sandia National Laboratories, operated for the United States Department of Energy by National Technology & Engineering Solutions of Sandia, LLC.

Available to DOE and DOE contractors from
U.S. Department of Energy
Office of Scientific and Technical Information
P.O. Box 62
Oak Ridge, TN 37831

Telephone: (865) 576-8401
Facsimile: (865) 576-5728
E-Mail: reports@osti.gov
Online ordering: http://www.osti.gov/scitech

Available to the public from
U.S. Department of Commerce
National Technical Information Service
5301 Shawnee Rd
Alexandria, VA 22312

Telephone: (800) 553-6847
Facsimile: (703) 605-6900
E-Mail: orders@ntis.gov
Online order: https://classic.ntis.gov/help/order-methods/

ABSTRACT

Bedded salt contains thin layers of clay, also known as clay seams, in-between far thicker layers of salt. These inhomogeneities are thought to have first-order effects on the closure of nearby drifts and potential roof collapses. Despite their importance, characterizations of the peak shear strength and residual shear strength of clay seams in salt are extremely rare in the published literature.

A previous paper reported results from laboratory direct shear experiments on clay seam samples from the Permian Basin in New Mexico. These clay seams behaved similar to intact salt, which was attributed to the abundance of salt crystals intersecting the clay seams. None of those specimens contained a distinct ¼" – ½" (6 – 12 mm) thick clay seam, as has been observed in drifts at the Waste Isolation Pilot Plant (WIPP).

Due to the difficulty in obtaining WIPP samples with these types of clay seams, artificial seams of bentonite and brine sandwiched between sections of salt were created and shear tested. Eight 4" diameter samples were created with either a ¼" or a ½" thick seam and then consolidated at 3000 psi prior to shear testing. The direct shear tests on these samples were performed at nominal normal stresses representative of expected WIPP in-situ conditions (500 to 1500 psi). The resulting shear stress vs. shear displacement curves exhibited a peak followed by a gradual decay of shear strength. The shear stress never transitioned to a true residual shear stress plateau, so the final shear strength at the end of each test (0.75" of shear displacement) was analyzed instead. Both the peak shear strength and the final shear strength conformed to Mohr-Coulomb behavior with friction angles and cohesion strengths consistent with a saturated, highly consolidated, clay. These new artificial clay seam results and the previous clay-interspersed-with-salt results likely bound the expected shear behavior of WIPP clay seams.

ACKNOWLEDGEMENTS

This research is funded by WIPP radioactive waste repository programs administered by the Office of Environmental Management (EM) of the U.S Department of Energy.

The authors would like to acknowledge and the technical staff of RESPEC Inc. in Rapid City, South Dakota. The tests documented in this SAND report were performed by RESPEC under a contract with Sandia. We would also like to thank Courtney Herrick and Benjamin Reedlunn of Sandia National Laboratories; Frank Hansen of Sandia National Laboratories and RESPEC; Paul Shoemaker from Sandia's WIPP organization; Andreas Hampel of Hampel Consulting; and the US-German collaboration on repositories in salt for their review and support of this work.

CONTENTS

LIST OF FIGURES

LIST OF TABLES

INTRODUCTION

1.1. Background and objective

Extensive collaborations between American and German salt repository researchers have identified four key research areas to better understand the behavior of salt (halite) for radioactive waste repositories (Hansen et al., 2016a, 2016b and 2017). One subject area includes the influence of inhomogeneities, which are thought to have first-order effects on excavation behavior. Included among these inhomogeneities are clay seams in bedded salt, or other interfaces such as halite/anhydrite and halite/polyhalite. These interfaces are prevalent in bedded salt formations, such as in the Delaware Basin, where the Waste Isolation Pilot Plant (WIPP) resides, near Carlsbad, New Mexico, USA. An idealized WIPP stratigraphy used for rock mechanics calculations with many seams and interfaces is illustrated in Figure 1-1. This figure also shows the location of two prominent clay seams, F and G, which are in the vicinity of many of the drifts and storage rooms at WIPP (Reedlunn, 2016, 2017, & 2018).

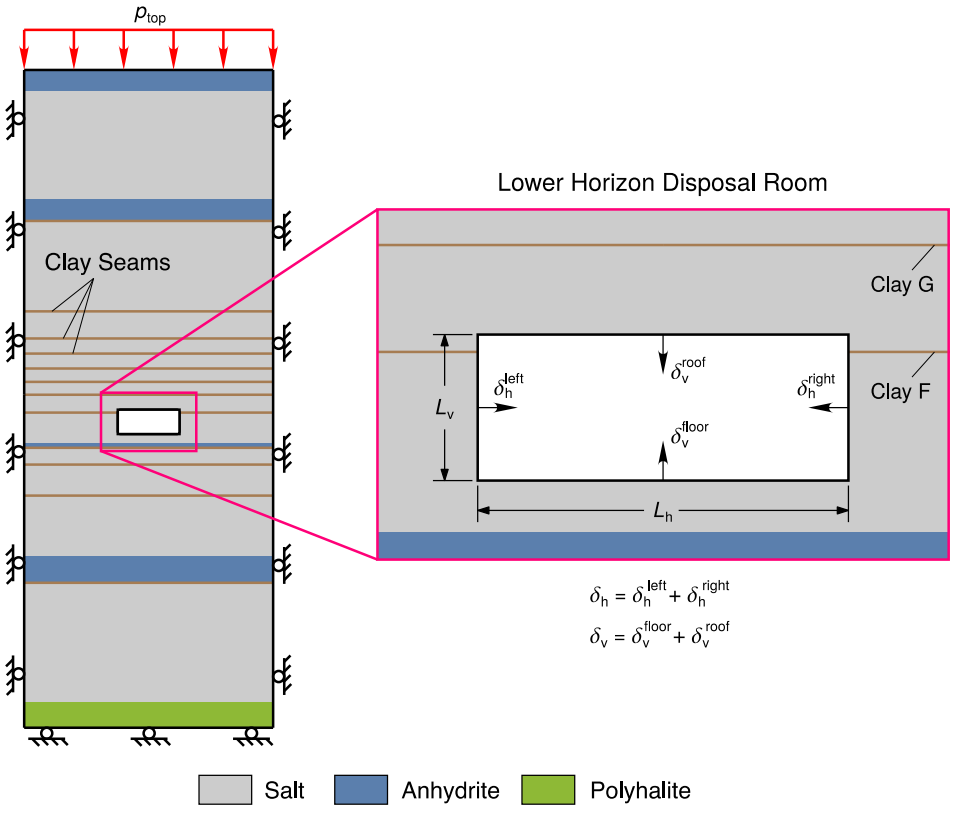

Figure 2-1. Idealized WIPP stratigraphy.

The effects of shear along these interfaces have long been thought to have significant impacts on the mechanical behavior of disposal rooms built for the long-term disposal of radioactive waste; particularly as they pertain to the evolution of room closure, roof falls, and changes in strength and permeability at these interfaces. Figure 1-2 shows a photograph looking into a vertical borehole in a drift roof at WIPP, where three interfaces have clearly slid since the borehole was originally drilled.

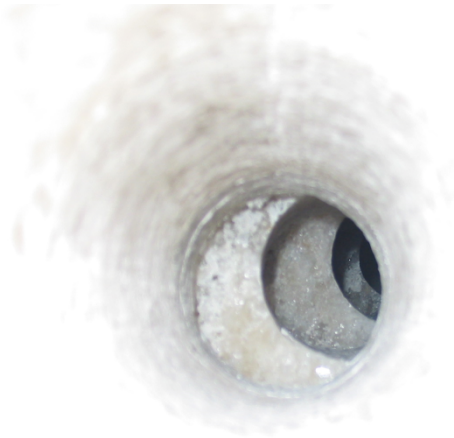

Figure 2-2. Example of interface sliding in a borehole at WIPP

There are essentially no published in situ measurement data for bedded salt deposits characterizing shear strength of an interface in salt and resulting effects of interface displacement and permeability. Munson and Matalucci (1983) proposed an in situ test for the WIPP site, with direct shear across a clay seam. A 1-by-1-m block in a wall containing a representative clay seam was to be isolated by cutting around it. Flatjacks were to be installed in slots cut around the block to apply shear and normal stresses. Displacements along and across the seam would be measured as a function of applied stress. This proposed test never occurred.

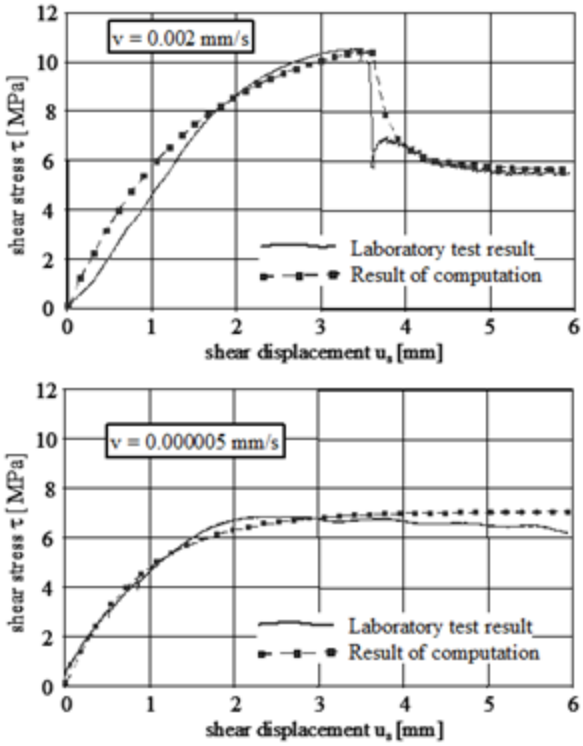

Figure 2-3. Shear stress vs. displacement for different shear velocities on carnallitite—halite interfaces (Minkley and Mühlbauer, 2007).

Some laboratory investigations have evaluated the slip along interfaces under several different stress environments. Minkley and Mühlbauer (2007) documented direct shear laboratory tests on carnallitite and salt blocks under varying normal and shear loads and shear velocities. With these data, they developed a shear model for interfaces that accounts for both velocity-dependent and displacement-dependent shear softening mechanisms. The plots in Figure 1-3, taken from Minkley and Mühlbauer (2007), show the evolution of shear stress as a function of shear displacement for two different shear velocities. Their results showed that under higher shear velocities, adhesive frictional resistance must first be exceeded before a loss of shear strength occurs; at lower shear velocities, no adhesion is apparent, and cohesion is maintained. They observed that the ultimate residual stress should be a function of normal stress and cohesion and not of shear velocity, which the plots in Figure 1-3 would support.

WIPP contains halite/clay/halite (clay seam), halite/anhydrite, and halite/polyhalite interfaces, not halite/carnallite interfaces, therefore the Minkley and Mühlbauer (2007) results are not directly applicable. In the absence of experimental data, the clay seams at WIPP have been modeled using Coulomb friction with an assumed friction coefficient of 0.2, while other interfaces have been assumed to be perfectly bonded with infinite strength. Figure 1-4 shows the results of analyses on the horizontal and vertical closure of a disposal room at WIPP that apply these lower and upper bounds of the friction coefficients on the seams. Clearly, the wide range of predicted times of full closure indicate it would be preferable to have interface models based on laboratory tests for WIPP performance assessment simulations.

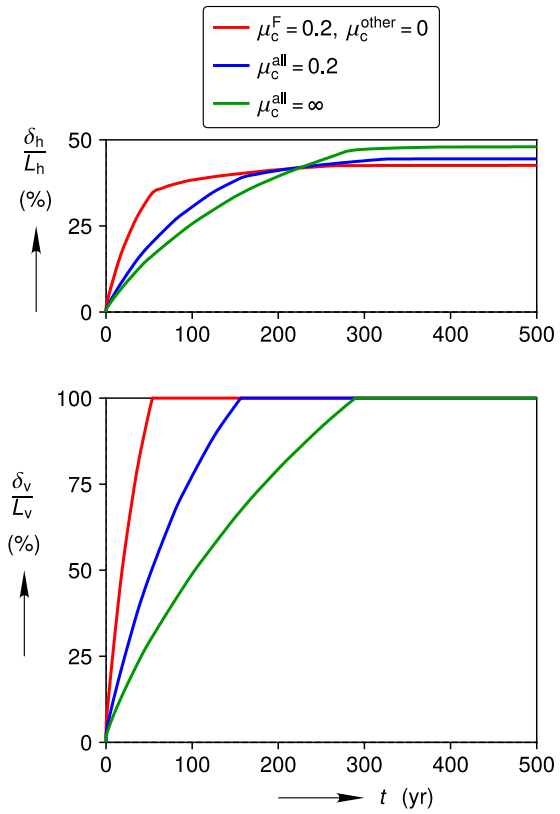

Figure 2-4. Effects of friction coefficient on predicted horizontal, vertical room closure at WIPP (Reedlunn & Bean, 2020).

A recent series of laboratory direct shear tests were performed to measure, evaluate, and quantify the effects of shear displacement along a bedding interface or clay seam, on shear and fracture strength of the interface and accompanying salt (Buchholz, 2019; Sobolik et al. 2019; Sobolik & Reedlunn, 2019). Thirty samples were tested from six salt specimen types: two halite-clay contact types, a polyhalite-halite contact, a mixed halite, a pure halite, and a halite-anhydrite contact. The tests ran according to procedure (Sobolik, 2019), and both maximum shear strength and residual shear strength were determined for each rock type. Regardless of the rock type (i.e., with or without contacts), the specimens behaved and broke like solid salt rock. Each rock type reasonably conformed to Mohr-Coulomb behavior. The mixed halite consistently tested as the strongest sample group for peak shear stress and residual shear stress. The samples with halite-clay-halite contacts were expected to be the weakest interfaces, but their residual shear stresses were similar to the pure halite. Numerous halite crystals were found spanning the clay-halite interface rather than a solid layer of clay. None of these samples featured a distinct clay seam between salt strata. Such clay seams, for example G (a distinct thin clay seam) and F (a less-distinct seam of mixed clay and salt with varying thickness and undulations) as shown in Figure 1-1, have been observed at the WIPP site. Unfortunately, programmatic priorities at the WIPP site have to date prevented the excavation of samples containing clay seams that can be used for testing.

The series of laboratory direct shear tests reported in this report were designed to measure, evaluate, and quantify the effects of shear displacement along an artificial clay seam created between sections of salt. These lab tests will be used to develop constitutive models for sliding and fracturing along clay seams at WIPP. In addition to applications directly related to WIPP, the data from these tests will be used to support US-German collaborative model development efforts for Joint Project WEIMOS (2016 – 2021; "Further Development and Qualification of the Rock Mechanical Modeling for the Final HAW Disposal in Rock Salt") (Lüdeling et al., 2018).

1.2. Salt interface shear tests

The previously mentioned series of laboratory direct shear on salt samples with and without interfaces (Buchholz, 2019; Sobolik et al. 2019; Sobolik & Reedlunn, 2019) were performed with samples of materials from a potash mine in the Permian Basin in New Mexico. The tests were run according to a procedure similar to that discussed later for the current series of tests, and both maximum shear strength and residual shear strength were determined for each rock type. Regardless of the rock type (i.e., with or without contacts), the specimens behaved and broke like solid salt rock. The samples that were of the highest interest were those with a halite-clay-halite contact. The interface between the halite layer and the clay section was somewhat well-defined visually when looking at the exterior surface of the sample.

Figures 1-5 and 1-6 show the data fits for peak shear stress versus the normal stress for the intact and residual strengths, respectively, for the interface shear tests. The stresses were calculated using the original cross-sectional area of the interface. The computed values for the cohesion (S_0) and friction angle (Φ) are also shown on the plots. Data from the residual tests performed following each intact test are not plotted and were not included in the data fits because of the inconsistent behavior exhibited by the samples after the breaking of the interfaces. The simple Mohr-Coulomb fits reasonably capture each interface type. The Mohr-Coulomb shear strength criterion is defined as

$$\tau = \sigma_{\mathrm{n}} \tan \Phi + S_0,$$

where τ is alternately the peak shear stress at failure (Figure 1-5), or the residual shear stress (Figure 1-6), σ_n is the normal stress on the shear surface, Φ is the friction angle, and S_0 is the cohesion strength. Notably, the cohesion strength is non-zero in all cases, suggesting the interfaces have a non-zero shear strength at zero normal stress.

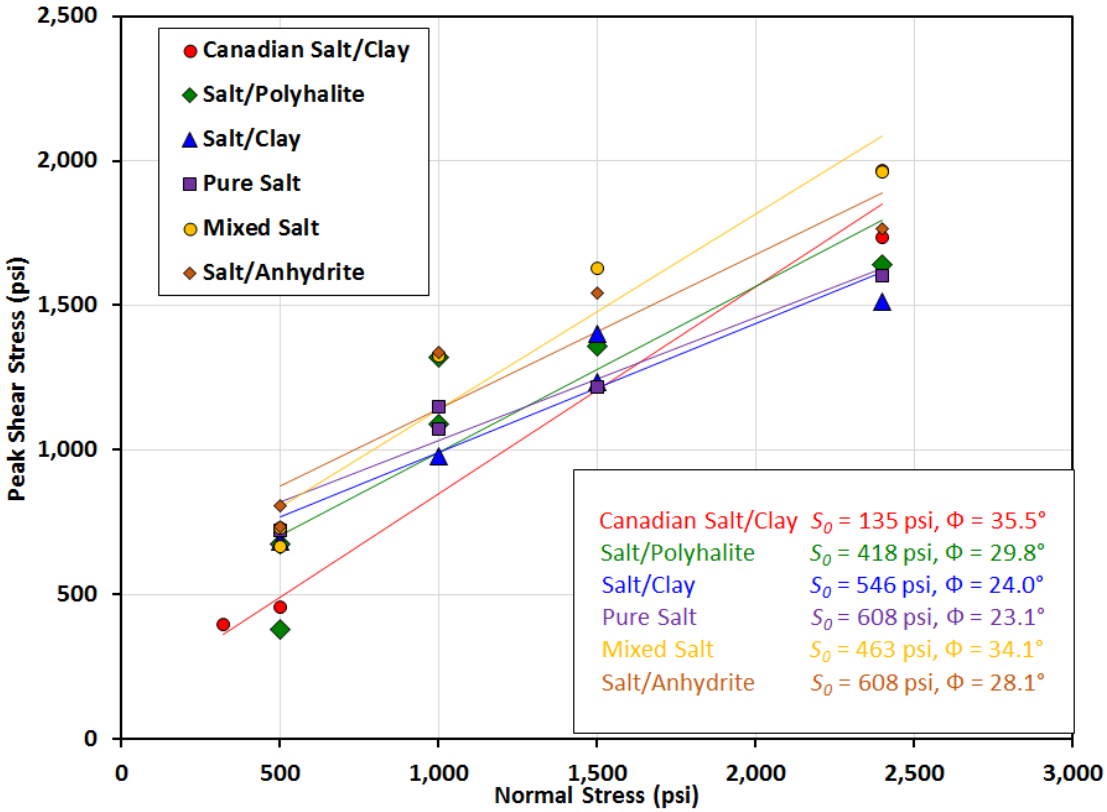

Figure 1-5. Nominal Peak Shear Stress as a Function of Nominal Normal Stress for Interface Shear Tests (Sobolik et al., 2019).

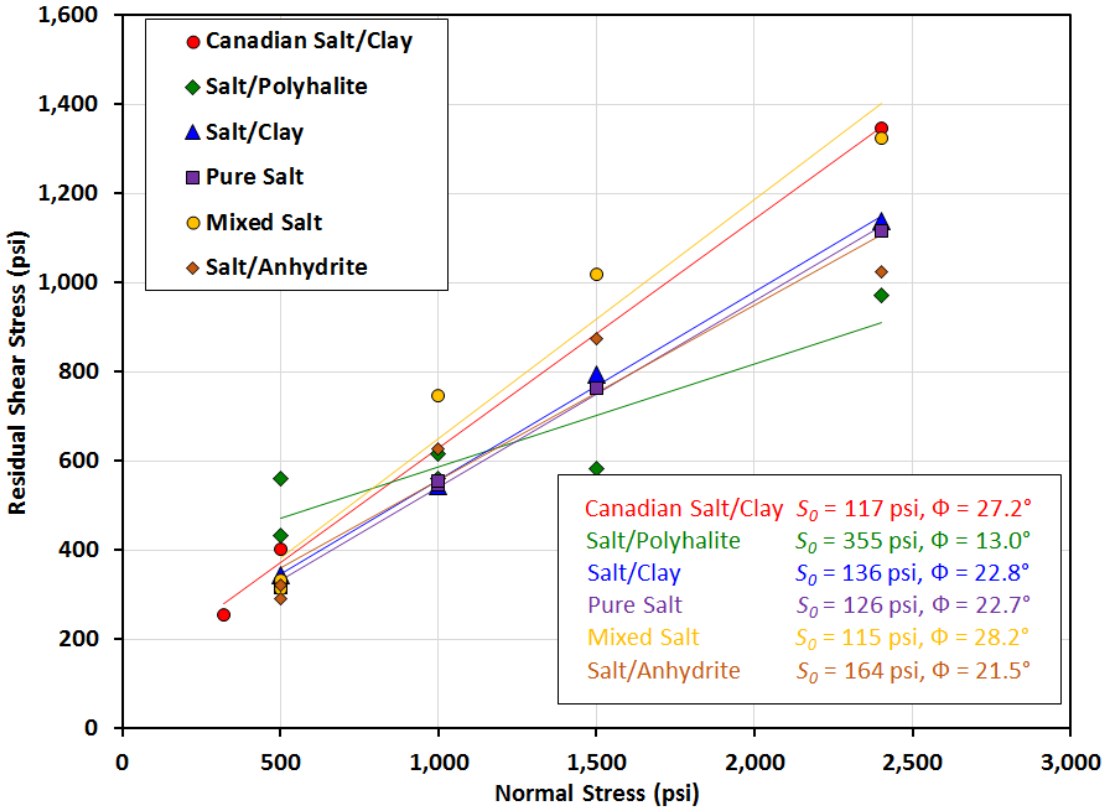

Figure 1-6. Nominal Residual Shear Stress as a Function of Nominal Normal Stress for Interface Shear Tests (Sobolik et al., 2019).

The halite/clay interface is particularly of interest because of the presence of several clay seams in the region surrounding the WIPP site (see Figure 1-1). Given the prevalence of clay seam sliding at WIPP (see Figure 1-2), the clay interface was expected to have the lowest cohesion and friction angle, yet its behavior is more similar to that of pure salt. One potential reason for the large clay strengths was found upon examining the broken interfaces. The clay interfaces had salt crystals spanning the interface, such that the shear test was measuring the sliding of these crystals against one another with little clay to lubricate the interface. This condition has been observed at other interfaces at the WIPP site (Holt and Powers, 2011), which is different than other less stiff clay interfaces at WIPP, such as those in Figure 1-2.

The clay seams observed at WIPP typically have a thickness between 0.125-2 inches (3-50 mm). Clay seam samples from depths closer to the WIPP horizon are currently difficult to obtain due to ventilation issues. For this reason, additional testing has been performed to include samples with artificially manufactured bentonite seams with thicknesses in the range described above. The tests detailed in the report will help interpret future tests on clay seam samples from the WIPP horizon.

1.3. Report organization

This report is organized in the following fashion: Section 2 describes the procedure for specimen acquisition and preparation as well as the test procedure. Section 3 describes in detail the results of the tests. Section 4 summarizes the results and provides concluding remarks.

2. EXPERIMENTAL PROCEDURE

A series of laboratory experiments was performed that consisted of fabricating consolidated clay seams within salt (predominately halite) and performing direct shear tests on those clay seams. These tests were conducted at several normal and shear loads up to the expected in situ pre-mining stress conditions, and at a single shear ram advancement velocity of 0.01 in/min (0.004 mm/sec). This shear velocity is currently the slowest capable on the direct shear machine used, thus these tests were unable to evaluate potential velocity-dependent shear stress evolution. The direct shear test method was designed to measure the complete shear stress-strain curve and characterize the following mechanical properties:

- Intact normal and shear stiffness
- Dependence of shear yield, ultimate, and residual strength on normal stress
- Residual normal and shear stiffness

Ultimate strength was the maximum shear stress measured during the test. Residual strength corresponds to the shear stress when the specimen shows perfectly plastic shear deformation behavior and was chosen as the lowest value of shear stress after decreasing to a nominally constant value. The test program followed two distinct phases, each of which is covered in the following subsections:

1. Experiment preparation, including test sample preparation and setup of the direct shear machine.

2. Execution of a suite of direct shear tests on 8 specimens, varying the thickness of the artificial clay seam and the applied normal stresses.

The project's test plan (Sobolik, 2019) includes further details of specimen preparation, test setup, multi-stage shear tests, and data processing. A full discussion of the testing procedure and results was provided in Keffeler (2020); much of Sections 2.1, 2.2, and 2.3 was taken directly from that report. The entire Keffeler report is included in Appendix A.

2.1. Specimen preparation

A total of eight artificial clay seam specimens were created. The test samples were from the same set of cores extracted from a potash mine in 2017 for the tests described in Buchholz (2019) Sobolik et al. (2019), and Sobolik and Reedlunn (2019), and the reader may refer to those documents for a full description. The specimen preparation method is summarized as:

1. 4-inch-diameter by approximately 3-inch-long salt cylinders were subcored from the 12-inch-diameter core obtained from the potash mine near WIPP. Bright-Cut NHG metal working fluid was used as a lubricant during subcoring to prevent washing of the evaporite materials. The specimens were then cleaned using an alcohol-based degreaser.
2. A series of 0.05-inch-deep circular grooves were machined, radially spaced 0.25 inch apart, into one face of each subcore, as shown in Figure 2-1.
3. Bentonite powder was mixed with saturated salt (halite) brine to a fresh-water moisture content (by weight) of approximately 60 percent.
4. A ¼-inch- or ½-inch-thick layer of the bentonite-brine mix was applied to the grooved surface of a subcore. A second subcore was placed onto the bentonite-brine mix with the grooved

surface facing the bentonite-brine mix. This assembly constituted an unconsolidated test specimen.

5. The unconsolidated test specimen was wrapped in filter fabric and placed into a consolidation vessel. The specimen was protected from the confining oil using neoprene jackets, and the platens were vented to the atmosphere.
6. The test specimen was consolidated under an isostatic stress of 3,000 pounds per square inch (psi) (nominal) at 21 degrees Celsius (°C) for 14 days. (For comparison, the lithostatic pressure at the WIPP horizon is approximately 2150 psi.) Excess pore fluid from the bentonite mixture was expelled through the vents.
7. The consolidated test specimen was removed from the consolidation vessel, and the diameter of the clay seam was measured.
8. The consolidated test specimens were coated in clear acrylic to protect them from the encapsulation grout used in the shear boxes.
9. The test specimens were photographed. An example photograph of a consolidated specimen is provided in Figure 2-2.

Four of the specimens had pre-consolidation seam thicknesses of ½ inch, and the remaining four had pre-consolidation seam thicknesses of ¼ inch. The post-consolidation seam thicknesses were approximately 1/16 inch and 3/16 inch for the ¼- and ½-inch pre-consolidation seam thicknesses, respectively. Specimen seam diameters are listed in Table 2-1.

Figure 2-1. Grooves machined into a face of a 4-inch-diameter salt subcore.

Figure 2-2. Photograph of consolidated test specimen.

Table 2-1. Consolidated test specimen seam diameters.

Specimen ID	Pre-Consolidation Seam Thickness	Post-Consolidation Seam Thickness	Pre-consolidation Average Seam Diameter	Post-consolidation Average Seam Diameter
	(inches)	(inches)	(inches)	(inches)
Carlsbad/Art-Seam/1A-1B	1/4	1/16	4.00	3.95
Carlsbad/Art-Seam/2A-2B	1/4	1/16	4.00	3.91
Carlsbad/Art-Seam/3A-3B	1/2	3/16	4.00	3.90
Carlsbad/Art-Seam/4A-4B	1/2	3/16	4.00	3.85
Carlsbad/Art-Seam/5A-5B	1/2	3/16	4.00	3.91

Specimen ID	Pre-Consolidation Seam Thickness	Post-Consolidation Seam Thickness	Pre-consolidation Average Seam Diameter	Post-consolidation Average Seam Diameter
Carlsbad/Art-Seam/6A-6B	1/4	1/16	4.00	3.96
Carlsbad/Art-Seam/7A-7B	1/2	3/16	4.00	3.87
Carlsbad/Art-Seam/8A-8B	1/4	1/16	4.00	4.05

2.2. Test Equipment

Normal stresses of 500–2,400 psi (3.5–17 MPa) were required to approximate in situ overburden stress conditions at WIPP (approximately 15 MPa). For this reason, tests were performed using a rock direct shear testing machine designed and fabricated by RESPEC, which is shown in Figure 2-3. It has an axial and shear load capacity of 30,000 pounds (130 kN) each, which meets the 1,500 psi (10 MPa) requirement for the 4-inch- (100-mm-) diameter cylinders. The machine consists of shear boxes (that hold the test specimen), a normal load ram, a shear load ram, and hydraulic controls. The shear load ram is controlled by a mechanical-over-hydraulic intensifier that advances the shear load ram at a set displacement rate. The normal load ram is controlled by a pressure regulator that maintains the normal load within 1 percent of the set point. The test specimen is encapsulated into the shear boxes using quick-setting, high-strength grout.

Normal load is applied to the shear boxes through a roller contact and spherical seat. Shear load is applied to the shear box through pinned connections, and the shear load ram is vertically aligned with the center of the gap between the shear boxes. The normal and shear forces are measured using load cells. Shear displacement is measured using a linear variable displacement transformer (LVDT). Normal displacement between the upper and lower shear boxes is monitored using four precision linear potentiometers. The sensor brackets are attached to the lower shear box and the sensor plungers ride against steel blocks on the upper shear box. Figure 2-4 shows the location of the normal displacement gages on the shear machine. These steel blocks are ground parallel to the bottom surface of the upper shear box; error in parallelism is about 0.001 inch. Non-uniform loading of the shear area is a known problem with direct shear tests. Typically, the shear force is applied slightly above the interface, which creates a moment on the specimen. This moment causes the front edge (furthest away from shear load ram) of the specimen to experience greater than the target normal stress and the back of the specimen to experience less than the target normal stress. The normal displacement of the front edge was measured by potentiometers number 1 and 4 in Figure 2-4, and these gages usually had the highest displacement readings. The average difference between minimum and maximum measured normal displacements was 0.0265”; over the 8” span of the shear box, which correlates to an angle of 0.19°. For routine applications of this test data, calculations typically assume nominal uniform stresses even though the actual distribution of stresses is nonuniform and changes with shear force. The machine’s stiffness to shear and normal loading was also measured; these results are shown in Appendix A. The load cells and linear displacement sensors were calibrated to standards traceable to the National Institute of Standards and Technology (NIST).

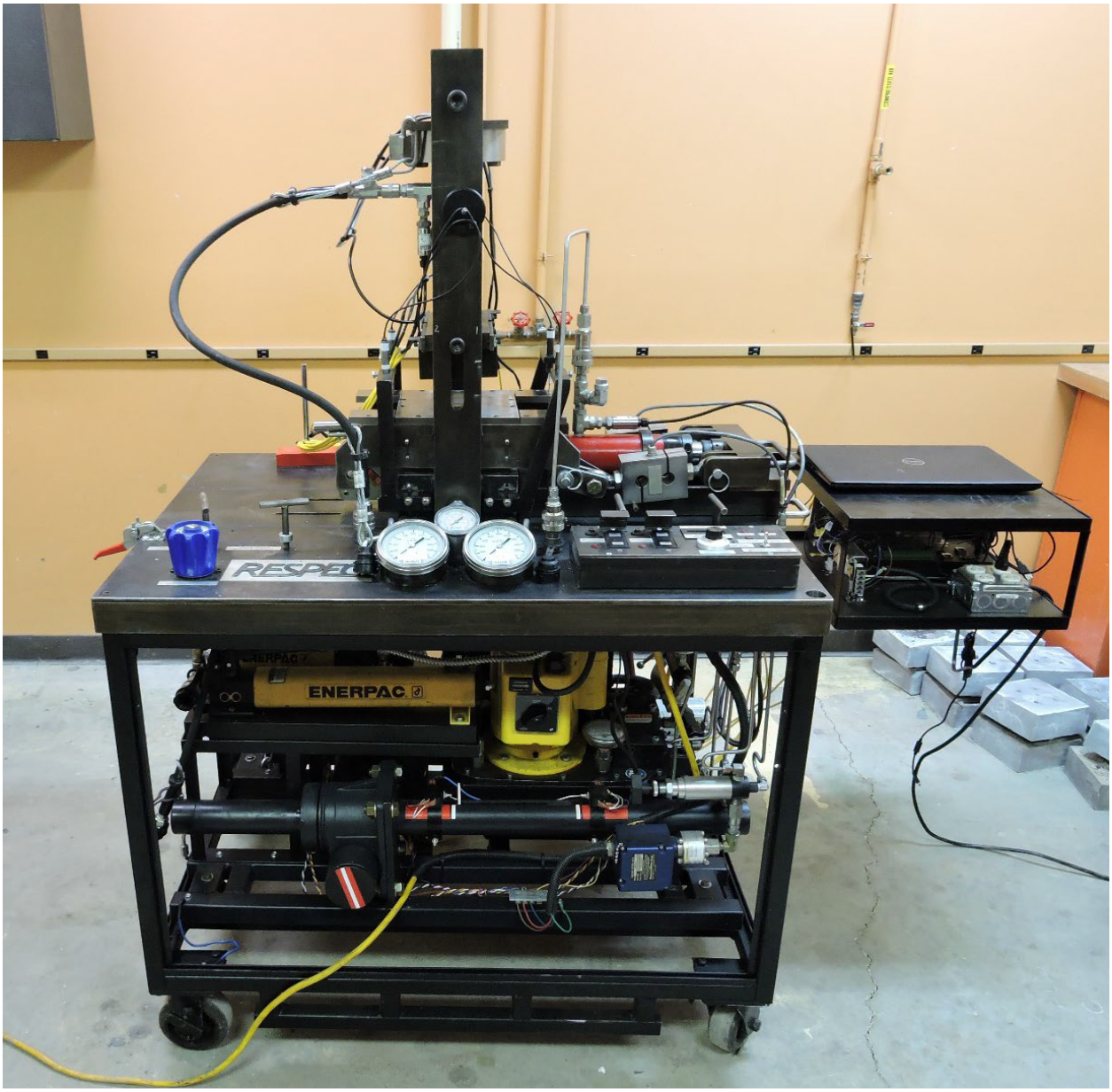

Figure 2-3. RESPEC direct shear machine.

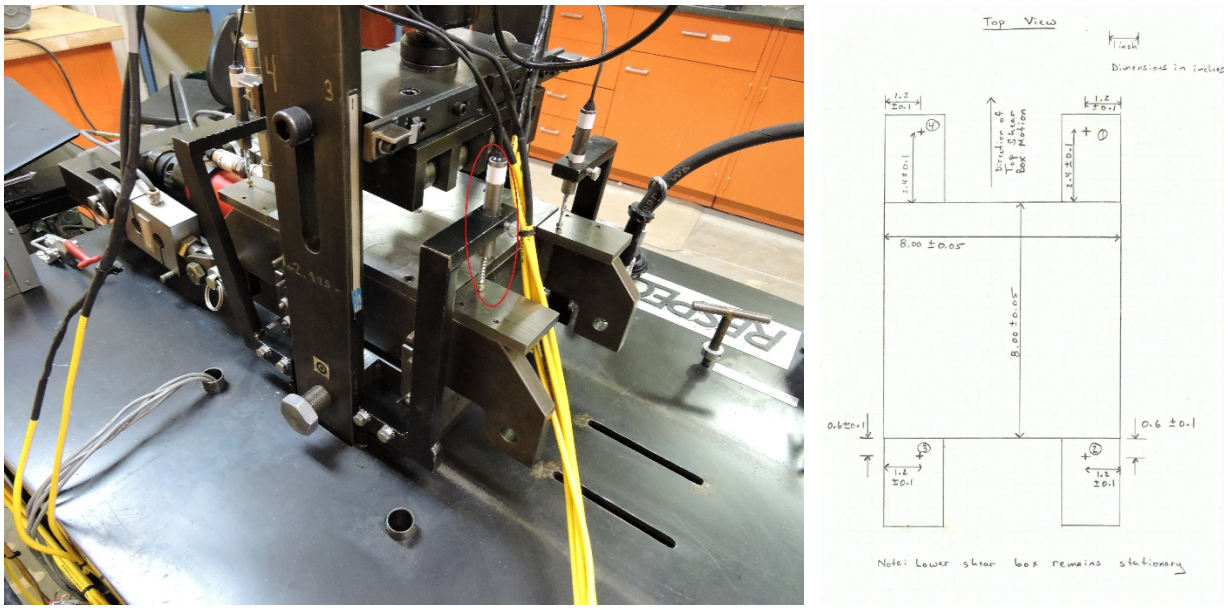

Figure 2-4. Location of normal displacement potentiometers numbered 1-4 (Number 3 highlighted with red oval).

2.3. Test Procedure

The direct shear testing method is summarized as:

- Encapsulate consolidated test specimen into the shear boxes using fast-setting grout while leaving a ½-inch gap between the boxes.
- Allow grout to cure overnight.
- Mount the shear boxes into the direct shear testing machine.
- Set up shear and normal displacement transducers.
- Initial normal loading:
    - Bring normal ram into contact with the upper shear box.
    - Increase normal load to the target value.
    - Measure the normal stiffness. Reduce normal load to approximately 600 pounds. Increase normal load to the target value (i.e., an unload/reload cycle).
    - Hold normal load constant for approximately 10 minutes to allow normal displacement to stabilize.
    - Hold normal load constant during shear loading.
- Shear loading:
    - Apply shear load by advancing the shear ram at a rate of 0.01 inch per minute (0.004 mm/s; this rate is the same used in the Buchholz (2019)/Sobolik et al. (2019) study, more than double the fastest rate in the Minkley and Mühlbauer (2007) study and orders of magnitude above the in situ rate, but it was the slowest rate the testing machine was capable of performing.).
    - Measure the shear stiffness. When the shear load is approximately 20 percent of the normal load, reduce the shear load to approximately 250 pounds by retracting the shear ram at 0.01 inch per minute. Reapply shear load by advancing the shear ram at 0.01 inch per minute (i.e., an unload/reload cycle).

    - Continue to advance the shear ram at 0.01 inch per minute until a residual shear strength has been established or shear displacement equals 0.8 inch (whichever is achieved first).
    - Measure the shear stiffness again. Reduce shear load to approximately 250 pounds by retracting the shear ram at 0.01 inch per minute. Reapply shear load by advancing the shear ram at 0.01 inch per minute until the shear plane slips (i.e., an unload/reload cycle).
    - Remove the shear load by retracting the shear ram at 0.01 inch per minute.
- Post-test normal loading:
    - Measure the normal stiffness. Reduce the normal load to approximately 600 pounds. Increase the normal load to the value at which the test was performed (i.e., an unload/reload cycle).
    - Remove the normal load.

If the test specimen was still in testable condition after the procedure described above, the shear boxes were reset to their original position and the shear testing procedure was repeated. Once the shear specimen could no longer be tested, the shear boxes were removed from the testing machine and separated. Debris was removed and post-test photographs were taken of the sheared surfaces. The testing room was kept at an ambient temperature of 68°F (20°C) during all tests.

One source of error was the shear displacement, causing the top half of the specimen to protrude over the bottom half. The maximum shear displacement reached as high as 0.80 inch. This overhang led to a decrease in modified cross-sectional area A_δ available to resist the normal and shear loads P and S. This modified cross-sectional area can be calculated as the overlap between two offset circles as

$$A_\delta = (\theta - \sin\theta)\left(\frac{d_0}{2}\right)^2,\ \theta = 2\cos^{-1}\frac{\delta}{d_0},$$

where d_0 is the initial specimen diameter. Nevertheless, the normal and shear stresses were first calculated assuming the initial area of the specimens $A_0 = \pi\ d_0^2 / 4$,. The error that results from assuming constant area is negligible for the intact portion of the tests as shear displacement is small prior to exceeding the ultimate shear strength of the specimens. For the portions of the intact tests after seam fracture (ultimate shear strength), the shear displacement and area loss are larger; neglecting the changing area resulted in roughly 15-25% errors in calculated stresses at the end of the test. In the Mohr-Coulomb strength criterion fits discussed below, calculations of shear stress calculated with original and modified contact area are compared.

3. RESULTS

The data from each test were analyzed to determine the following:

- Pretest normal stiffness (psi per inch [psi/inch])
- Pretest shear stiffness (psi/inch)
- Peak shear strength (psi)
- Shear strength at 0.75 inch of shear displacement (psi)
- Posttest shear stiffness (psi/inch)
- Posttest normal stiffness (psi/inch).

This section begins with results from one specimen, followed by comparisons across the various specimen groups.

3.1. Specimen Carlsbad/Art-Seam/2A-2B

Figures 3-1 through 3-3 show the stiffness and shear stress results of the tests on the sample Carlsbad/Art-Seam/2A-2B which was tested as an intact sample at a normal stress of P/A_0 = 1494 psi (10.3 MPa). In these plots, nominal stresses were used throughout the calculations. Nominal stresses are calculated using the original shear area of the specimens (i.e., change in area during the test is not accounted for). A plot of normal stress versus normal displacement for a normal unload/reload cycle is shown in Figure 3-1. Joint stiffness is defined as the slope of the stress-displacement curve. Normal stiffness was calculated from the slope of a line fit to the normal stress reload curve; because many of the normal reloads were noticeably nonlinear, the line was fit between 40 percent and 100 percent of the target normal stress to ensure consistency between tests. A shear-reloading plot is shown in Figure 3-2. Shear stiffness was calculated from the slope of a line fit to the linear portion of the shear stress reload curve. Normal and shear stiffness curves for all the tests in this report are included in Keffeler (2020) in Appendix A.

A plot of shear stress versus shear displacement for sample 2A-2B is shown in Figure 3-3. The peak shear strength was defined as the maximum nominal shear stress recorded during the test. By using the original shear area to calculate the shear stress, the plot shows that a residual stress was not established within 0.8 inch of shear displacement for any of the tests. Consequently, the computed shear stress at 0.75 inch was used as a means to compare post-peak strengths between the specimens. In the figures in the next section, two separate representations of shear stress will be plotted – one based on the original contact area, and another based on the area as defined by the shear displacement.

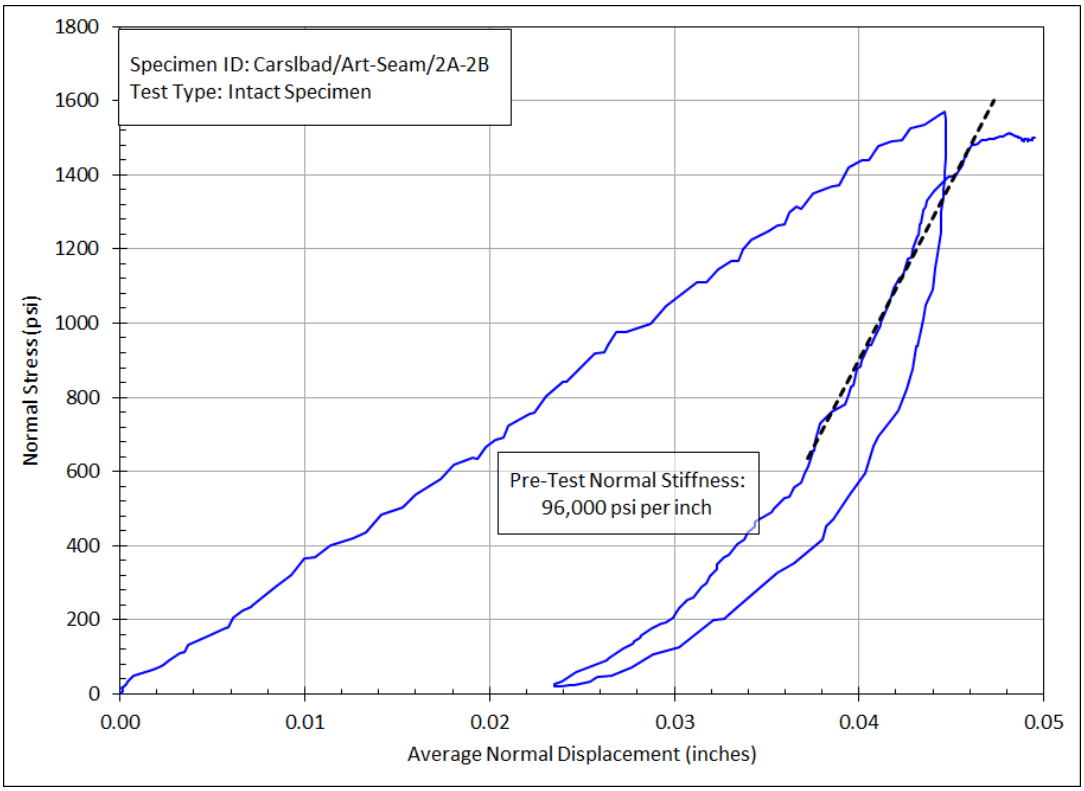

Figure 3-1. Nominal Normal Stress Versus Normal Displacement Plot Used to Calculate Normal Stiffness.

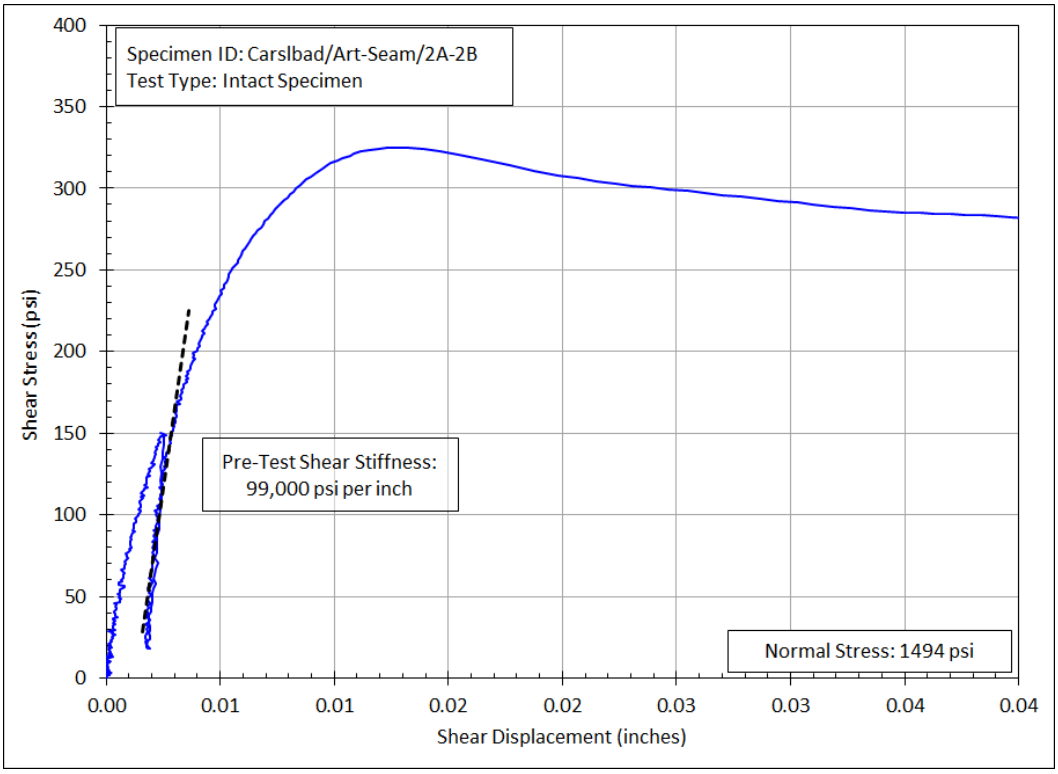

Figure 3-2. Nominal Shear Stress Versus Shear Displacement Plot Used to Calculate Shear Stiffness.

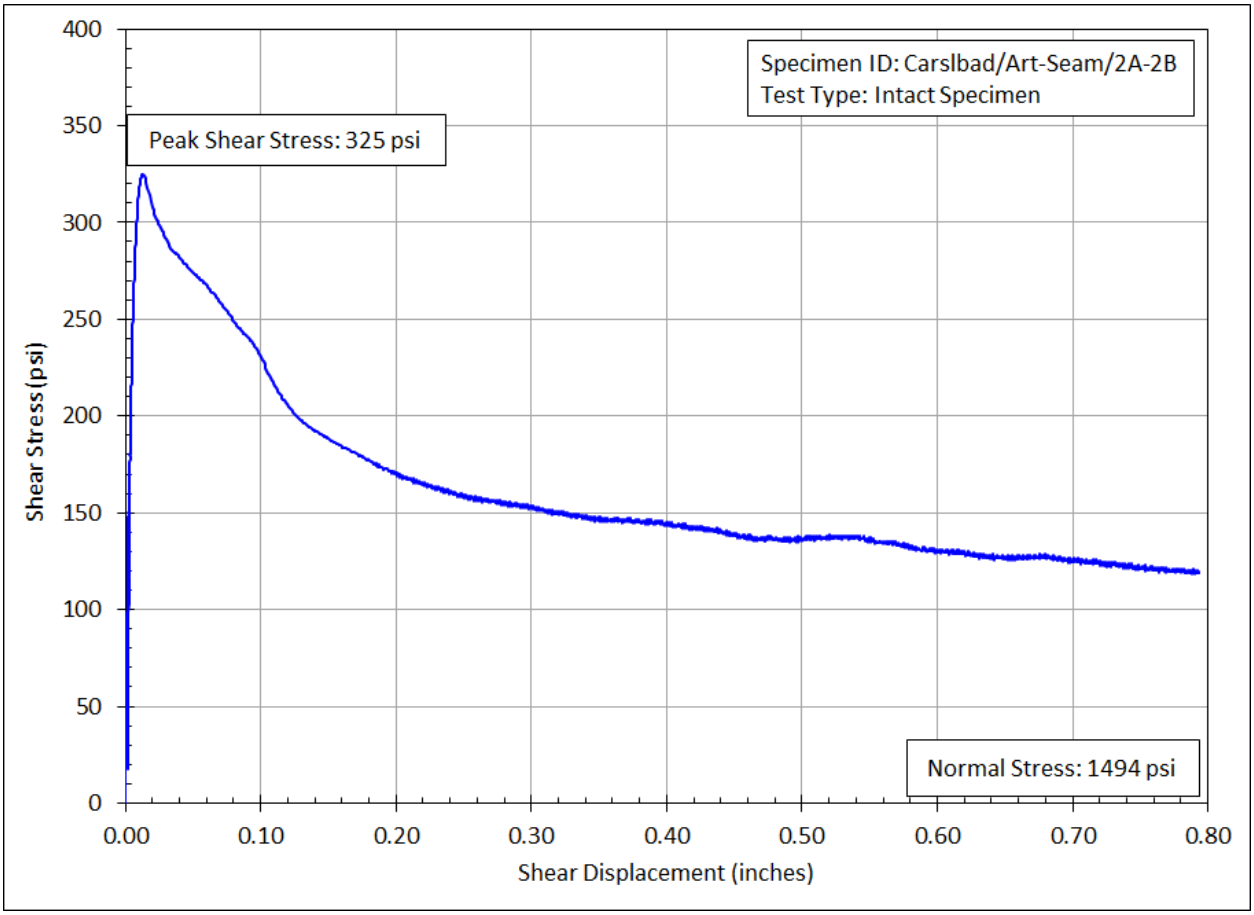

Figure 3-3. Nominal Shear Stress-Displacement Plot for a Direct Shear Test on Intact Specimen 2A-2B.

3.2. Results

A summary of the measured peak and residual shear stresses for all the tests is listed in Table 3-1, with shear stress values based on the modified contact area A_δ. Figures 3-4 through 3-11 plot the shear stress versus shear displacement δ curves for the eight intact sample tests. The results from the four previously failed specimens are included in Appendix A. All stresses in the table have units of psi. For Figures 3-4 through 3-11, two values are plotted for shear stress: the blue curves represent shear stress calculated with the original seam contact area, S/A_0, calculated with the average original seam diameter d_0; and the orange curves represent the shear stress calculated using the modified contact area reduced by the shear displacement S/A_δ.

Table 3-1 lists the tests in specimen ID numerical order. However, the seam thicknesses and applied normal stresses do not correspond to the same order, so Figures 3-4 through 3-11 are grouped first by seam thickness, then by normal stress. Figures 3-4 through 3-7 are for the tests with the ¼" seam: specimens #1 and #8 at 500 psi, #6 at 1000 psi, and #2 at 1500 psi. Figures 3-8 through 3-11 are for the tests with the ½" seam: specimen #4 at 500 psi, #3 and #7 at 1000 psi, and #5 at 1500 psi. Test #8 was a repeat with a different specimen of Test #1 due to noisy data in Test #1; Test #7 was a retest of Test #3 to verify results.

For each of the tests in Figures 3-4 through 3-11, a peak stress was established, after which the seam "broke" or exceeded its static friction and began to slide with reduced stress. This behavior is similar to that of the higher speed test by Minkley and Mühlbauer (2007), and to the salt interface test by Buchholz (2019) and Sobolik et al. (2019). In the initial analysis of all eight tests using the original seam contact area, two tests at most appeared to have achieved a residual shear stress through 0.75" shear displacement. After recalculating the shear stress based on the displacement-reduced contact area, four tests appear to have achieved a residual stress: Test #8 (~150 psi), Test #2 (~164 psi), Test #4 (~130 psi), and Test #7 (~150 psi). It is unclear why the other tests failed to reach a residual stress condition.

Table 3-1. Direct shear testing strength results.

Specimen and Test ID	Specimen Type	Pre-Consolidation Seam Thickness	Nominal Normal Stress	Peak Nominal Shear Stress	Nominal Shear Stress at 0.75 inch Displacement
		(inches)	(psi)	(psi)	(psi)
Carlsbad/Art-Seam/1A-1B	Intact	1/4	504	140	96
Carlsbad/Art-Seam/1A-1B	Previously Failed	1/4	1004	137	125
Carlsbad/Art-Seam/2A-2B	Intact	1/4	1494	325	161
Carlsbad/Art-Seam/3A-3B	Intact	1/2	1000	215	76
Carlsbad/Art-Seam/4A-4B	Intact	1/2	507	277	104
Carlsbad/Art-Seam/4A-4B	Previously Failed	1/2	992	166	156
Carlsbad/Art-Seam/5A-5B	Intact	1/2	1487	427	155
Carlsbad/Art-Seam/6A-6B	Intact	1/4	992	282	136
Carlsbad/Art-Seam/6A-6B	Previously Failed	1/4	1501	199	157
Carlsbad/Art-Seam/7A-7B	Intact	1/2	990	239	149
Carlsbad/Art-Seam/8A-8B	Intact	1/4	496	234	144
Carlsbad/Art-Seam/8A-8B	Previously Failed	1/4	990	235	209

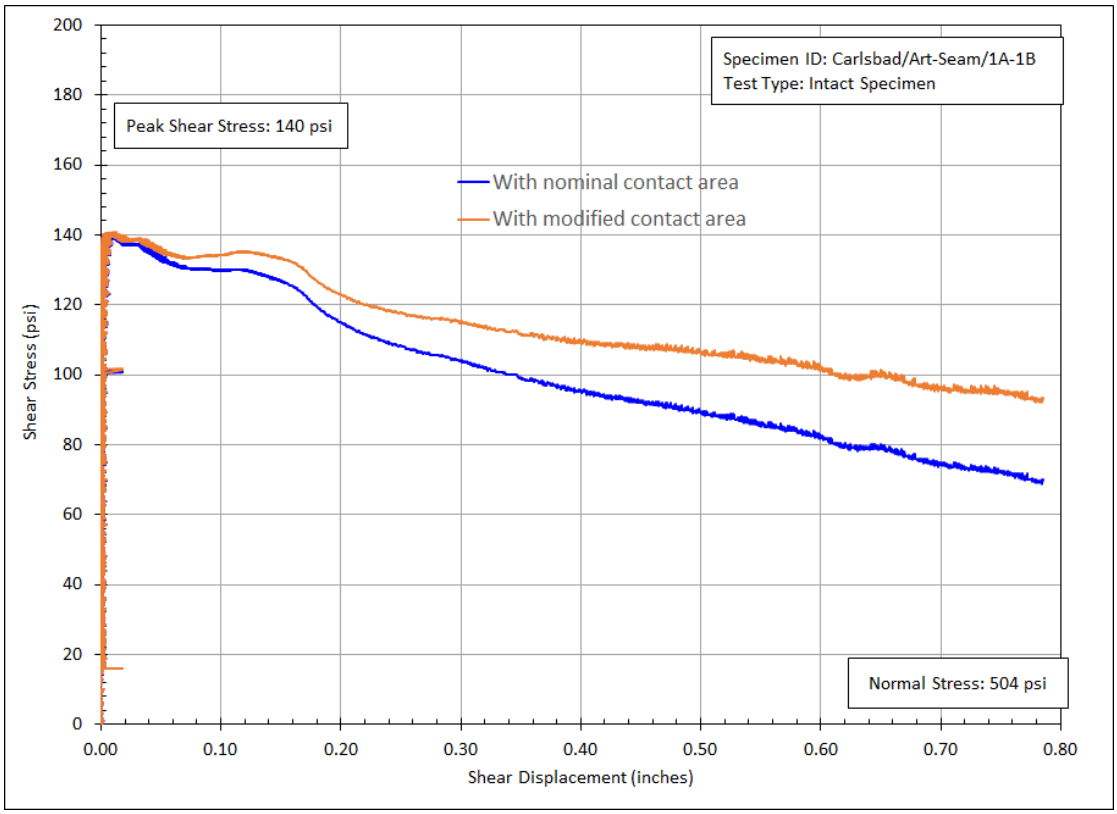

Figure 3-4. Carlsbad/Art-Seam/1A-1B Intact Shear Stress Versus Shear Displacement.

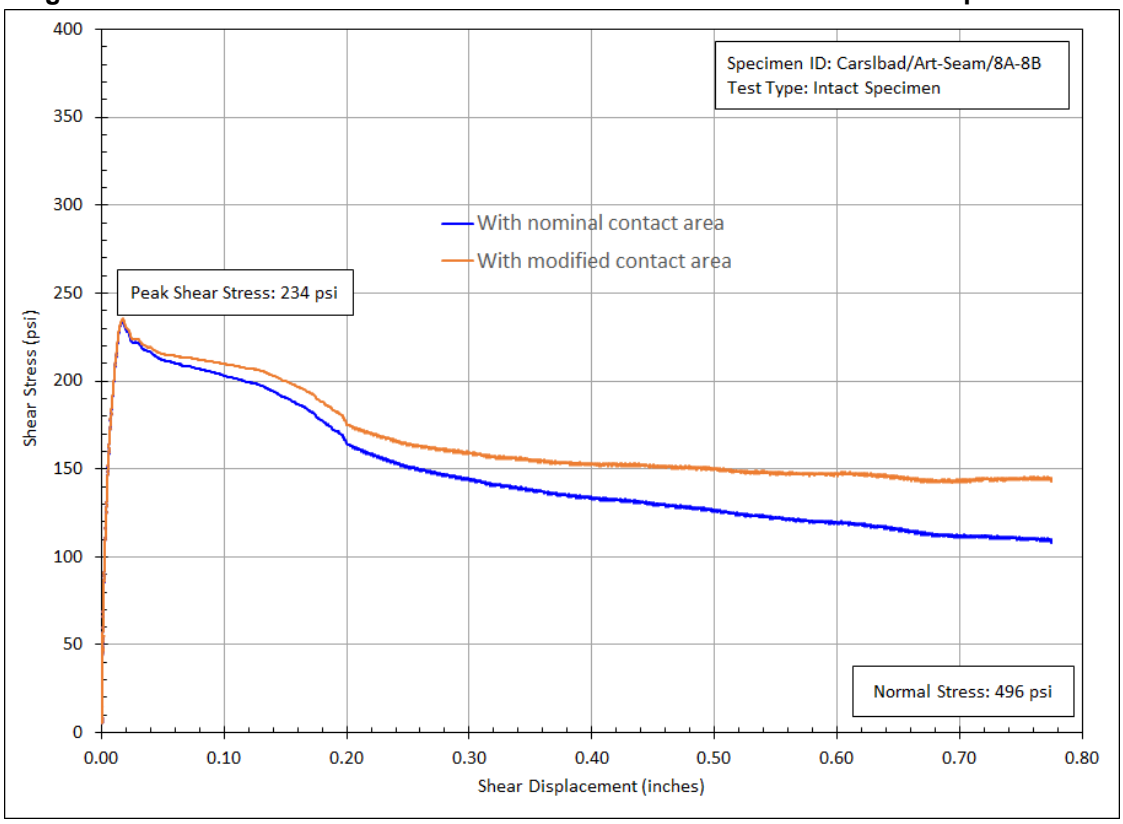

Figure 3-5. Carlsbad/Art-Seam/8A-8B Intact Shear Stress Versus Shear Displacement.

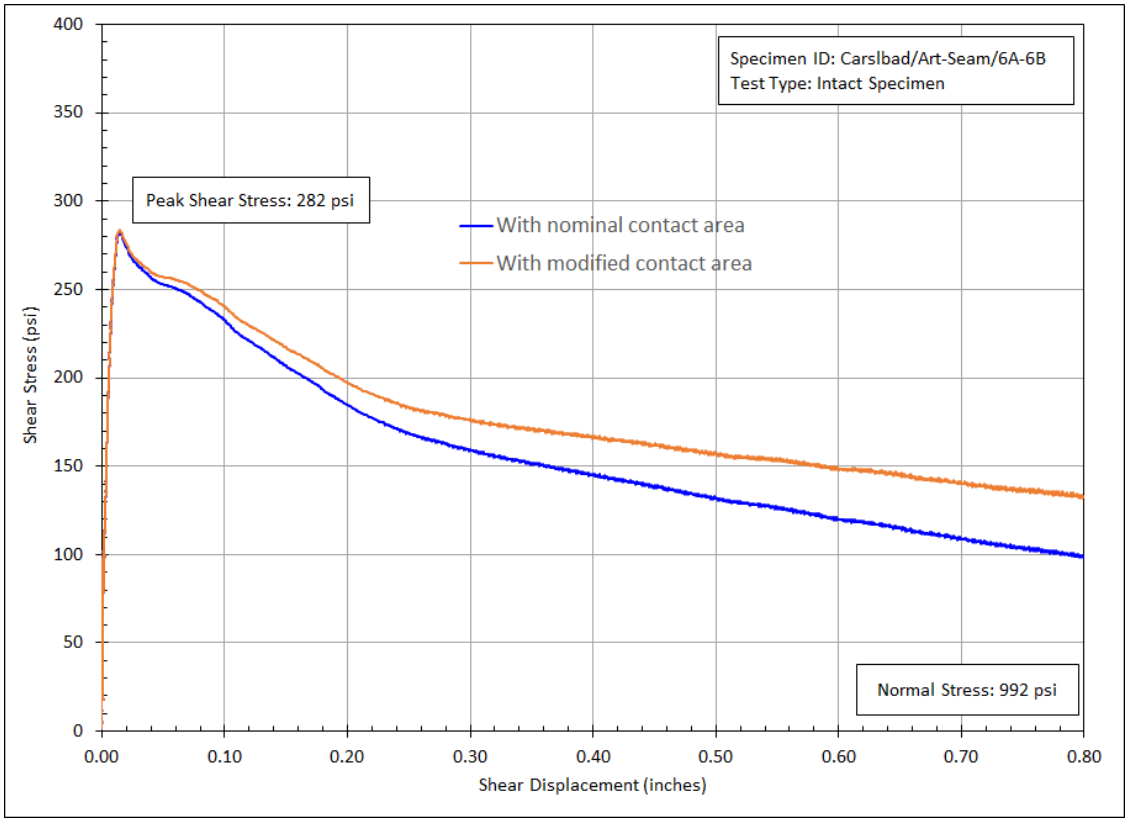

Figure 3-6. Carlsbad/Art-Seam/6A-6B Intact Shear Stress Versus Shear Displacement.

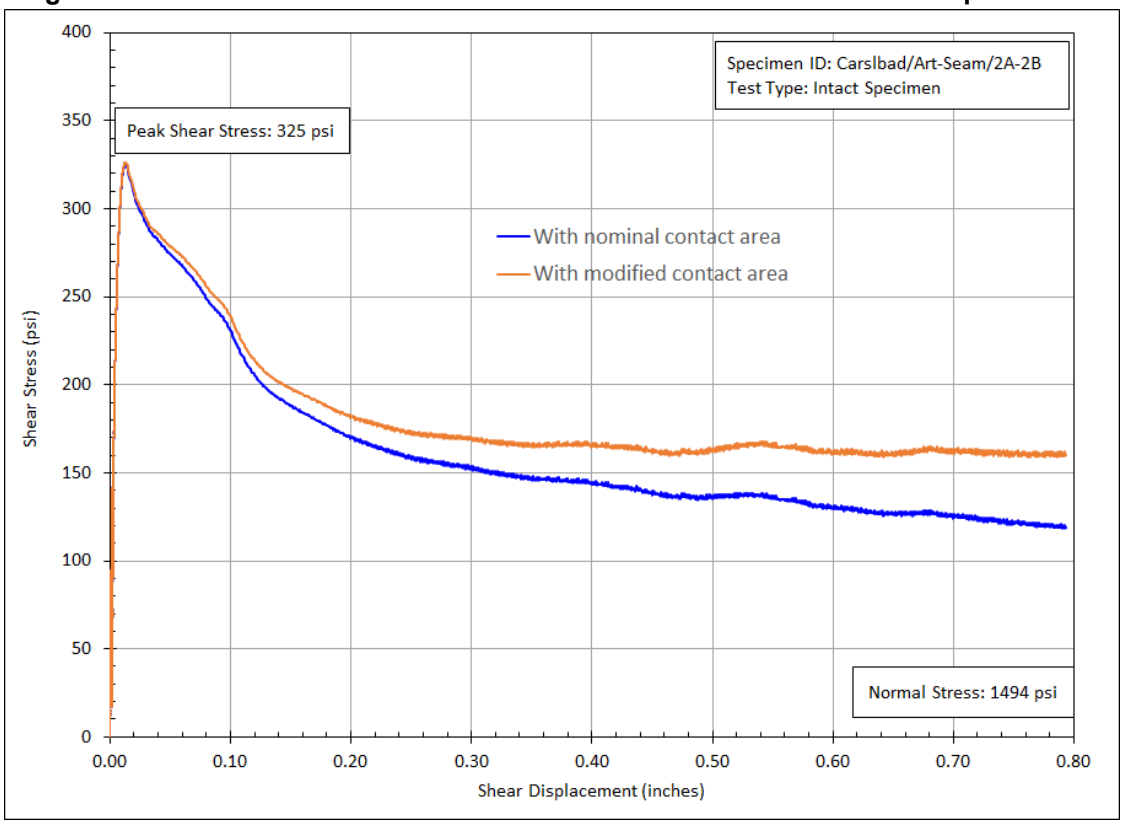

Figure 3-7. Carlsbad/Art-Seam/2A-2B Intact Shear Stress Versus Shear Displacement.

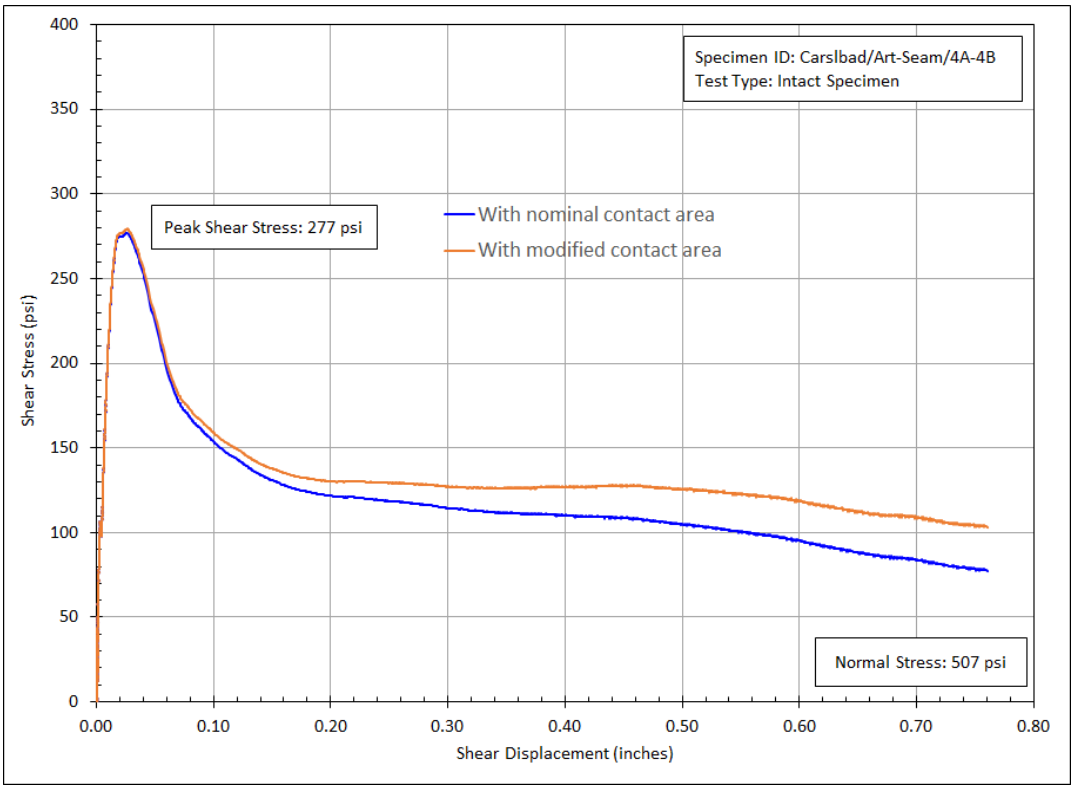

Figure 3-8. Carlsbad/Art-Seam/4A-4B Intact Shear Stress Versus Shear Displacement.

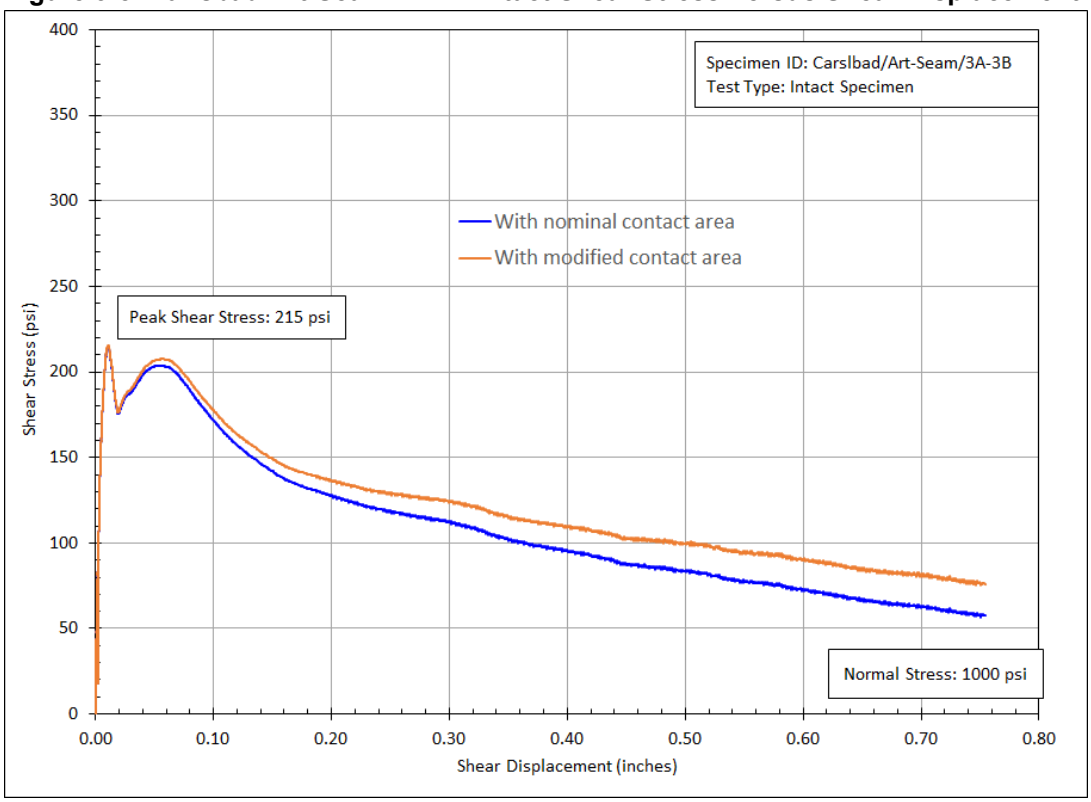

Figure 3-9. Carlsbad/Art-Seam/3A-3B Intact Shear Stress Versus Shear Displacement.

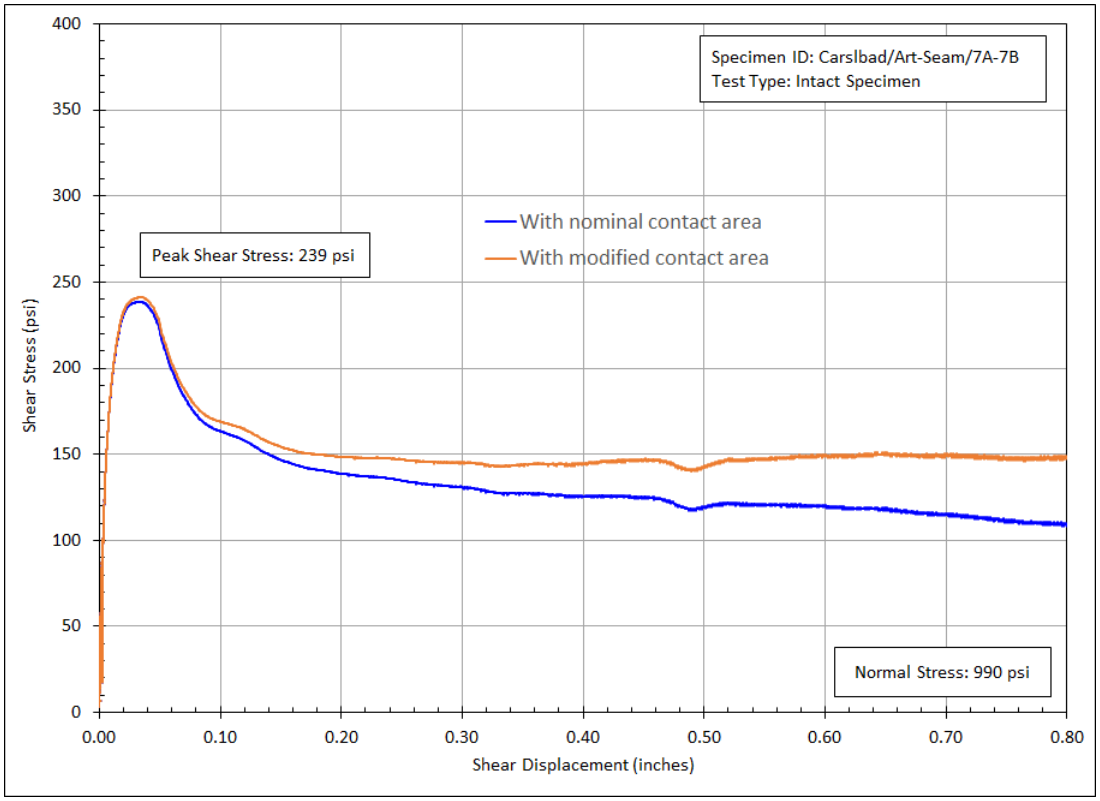

Figure 3-10. Carlsbad/Art-Seam/7A-7B Intact Shear Stress Versus Shear Displacement.

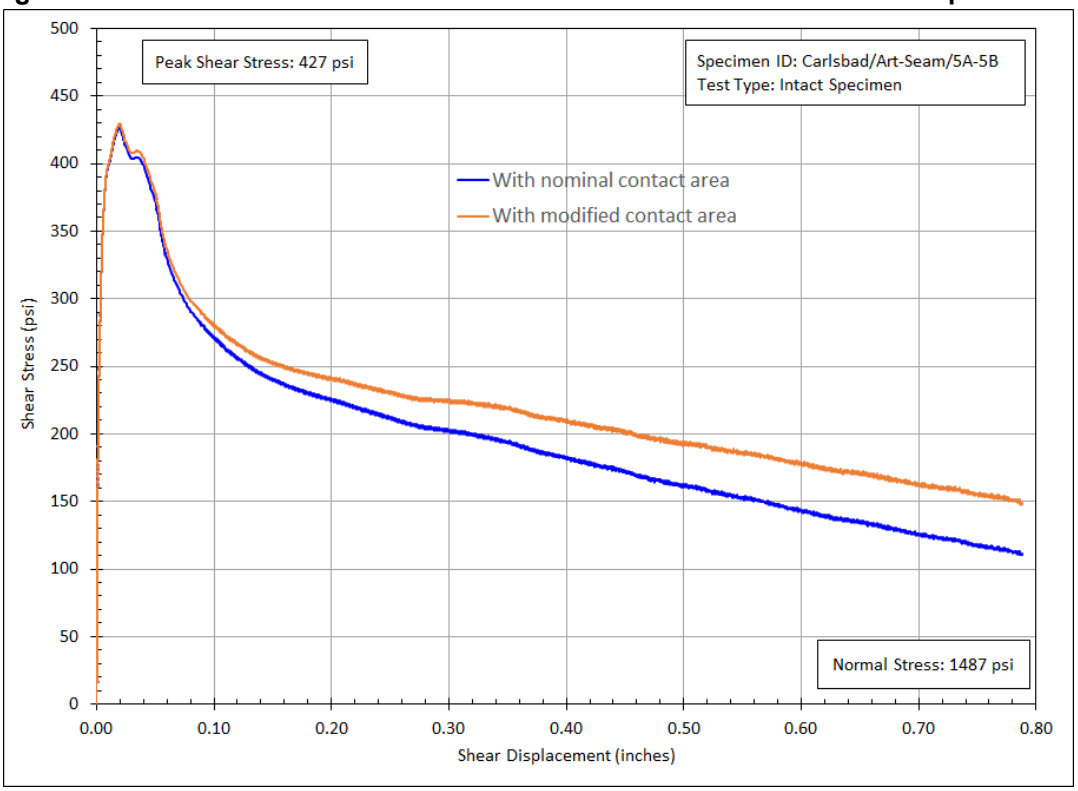

Figure 3-11. Carlsbad/Art-Seam/5A-5B Intact Shear Stress Versus Shear Displacement.

While calculating the shear stress using the displacement-reduced contact area indicated that four of the shear tests reached a residual shear stress, that same method changes the calculation of the normal stress during the test. Figure 3-12 plots the normal stress for one of the tests by both methods, against the shear displacement. As the normal forces remains essentially constant, the reduction in area causes an increase in normal stress on the contact area by about 33%. This is a curious result, because there is no corresponding increase in the shear stress with decreasing contact area; it would have been expected that an increasing Cauchy normal stress would have resulted in an increasing Cauchy shear stress. This result complicates the notion that the shear tests actually reached a residual shear stress and somewhat skews any analysis of the shear behavior. For now, the analysis in the next chapter simply utilizes the final shear strength measured at 0.75" of shear displacement.

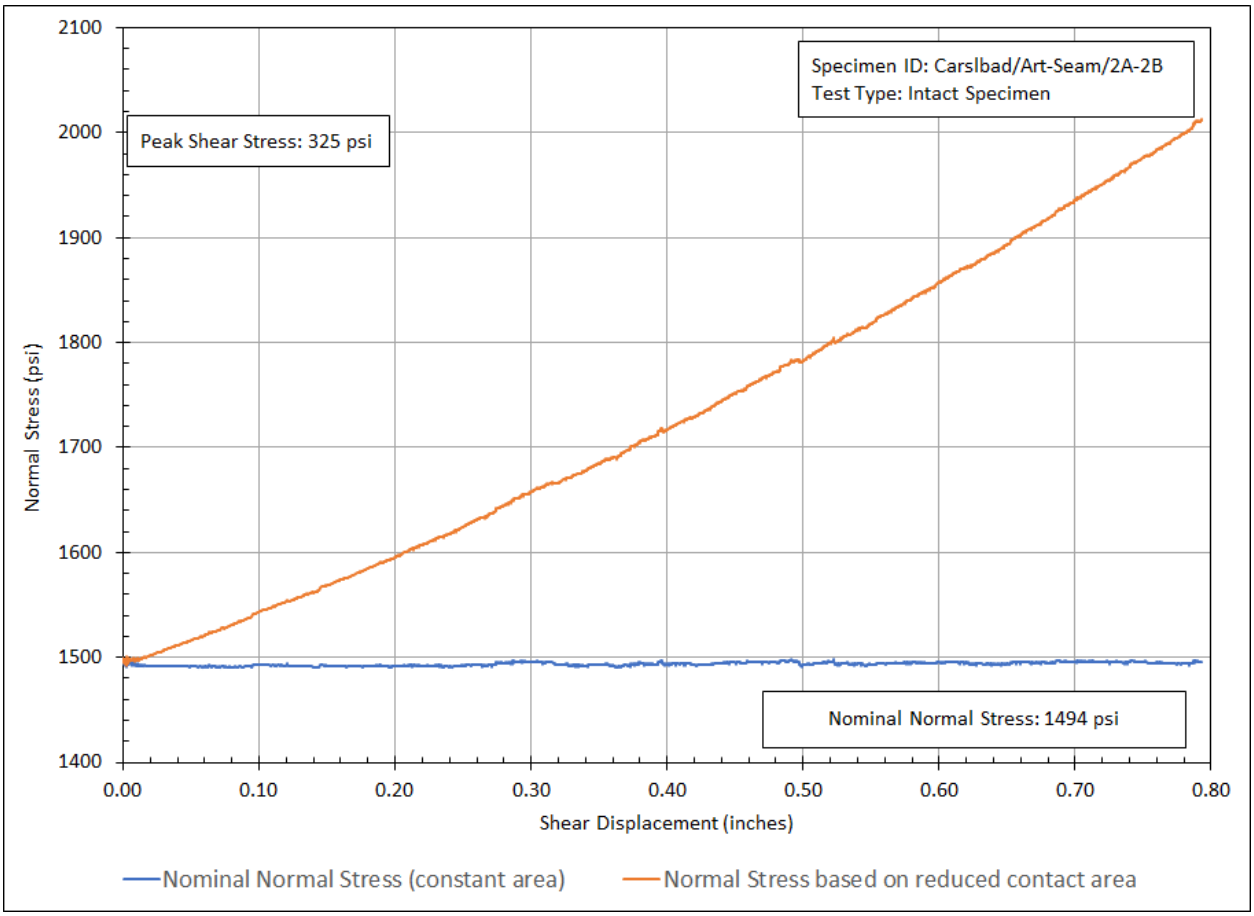

Figure 3-12. Carlsbad/Art-Seam/2A-2B Intact Normal Stress Versus Shear Displacement.

3.3. Analysis of Clay Seam Shear Results

Figures 3-13 through 3-15 show the data fits for peak shear stress, nominal residual shear stress, and displacement-corrected (Cauchy) residual shear stress, respectively, versus the normal stress. Results from both the artificial seam shear tests, and the halite-salt interface shear tests (Figures 1-5 and 1-6, Sobolik et al., 2019) are plotted together. Figure 3-13 is a comparison of similar values, with all stresses referenced to the original contact area A_0. Because only four of the clay seam shear tests reached a constant Cauchy shear stress, a condition caveated by the fact that the Cauchy nominal

normal stress increased because of the decreasing contact area (as shown in Figure 3-12), it is difficult to make a true comparison of residual stress test results between the clay seam tests and the earlier interface tests. For Figure 3-14, the shear and normal stresses for both the artificial clay seam tests and the interface shear tests were calculated using the original contact area A_0. The clay seam shear strengths correspond to 0.75" shear displacement, whereas the interface residual shear stress values correspond to those in Figures 1-5 & 1-6. For Figure 3-15, the shear and normal stresses for the both sets of tests were calculated using the reduced cross-sectional area of the interface A_δ. For the clay seam tests, the shear stresses at 0.75" displacement for all eight tests are included; for the interface tests, the shear stresses at the maximum displacement (ranging from 0.4" to 0.75") of the test were used. Note that the nominal shear stress and Cauchy shear stress were not necessarily computed at the exact same shear displacement for the interface tests. The results of the tests have been fitted to a Mohr-Coulomb shear strength criterion, defined as

$$\tau = \sigma_n \tan \Phi + S_0,$$

where τ is alternately the peak shear stress at failure (Figure 3-13), or the residual/final shear stress (Figures 3-14 & 3-15), σ_n is the normal stress on the shear surface, Φ is the friction angle, and S_0 is the cohesion.

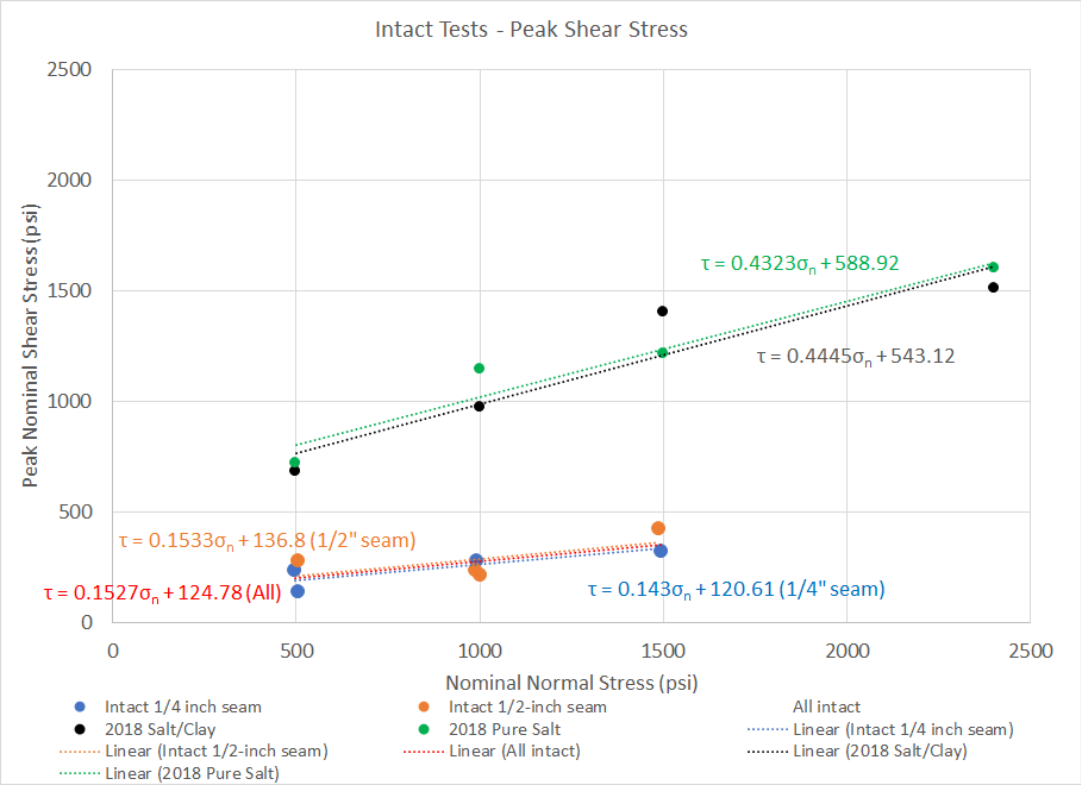

Figure 3-13. Peak shear stress as a function of normal stress, halite-salt interface tests and artificial seam tests.

For the artificial shear intact tests shown in Figure 3-13, the least square fit values for friction angle was $\Phi = 8.7°$, and for cohesion was S_0~125 psi. These values are much lower than those for previous salt interface tests, which had friction angle values ranging from Φ= 24-30° and cohesion of S_0~418-608 psi. Among the individual tests, the test for Sample 1 (¼", 500 psi normal, 140 psi

shear) had noisy data, which probably did not affect the result; the test for Sample 8 was a repeat of that test. In addition, the tests for Samples 3 & 7 (½", 1000 psi normal) had similar results to each other.

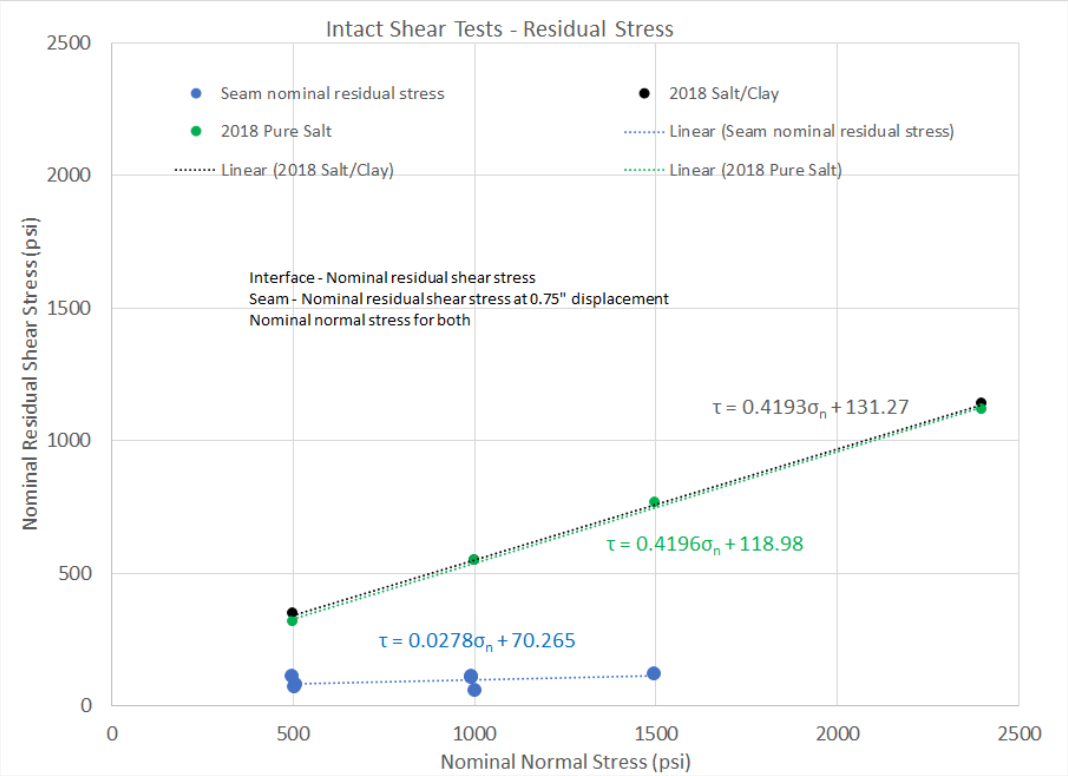

Figure 3-14. Nominal residual/final shear stress as a function of nominal normal stress, halite-salt interface tests and artificial seam tests.

The final shear strengths were also much lower than those from the previous salt interface tests. Figures 3-14 and 3-15 show that these samples had least squares fit values of friction angle Φ= 1.6°, and cohesion of ~70 and 93 psi for nominal and Cauchy stresses, respectively. For comparison, the value ranges for the pure salt and salt/clay interface tests are friction angle Φ = 22.1-23.4°, cohesion S_0~119-193 psi*. For an additional reference point, a friction coefficient of 0.2, which is equivalent to Φ = 11.3° and S_0=0, has historically been assumed in WIPP geomechanical analyses.

The softness of clay and small asperity size in the artificial clay seams may explain the low Mohr-Coulomb parameter measurements, particularly the friction angles. When examining the collection of tests in Figures 3-13 to 3-15, it was surprising that the 1/4" and 1/2" artificial seams underwent approximately the same behavior, with similar Mohr-Coulomb cohesion and friction angle values. This suggests that the tests may be measuring the shear strength of the clay, rather than the shear strength of a bumpier clay-salt interface where the salt must deform somewhat to permit sliding. There did not appear to be any salt asperity-to-salt asperity contact during shearing, so the behavior

* Switching from nominal stress in Figure 3-14 to Cauchy stress in Figure 3-15 causes the pure salt and salt/clay interface friction angles Φ to change slightly and the cohesion strengths S_0 to change more substantially. Friction angles are typically independent of stress measure, but the nominal shear stresses in Figure 3-14 do not exactly correspond to the Cauchy shear stresses in Figure 3-15, because, as mentioned above, they were computed at slightly different shear displacements.

was likely dominated by the saturated, consolidated, clay properties. This conclusion is supported by the calculated values of the Mohr-Coulomb constants. Clays typically exhibit non-zero cohesion. The values of cohesion in Figures 3-13 to 3-15 range from 70 to 125 psi, (0.48-0.86 MPa), which is larger than most references cite for clays (ranging from 10 to 110 psi for most clays, with hard clays having greater than 100 psi). Saturated consolidated clays, however, typically show cohesion with values as high as 110 psi, which is close to the values measured in the Figure 3-13.

It is intended that future laboratory tests with samples from Clay Seam G (generally thin and soft) and Clay Seam F (wide variation in thickness and hardness) will provide more insight into the variability of seam shear behavior. It is expected that the salt interface results and artificial seam results shown in Figures 3-13 through 3-15 will be bounding curves for Clay Seams F & G.

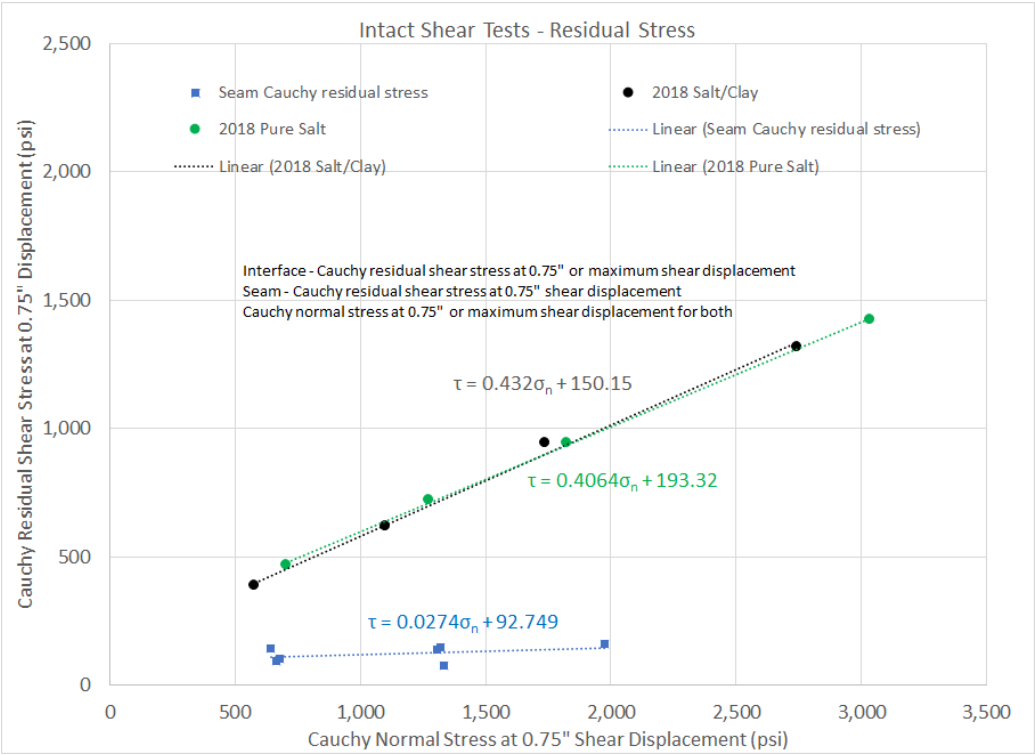

Figure 3-15. Cauchy residual/final shear stress as a function of Cauchy normal stress, halite-salt interface tests and artificial seam tests.

A first attempt at a clay seam constitutive model would likely ignore the intact peak stress and focus on capturing the residual strength using a Mohr-Coulomb model for two reasons. First, the intact peak stress may only be relevant as a room is being excavated. The clay seams near a room will likely develop cracks during excavation, and the remainder of the room closure period will involve crack propagation and sliding along the clay seam. It could be worth trying to incorporate crack propagation, which generally requires less stress than initiation, into a model, but we have not quantified the propagation behavior. Accordingly, it is prudent to assume the propagation strength is equal to the residual strength to begin with. Second, there may be a shear rate dependence on the behavior of clay seams in shear, similar to that found by Minkley and Mühlbauer (2007) on salt/ carnallitite. It is thought that the creeping of salt around rooms at WIPP will induce a shear velocity $\dot{\delta}$ on the seams much lower than that performed during the experiments herein, so that a shear response more like the bottom graph in Figure 1-3 would occur.

4. CONCLUSIONS

Eight samples of salt with artificial clay seams of two different thicknesses were subjected to displacement-controlled direct shear tests at three different normal loads. The tests ran according to procedure, and both maximum shear strength and final shear strength were determined for each test. The test results were similar in that a peak stress was achieved at which the seam broke, and the shear stress lowered through continual shearing. Although none of the tests achieved a true residual stress plateau, the final shear stresses reasonably conformed to Mohr-Coulomb behavior. The Mohr-Coulomb parameters were similar to those of a highly consolidated, saturated, clay, which is to say they were quite low.

These artificial clay seam results and previous direct shear test results on salt with diffuse clay interfaces appear to provide lower and upper bounds for the expected strength of clay seams from the WIPP site. This hypothesis will be tested if more relevant clay seams from the WIPP site (probably Clay Seams F and G) can be extracted and tested as planned. One improvement being considered for these future shear tests is reducing the shear velocity to something closer to expected in situ rates. Additionally, the need for tension tests on clay seams has been recognized, and discussions are underway on how to perform such tests.

REFERENCES

Brady, B.H.G., & Brown, E.T., 2006. Rock Mechanics for Underground Mining, Springer, The Netherlands.

Buchholz, S.A., 2019. Technical Letter Memorandum RSI/TLM-190, Direct Shear Testing of Bedded Interfaces and Clay Seams, RESPEC, Rapid City, South Dakota, January 11, 2019.

Hansen, F.D., Sobolik S.R., & Stauffer, P., 2016a. Intermediate Scale Testing Recommendation Report, FCRD-UFD-2016- 000030 Rev. 0, SAND2016-9041R, Sandia National Laboratories, Albuquerque, NM.

Hansen, F.D., Steininger, W., & Bollingerfehr W., 2016b. Proceedings of the 6th US/German Workshop on Salt Repository Research, Design, and Operation. FCRD-UFRD-2016-00069. SAND2016-0194R, Dresden, Germany, Sept. 2015. Sandia National Laboratories, Albuquerque, NM.

Hansen, F.D., Steininger, W., & Bollingerfehr, W., 2017. Proceedings of the 7th US/German Workshop on Salt Repository Research, Design, and Operation, SFWD-SFWST-2017-000008. SAND2017-1057R, Arlington, VA, Sept. 2016, Sandia National Laboratories, Albuquerque, NM.

Holt, R.M., and Powers, D.W., 2011. Synsedimentary dissolution pipes and the isolation of ancient bacteria and cellulose, Geological Society of America Bulletin, published online on 11 February 2011 as doi:10.1130/B30197.1.

Keffeler, E.D., 2020. Technical Letter Memorandum RSI/TLM-191, Direct Shear Testing of Artificial Clay Seams, RESPEC, Rapid City, South Dakota, July 15, 2020?.

Lüdeling, C., Salzer, K., Günther, R. -M., Hampel, A., Yildirim, S., Staudtmeister, K., Gährken, A., Stahlmann, J., Herchen, K., Lux, K.-H., Reedlunn, B., Sobolik, S., Hansen, F.D. & Buchholz, S.A. (2018). WEIMOS: Joint Project on further development and qualification of the rock mechanical modeling for the final HLW disposal in rock salt. Overview and first results on tensile stress modeling. Proceedings of the 9th Conference on the Mechanical Behavior of Salt (Saltmech IX), 12-14 Sept. 2018, Hannover, Germany. Eds.: S. Fahland, J. Hammer, F.D. Hansen, S. Heusermann, K.-H. Lux & W. Minkley, published by BGR Hannover, ISBN 978-3-9814108-6-0, pp. 459-477.

Minkley, W. & M Mühlbauer, J., 2007. Constitutive Models to Describe the Mechanical Behavior of Salt Rocks and the Imbedded Weakened Planes. Wallner, M., K-H Lux, W. Minkley, H.R. Hardy, eds. The Mechanical Behavior of Salt: Understanding of THMC Processes in Salt. Taylor & Francis/Balkema, Leiden, The Netherlands.

Munson, D.E. & Matalucci, R.V., 1983. Planning, Developing, and Fielding of Thermal/Structural Interactions in situ Tests for the Waste Isolation Pilot Plant (WIPP). SAND83-2048. Sandia National Laboratories, Albuquerque NM.

Reedlunn, B. (2016). Reinvestigation into Closure Predictions of Room D at the Waste Isolation Pilot Plant. Tech. rep. SAND2016-9961. Albuquerque, NM, USA: Sandia National Laboratories. doi: 10.2172/1333709.

Reedlunn, B. (2017). Geomechanical Simulations of an Empty WIPP Disposal Room using Explicit Dynamics and Time-Temperature Scaling. Memorandum. SAND2017-13593, Sandia National Laboratories.

Reedlunn, B. (2018). "Joint Project III on the Comparison of Constitutive Models for the Mechanical Behavior of Rock Salt: Reinvestigation into Isothermal Room Closure Predictions at the Waste Isolation Pilot Plant". In: The Mechanical Behavior of Salt IX. Ed. By S. Fahland, J. Hammer, F. D. H. Hansen, S. Heusermann, K.-H. Lux, and W. Minkley. BGR (Federal Institute for Geosciences and Natural Resources). isbn: 978-3-9814108-6-0.

Reedlunn, B. and Bean, J. (2019). Simulations of Pipe Overpack Container Compaction at the Waste Isolation Pilot Plant. Tech. rep. SAND2019-12111. Sandia National Laboratories. doi: 10.2172/1570309.

Reedlunn, B., Bean, J., Wilkes, J., and Bignell, J. (2019). Simulations of Criticality Control Overpack Container Compaction at the Waste Isolation Pilot Plant. Tech. rep. SAND2019-3106, Sandia National Laboratories.

Reedlunn, B. and Bean, J. (2020). Impact of Properly Specifying the Clay F and Clay G Friction Coefficients in Disposal Room Closure Simulations at the Waste Isolation Pilot Plant, Sandia Letter SAND2020-3575, Sandia National Laboratories.

Sobolik, S., 2019. Experimental Investigation of WIPP Salt Samples and Clay Seams. Test Plan TP 17-03, Rev. 1.

Sobolik, S.R., S.A. Buchholz, E. Keffeler, S. Borglum, & B. Reedlunn, 2019. Shear Behavior of Bedded Salt Interfaces and Clay Seams. In Proceedings of the 53rd U.S. Rock Mechanics Symposium, ARMA 19-040, New York, New York, June 23-26, 2019.

Sobolik, S.R., & B. Reedlunn, 2019. Shear Behavior of Bedded Salt Interfaces under Direct Shear Loading. SAND2019-11843. Sandia National Laboratories, Albuquerque NM.

Appendix A: Technical Letter Memorandum RSI/TLM-191, Direct Shear Testing of Artificial Clay Seams RESPEC, Rapid City, South Dakota, July 15, 2020

DRAFT TECHNICAL LETTER MEMORANDUM RSI/TLM-191

To: Mr. Steven R. Sobolik
Sandia National Laboratories
Mail Stop 0751
P.O. Box 5800
Albuquerque, NM 87185-0771

cc: Project Central File 3197 — Category A

From: Dr. Evan R. Keffeler
Testing Specialist, Materials Testing Laboratory
RESPEC
P.O. Box 725
Rapid City, SD 57709

Date: June 29, 2020

Subject: Direct Shear Testing of Artificial Clay Seams

INTRODUCTION

Sandia National Laboratories (SNL) is tasked with modeling the long-term future behavior of the Waste Isolation Pilot Plant (WIPP). A shortcoming that hinders the accuracy of the geotechnical analyses is a lack of publicly available shear strength and deformation properties for geologic contacts and clay seams in bedded salt formations. In 2018, SNL commissioned RESPEC to obtain representative core samples from a potash mine near WIPP and perform direct shear tests on the geologic contacts and clay seams in those samples. RESPEC collected 12-inch-diameter core samples from the rib of a decline in the potash mine. The natural clay seams and geologic contacts that were recovered from the potash mine had intergrown halite crystals, and the shear strengths of the interfaces were similar to that of intact salt. Consequently, these strength results are likely an upper bound of the interface shear strength in bedded salt deposits. The results of this first phase of direct shear testing are summarized in Buchholz [2019].

To complement the results of the direct shear tests performed on clay seams and geologic contacts recovered from the potash mine, SNL and RESPEC personnel designed an experiment to establish a plausible lower bound of the shear strengths of clay seams at WIPP. This experiment and its results are documented in this Technical Letter Memorandum (TLM).

The experiment consisted of fabricating consolidated clay seams within salt (predominately halite) and performing direct shear tests on those clay seams. The direct shear tests were performed in a manner that allowed for the following properties to be measured:

3824 JET DRIVE
RAPID CITY, SD 57703
P.O. BOX 725 // RAPID CITY, SD 57709
605.394.6400

respec.com

- Intact normal and shear stiffnesses
- Residual normal and shear stiffnesses
- Dependence of yield, ultimate, and post-peak shear strength with normal stress.

The results of the direct shear tests reported in this TLM will be used by SNL to improve the accuracy of the models that predict the long-term geomechanical behavior of the WIPP.

SPECIMEN PREPARATION

A total of eight artificial clay seam specimens were created. The specimen preparation method is summarized as:

1. 4-inch-diameter by approximately 3-inch-long salt cylinders were subcored from the 12-inch-diameter core obtained from the potash mine near WIPP.
2. 0.05-inch-deep grooves were machined every 0.25 inch into one face of each subcore, as shown in Figure 1.
3. Bentonite powder was mixed with saturated salt (halite) brine to a fresh-water moisture content of approximately 60 percent.
4. A ¼-inch- or ½-inch-thick layer of the bentonite-brine mix was applied to the grooved surface of a subcore. A second subcore was placed onto the bentonite-brine mix with the grooved surface facing the bentonite-brine mix. This assembly constituted an unconsolidated test specimen.
5. The unconsolidated test specimen was wrapped in filter fabric and placed into a consolidation vessel. The specimen was protected from the confining oil using neoprene jackets, and the platens were vented to the atmosphere.
6. The test specimen was consolidated under an isostatic stress of 3,000 pounds per square inch (psi) (nominal) at 21 degrees Celsius (°C) for 14 days. Excess pore fluid from the bentonite mixture was expelled through the vents.
7. The consolidated test specimen was removed from the consolidation vessel, and the diameter of the clay seam was measured.
8. The consolidated test specimens were coated in clear acrylic to protect them from the encapsulation grout used in the shear boxes.
9. The test specimens were photographed. An example photograph of a consolidated specimen is provided in Figure 2.

Four of the specimens had preconsolidation seam thicknesses of ½ inch, and the remaining four had preconsolidation seam thicknesses of ¼ inch. The postconsolidation seam thicknesses were approximately $^{7}/_{16}$ inch and $^{3}/_{16}$ inch for the ¼- and ½-inch preconsolidation seam thicknesses, respectively. Specimen seam diameters are listed in Table 1, and postconsolidation photographs are provided in Attachment A.

TESTING METHOD

DIRECT SHEAR TESTING MACHINE

The tests were performed using a rock direct shear testing machine designed and fabricated by RESPEC, which is shown in Figure 3. The machine consists of shear boxes (that hold the test specimen), a normal load ram, a shear load ram, and hydraulic controls. The shear load ram is controlled by a mechanical-over-hydraulic intensifier that advances the shear load ram at a set displacement rate. The normal load ram is controlled by a pressure regulator that maintains the normal load within 1 percent of the set point. The test specimen is encapsulated into the shear boxes using quick-setting, high-strength grout.

Figure 1. Grooves Were Machined Into One Face of Each 4-Inch-Diameter Salt Subcore.

Figure 2. Photograph of Consolidated Test Specimen.

Table 1. Consolidated Test Specimen Seam Diameters

Specimen I.D.	Preconsolidation Seam Thickness (inches)	Postconsolidation Seam Thickness (inches)	Preconsolidation Average Seam Diameter (inches)	Postconsolidation Average Seam Diameter (inches)
Carlsbad/Art-Seam/1A-1B	¼	1/16	4.00	3.95
Carlsbad/Art-Seam/2A-2B	¼	1/16	4.00	3.91
Carlsbad/Art-Seam/3A-3B	½	3/16	4.00	3.90
Carlsbad/Art-Seam/4A-4B	½	3/16	4.00	3.85
Carlsbad/Art-Seam/5A-5B	½	3/16	4.00	3.91
Carlsbad/Art-Seam/6A-6B	¼	1/16	4.00	3.96
Carlsbad/Art-Seam/7A-7B	½	3/16	4.00	3.87
Carlsbad/Art-Seam/8A-8B	¼	1/16	4.00	4.05

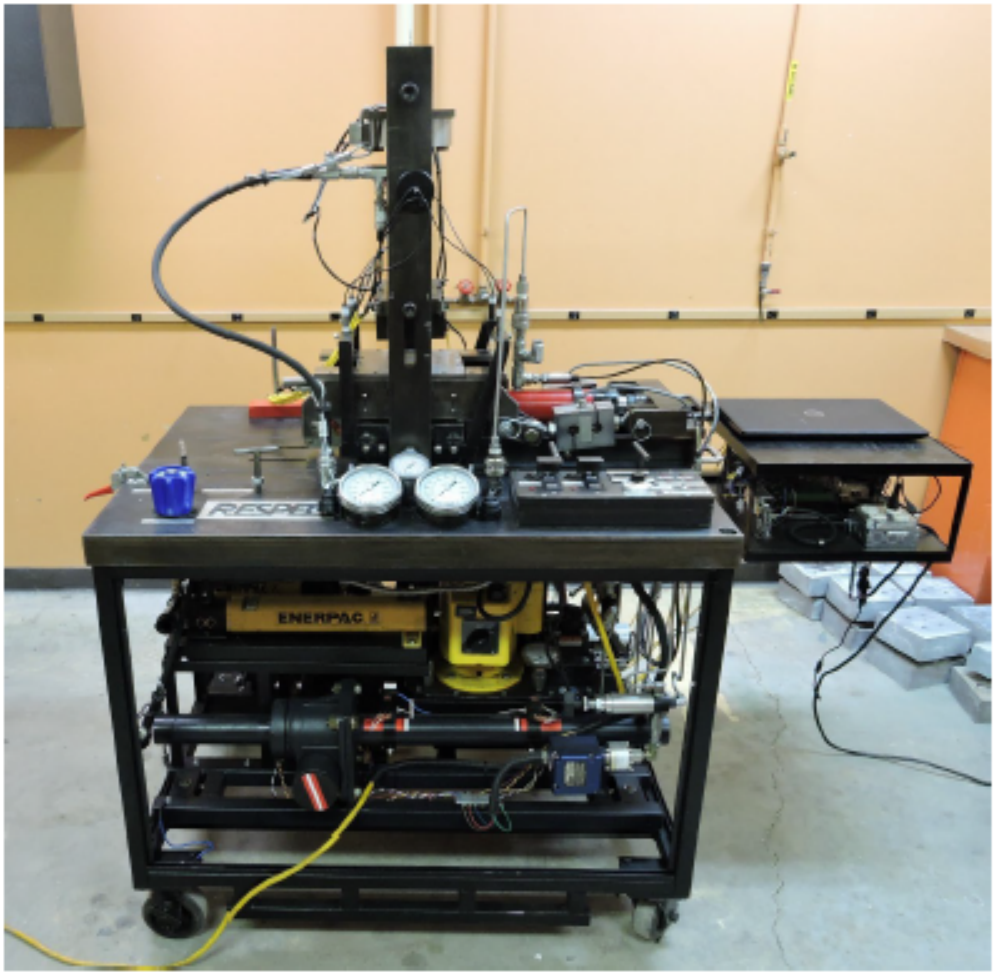

Figure 3. RESPEC Direct Shear Testing Machine.

Normal load is applied to the shear boxes through a roller contact and spherical seat. Shear load is applied to the shear box through pinned connections, and the shear load ram is vertically aligned with the center of the gap between the shear boxes. The machine has force capacities of 30,000 pounds in the normal and shear directions, and force is measured using load cells. Normal displacement is monitored using four precision linear potentiometers, and shear displacement is measured using a linear variable displacement transformer (LVDT). Displacements are measured between the shear boxes, thereby reducing error.

DIRECT SHEAR TESTING METHOD

The direct shear testing method is summarized as:

- Encapsulate consolidated test specimen into the shear boxes using fast-setting grout while leaving a ½-inch gap between the boxes.
- Allow grout to cure overnight.
- Mount the shear boxes into the direct shear testing machine.
- Set up shear and normal displacement transducers.
- Initial normal loading:
  - Bring normal ram into contact with the upper shear box.
  - Increase normal load to the target value.
  - Reduce normal load to approximately 600 pounds.
  - Increase normal load to the target value (i.e., an unload/reload cycle).
  - Hold normal load constant for approximately 10 minutes to allow normal displacement to stabilize.
- Shear loading:
  - Apply shear load by advancing the shear ram at a rate of 0.01 inch per minute.
  - When the shear load is approximately 20 percent of the normal load, reduce the shear load to approximately 250 pounds by retracting the shear ram at 0.01 inch per minute.
  - Reapply shear load by advancing the shear ram at 0.01 inch per minute (i.e., an unload/reload cycle).
  - Once a residual shear strength has been established or shear displacement equals 0.8 inch (whichever is achieved first), reduce shear load to approximately 250 pounds by retracting the shear ram at 0.01 inch per minute.
  - Reapply shear load by advancing the shear ram at 0.01 inch per minute until the shear plane slips (i.e., an unload/reload cycle).
  - Remove the shear load by retracting the shear ram at 0.01 inch per minute.
- Posttest normal loading:
  - Reduce the normal load to approximately 600 pounds.
  - Increase the normal load to the value at which the test was performed (i.e., an unload/reload cycle).
  - Remove the normal load.

If the test specimen was still in testable condition, the shear boxes were reset to their original position and the shear testing procedure was repeated. Once the shear specimen could no longer be tested, the shear boxes were removed from the testing machine and separated. Debris was removed and posttest photographs were taken of the sheared surfaces.

DATA ANALYSIS METHODS

The data from each test were analyzed to determine the following:

- Pretest normal stiffness (psi per inch [psi/inch])
- Pretest shear stiffness (psi/inch)

- Peak shear strength (psi)
- Shear strength at 0.75 inch of shear displacement (psi)
- Posttest shear stiffness (psi/inch)
- Posttest normal stiffness (psi/inch).

Nominal stresses were used throughout the calculations. Nominal stresses are calculated using the original shear area of the specimens (i.e., change in area during the test is not accounted for). An example plot of normal stress versus normal displacement for a normal unload/reload cycle is shown in Figure 4. Joint stiffness is defined as the slope of the stress-displacement curve. Normal stiffness was calculated from the slope of a line fit to the normal stress reload curve; because many of the normal reloads were noticeably nonlinear, the line was fit between 40 percent and 100 percent of the target normal stress to ensure consistency between tests. An example shear-reloading plot is shown in Figure 5. Shear stiffness was calculated from the slope of a line fit to the linear portion of the shear stress reload curve.

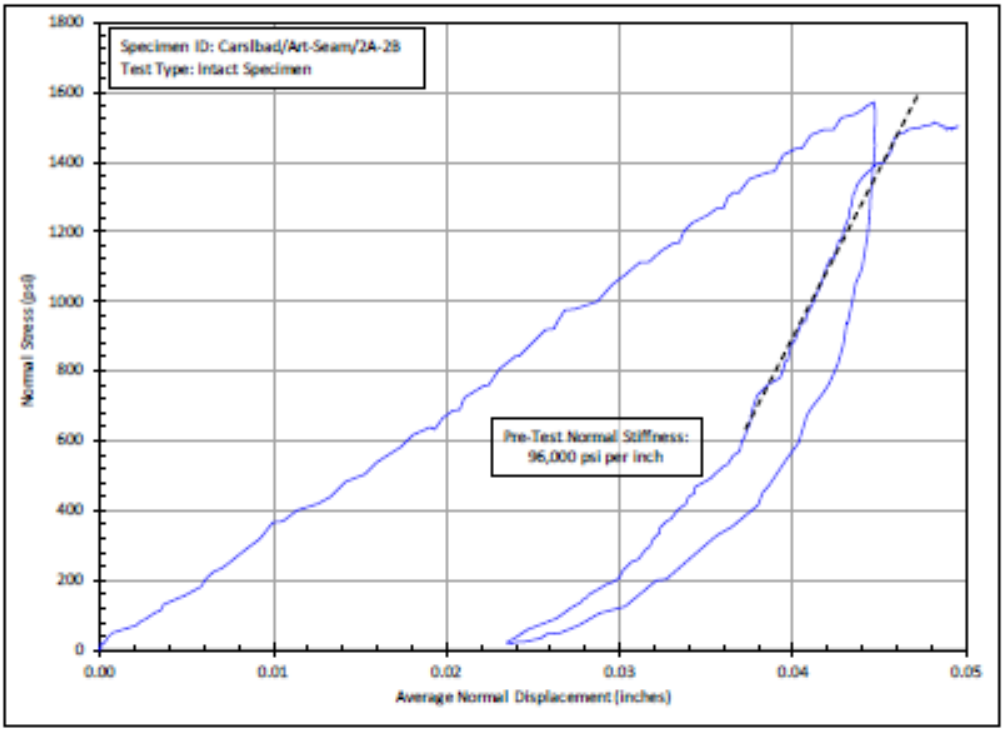

Figure 4. Example Normal Stress Versus Normal Displacement Plot Used to Calculate Normal Stiffness.

An example shear displacement plot is shown in Figure 6. The peak shear strength was defined as the maximum nominal shear stress recorded during the test. A residual was not established within 0.8 inch of shear displacement for any of the tests. Consequently, the shear stress at 0.75 inch was used as a means to compare post-peak strengths between the specimens.

RESULTS

A summary of the results of the direct shear tests on the artificial clay seams is provided in this section. Posttest photographs of the shear surfaces are provided in Attachment A, and plots of the test data are provided in Attachment B. The strength results are summarized in Table 2, and the intact peak strength

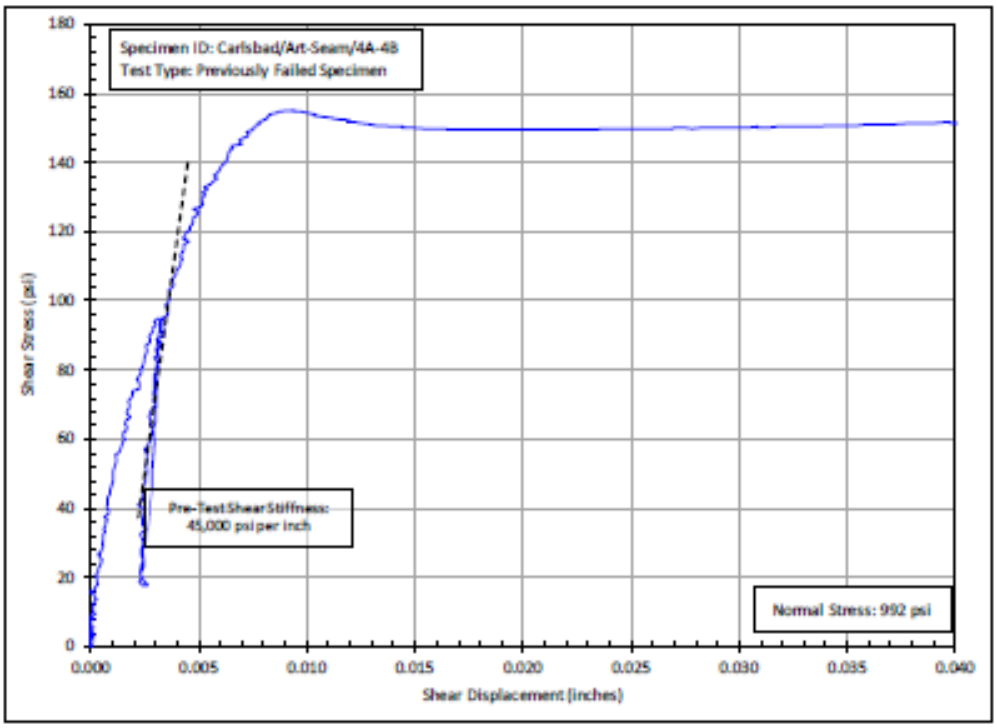

Figure 5. Example Shear Stress Versus Shear Displacement Plot Used to Calculate Shear Stiffness.

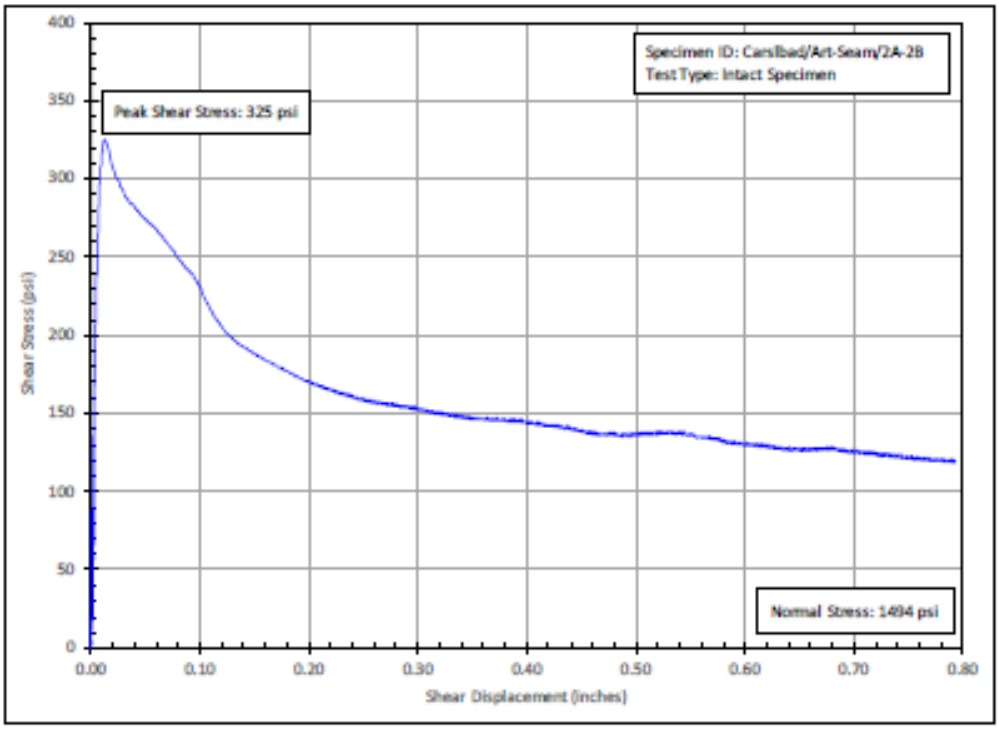

Figure 6. Example Shear Stress-Displacement Plot for a Direct Shear Test on an Intact Specimen.

results are plotted in Figure 7 along with a Mohr-Coulomb shear-strength criterion fit. The Mohr-Coulomb shear-strength criterion is defined as:

$$\tau = \sigma_n \tan\varphi + C \quad (1)$$

where:

τ = shear stress at failure

σ_n = normal stress on shear surface

φ = friction angle

C = cohesion.

The Mohr-Coulomb strength criterion parameters are determined by fitting a line to the shear-strength versus normal-stress data. The cohesion is equal to the intercept, the slope is the coefficient of friction, and the arctangent of the slope is the friction angle.

Table 2. Direct Shear Testing Strength Results

Specimen I.D.	Specimen Type	Seam Thickness Before Consolidation (inch)	Nominal Normal Stress (psi)	Nominal Peak Shear Stress (psi)	Nominal Shear Stress at 0.75 Inch Displacement (psi)
Carlsbad/Art-Seam/1A-1B	Intact	¼	504	140	72
Carlsbad/Art-Seam/1A-1B	Previously Failed	¼	1004	133	93
Carlsbad/Art-Seam/2A-2B	Intact	¼	1,494	325	122
Carlsbad/Art-Seam/3A-3B	Intact	½	1,000	215	58
Carlsbad/Art-Seam/4A-4B	Intact	½	507	277	79
Carlsbad/Art-Seam/4A-4B	Previously Failed	½	992	158	118
Carlsbad/Art-Seam/5A-5B	Intact	½	1,487	427	110
Carlsbad/Art-Seam/6A-6B	Intact	¼	992	282	105
Carlsbad/Art-Seam/6A-6B	Previously Failed	¼	1,501	192	118
Carlsbad/Art-Seam/7A-7B	Intact	½	990	239	111
Carlsbad/Art-Seam/8A-8B	Intact	¼	496	234	111
Carlsbad/Art-Seam/8A-8B	Previously Failed	¼	990	211	156

The intact specimen peak shear strengths were similar regardless of preconsolidation seam thickness. For the peak strength of the intact specimens, the friction angle is 9 degrees (coefficient of friction of 0.16) and cohesion is 125 psi.

In Figure 8, the following are plotted versus normal stress:

- Peak shear stress attained for previously tested specimens
- Shear stress at 0.75-inch shear displacement for tests on intact specimens
- Shear stress at 0.75-inch shear displacement for tests on previously tested specimens.

Figure 8 also shows a Mohr-Coulomb strength fit to the shear stresses at 0.75-inch shear displacement for all samples. The friction angle for this fit is 2 degrees (coefficient of friction of 0.03) and cohesion is 75 psi. The near-zero friction angle is consistent with the expected residual shear-strength behavior of highly plastic clays.

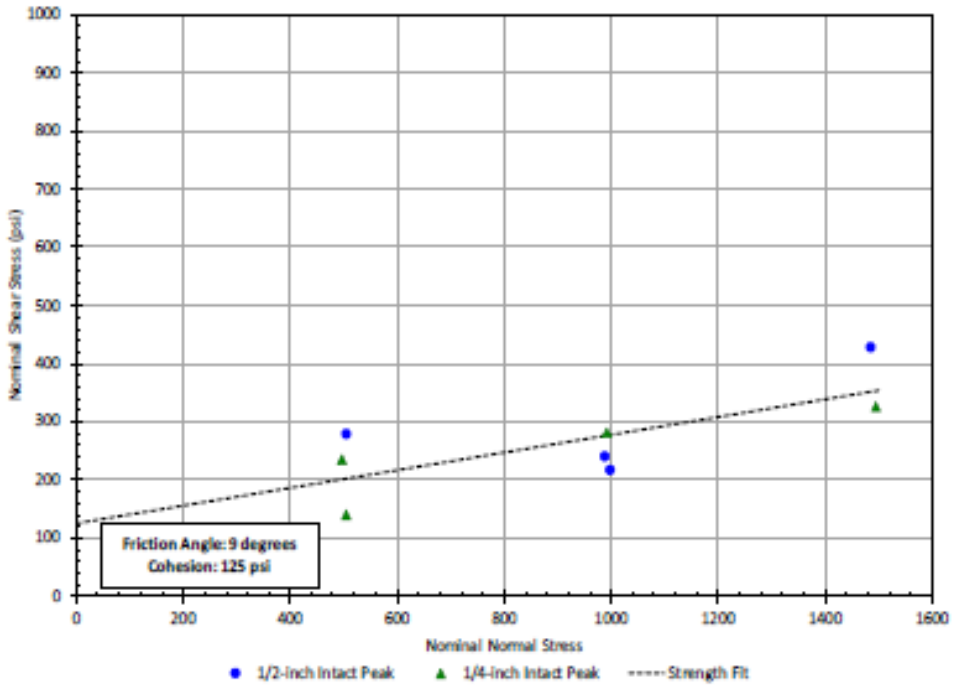

Figure 7. Plot of Peak Shear Stress Versus Normal Stress for Intact Specimens.

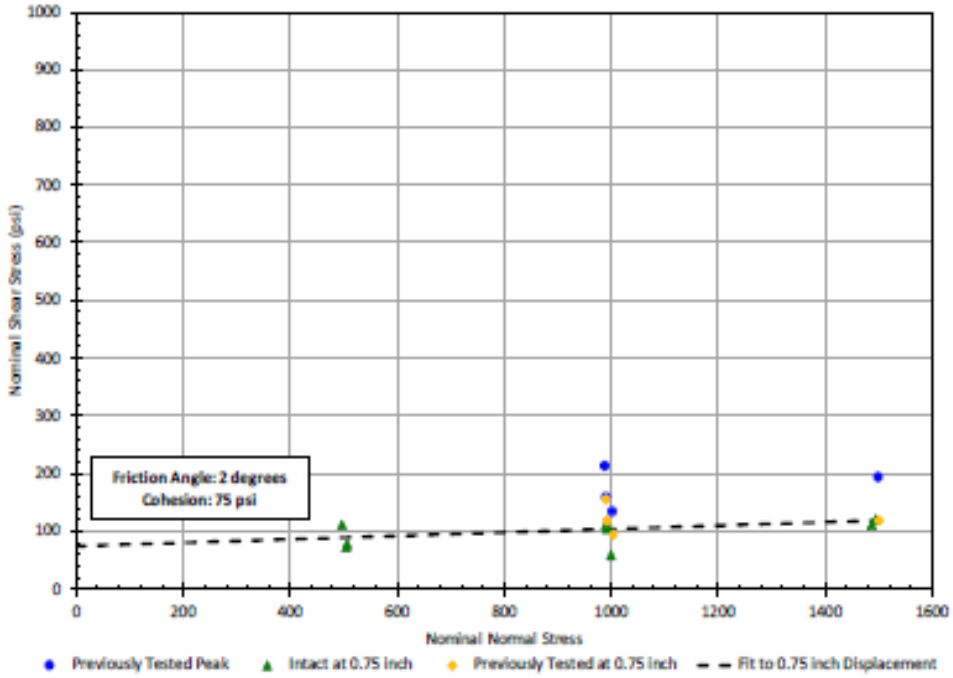

Figure 8. Plot of Peak Shear Strength for Previously Tested Specimens and Shear Strength for All Specimens at 0.75 Inch of Shear Displacement.

The stiffness values from each direct shear test are summarized in Table 3. Stiffness values are in the range of tens of thousands to hundreds of thousands of psi/inch. Normal stiffness tends to increase with normal stress, but shear stiffness does not correlate with normal stress. Posttest stiffness values tend to be greater than pretest stiffness values; whether this phenomenon results from increased consolidation of the clay seams during the tests or is an artifact of the measurement system is not known.

Table 3. Direct Shear Testing Stiffness Results

Specimen I.D.	Specimen Type	Nominal Normal Stress (psi)	Pretest Normal Stiffness (psi/inch)	Pretest Shear Stiffness (psi/inch)	Posttest Normal Stiffness (psi/inch)	Posttest Shear Stiffness (psi/inch)
Carlsbad/Art-Seam/1A-1B	Intact	504	61,000	—	86,000	—
Carlsbad/Art-Seam/1A-1B	Previously Failed	1,004	82,000	—	81,000	—
Carlsbad/Art-Seam/2A-2B	Intact	1,494	96,000	99,000	128,000	311,000
Carlsbad/Art-Seam/3A-3B	Intact	1,000	76,000	81,000	172,000	58,000
Carlsbad/Art-Seam/4A-4B	Intact	507	67,000	33,000	66,000	64,000
Carlsbad/Art-Seam/4A-4B	Previously Failed	992	68,000	45,000	82,000	79,000
Carlsbad/Art-Seam/5A-5B	Intact	1,487	107,000	81,000	135,000	134,000
Carlsbad/Art-Seam/6A-6B	Intact	992	89,000	29,000	89,000	75,000
Carlsbad/Art-Seam/6A-6B	Previously Failed	1,501	108,000	57,000	128,000	146,000
Carlsbad/Art-Seam/7A-7B	Intact	990	77,000	70,000	114,000	110,000
Carlsbad/Art-Seam/8A-8B	Intact	496	50,000	32,000	83,000	75,000
Carlsbad/Art-Seam/8A-8B	Previously Failed	990	89,000	72,000	107,000	110,000

An example posttest photograph of the shear surfaces is provided in Figure 9. The shear surfaces were striated, and the clay was hard for all tests. Moisture content analyses were performed on the clay seams after the direct shear tests were completed, and the results are summarized in Table 4. The fresh-water moisture content of the tested clays seams varied between 13 percent and 17 percent, which is approximately one-fourth of the moisture content of the unconsolidated clay seams.

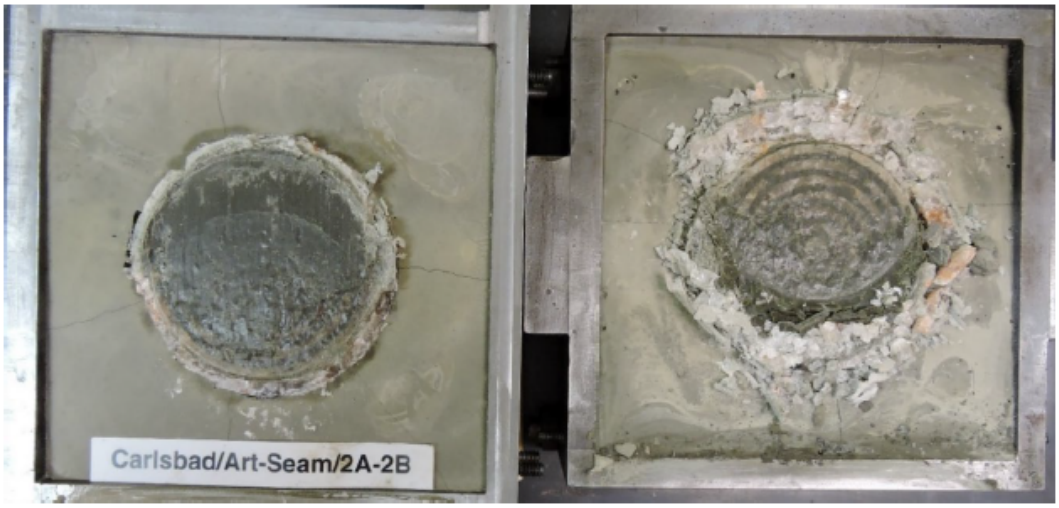

Figure 9. Posttest Photograph of Shear Surfaces for Carlsbad/Art-Seam/2A-2B.

Table 4. Moisture Contents of Tested Clay Seams

Specimen I.D.	Fresh-Water Equivalent Moisture Content (%)
Carlsbad/Art-Seam/1A-1B	16
Carlsbad/Art-Seam/2A-2B	16
Carlsbad/Art-Seam/3A-3B	17
Carlsbad/Art-Seam/4A-4B	13
Carlsbad/Art-Seam/5A-5B	14
Carlsbad/Art-Seam/6A-6B	14
Carlsbad/Art-Seam/7A-7B	15
Carlsbad/Art-Seam/8A-8B	14

SUMMARY AND CONCLUSION

This TLM summarizes the results of direct shear tests on manufactured clay seams in salt. The intent of this research was to establish a plausible lower bound for the shear strength of clay seams for geomechanical modeling of the excavations at the WIPP. The test specimens were prepared from salt (predominantly halite) recovered from a potash mine near the WIPP and a mixture of bentonite and halite brine. The specimens were consolidated at 3,000 psi for 14 days. At the end of the consolidation period, the clay seams were approximately one-fourth their original thickness and well indurated.

A Mohr-Coulomb criterion fit to the peak strength data resulted in a friction angle of 9 degrees (coefficient of friction of 0.16) and cohesion of 125 psi. Residual shear strengths were not obtained during the tests, so the shear stresses at 0.75 inch of shear displacement (approximately 20 percent relative displacement) were used a proxy for residual strength; the resulting Mohr-Coulomb criterion parameters for these strengths were a friction angle of 2 degrees (coefficient of friction of 0.03) and cohesion of 75 psi. Joint stiffness ranged from tens of thousands to hundreds of thousands of psi per inch.

REFERENCES

Buchholz, S. A., 2019. *Direct Shear Testing of Bedded Interfaces and Clay Seams (RFQ #973665),* RSI/TLM-190, prepared by RESPEC, Rapid City, SD, for Sandia National Laboratories, Albuquerque, NM, January 11.

ERK:lif

ATTACHMENT A

PRE- AND POSTTEST PHOTOGRAPHS OF TEST SPECIMENS

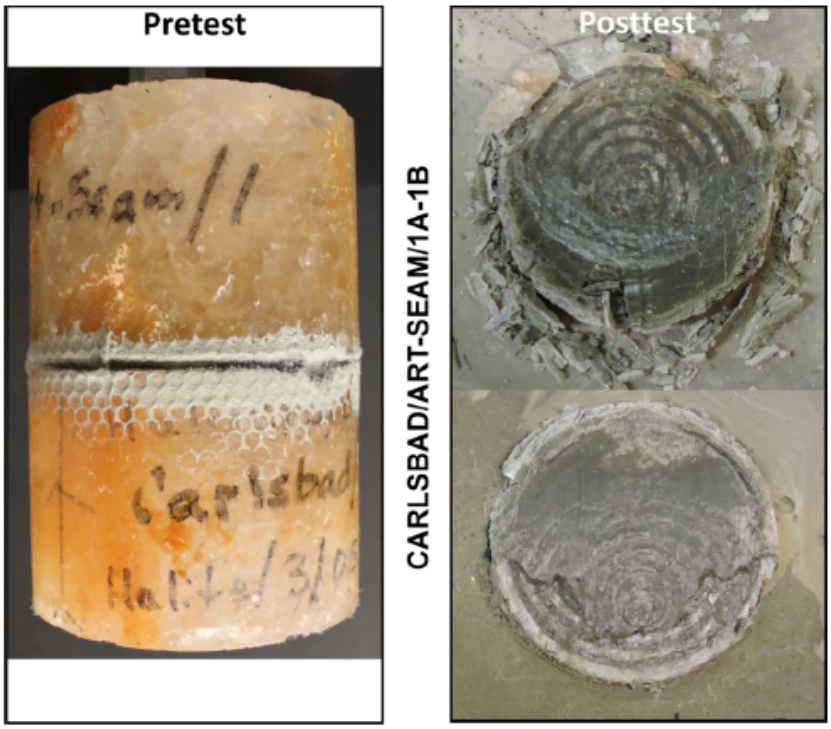

Figure A-1. Pre- and Posttest Photographs of Test Specimen Carlsbad/Art-Seam/1A-1B.

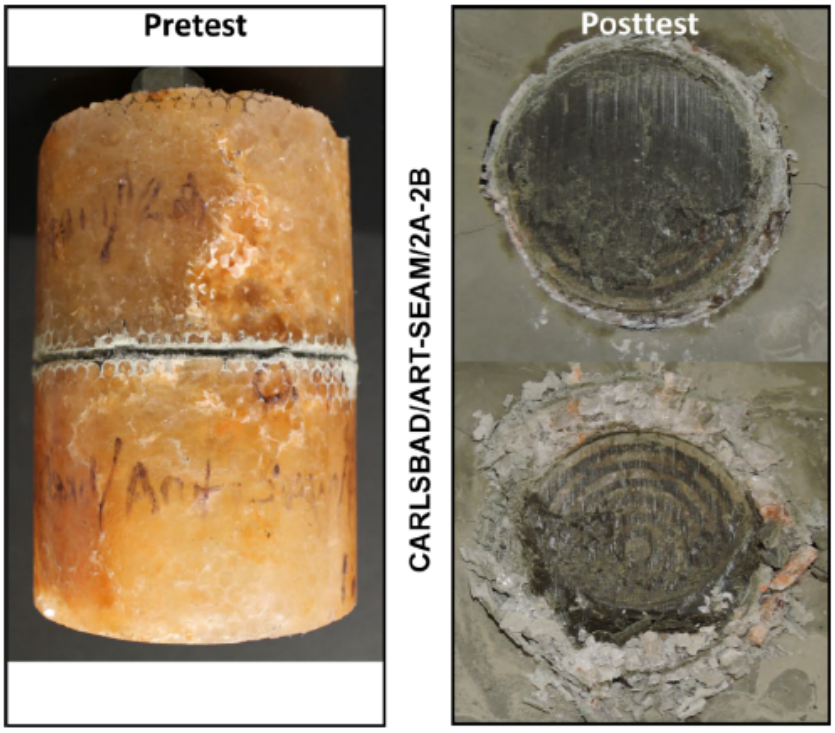

Figure A-2. Pre- and Posttest Photographs of Test Specimen Carlsbad/Art-Seam/2A-2B.

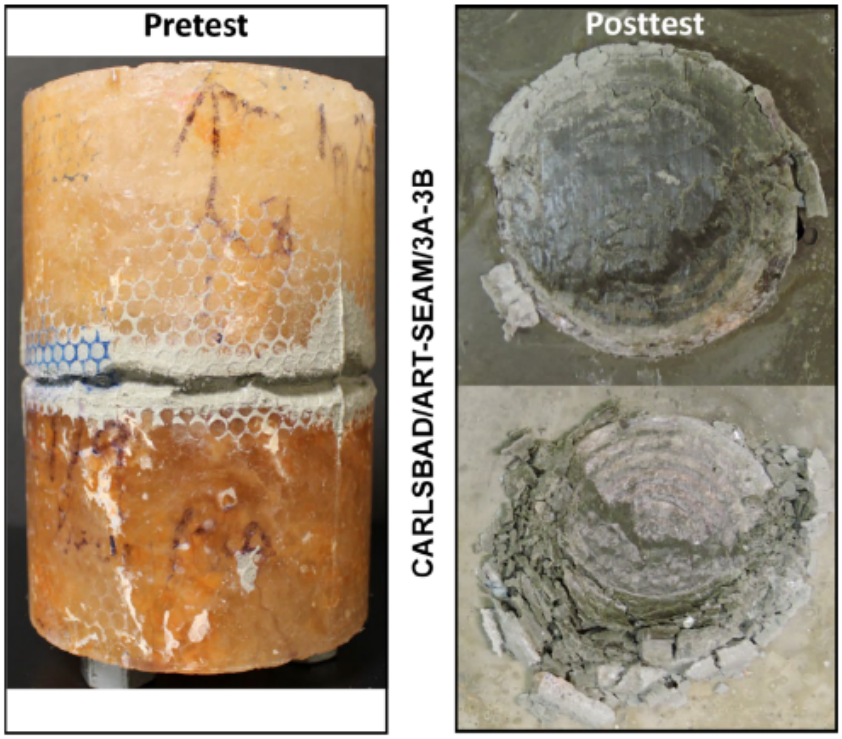

Figure A-3. Pre- and Posttest Photographs of Test Specimen Carlsbad/Art-Seam/3A-3B.

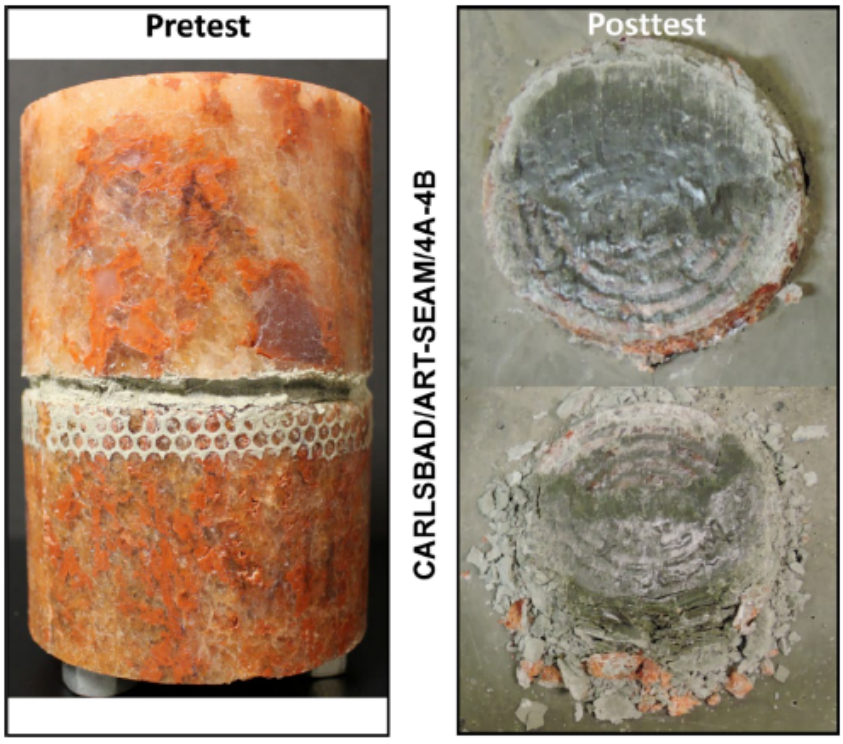

Figure A-4. Pre- and Posttest Photographs of Test Specimen Carlsbad/Art-Seam/4A-4B.

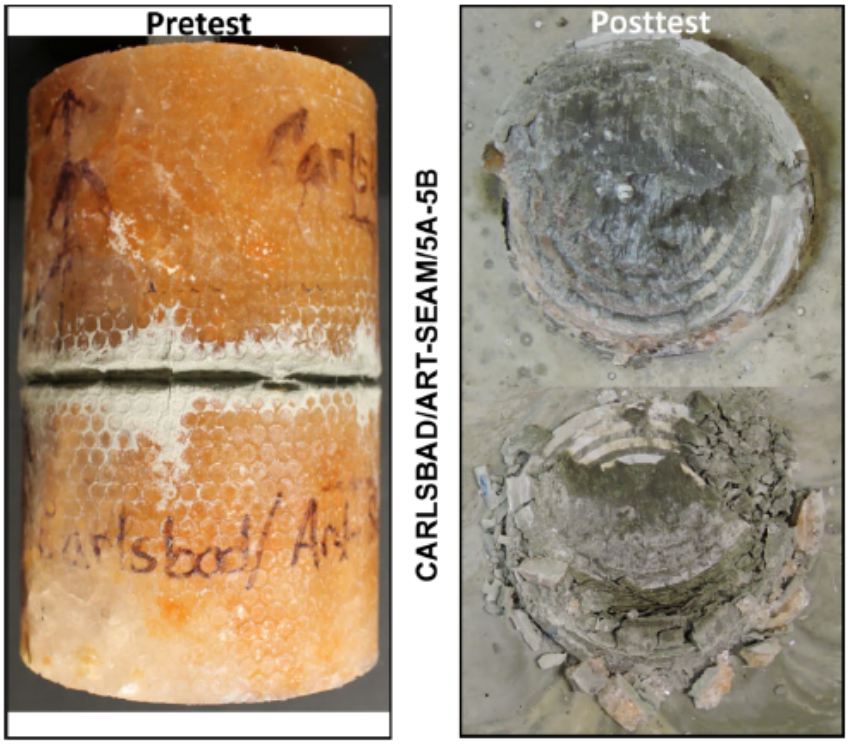

Figure A-5. Pre- and Posttest Photographs of Test Specimen Carlsbad/Art-Seam/5A-5B.

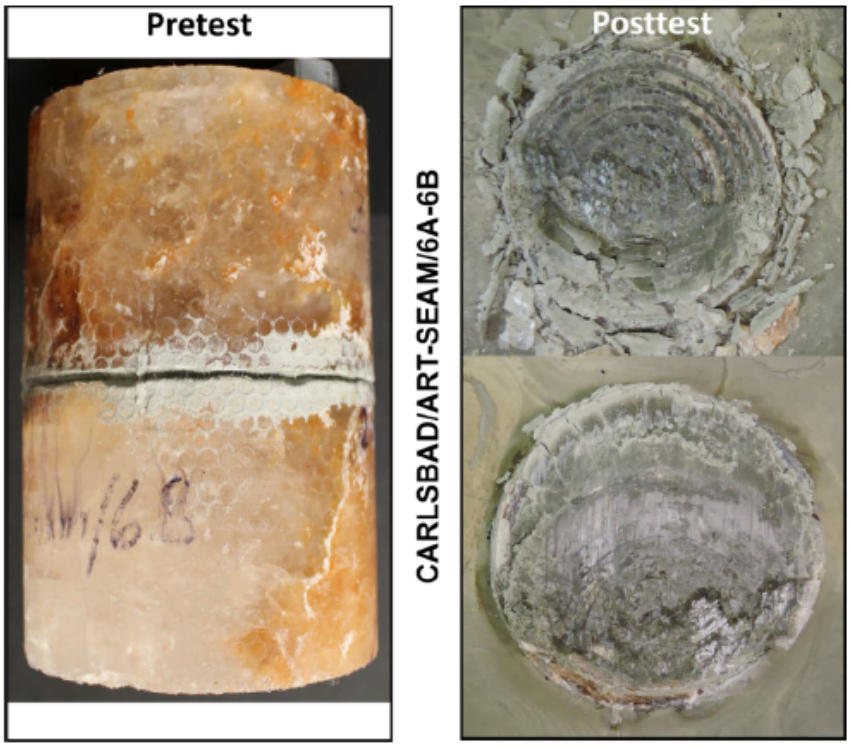

Figure A-6. Pre- and Posttest Photographs of Test Specimen Carlsbad/Art-Seam/6A-6B.

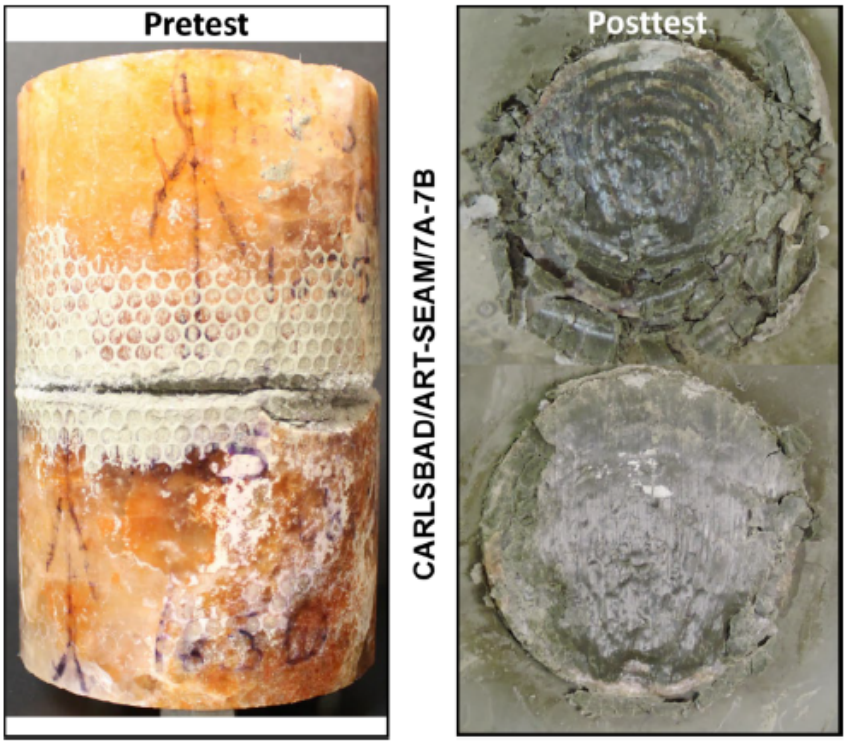

Figure A-7. Pre- and Posttest Photographs of Test Specimen Carlsbad/Art-Seam/7A-7B.

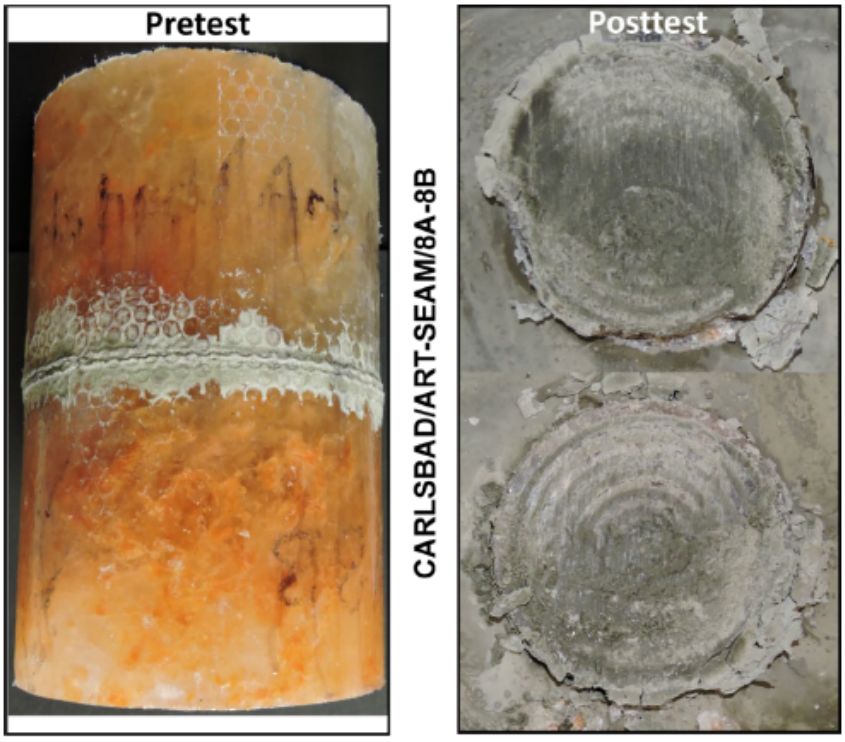

Figure A-8. Pre- and Posttest Photographs of Test Specimen Carlsbad/Art-Seam/8A-8B.

ATTACHMENT B

PLOTS OF TEST RESULTS

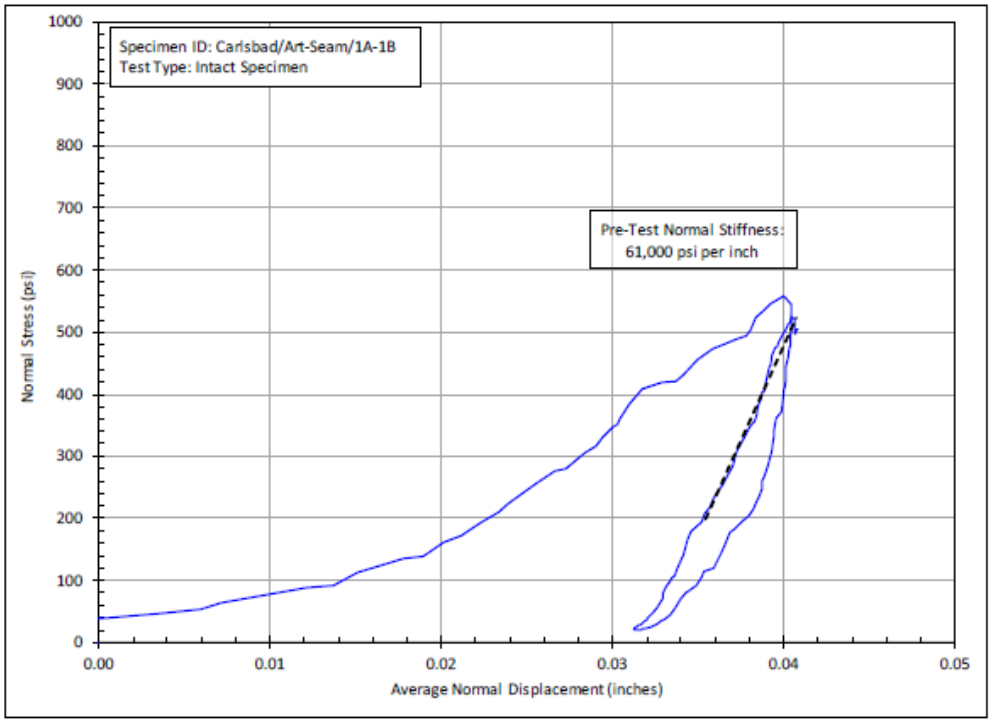

Figure B-1. Pretest Normal Stiffness Fit for Intact Specimen Carlsbad/Art-Seam/1A-1B.

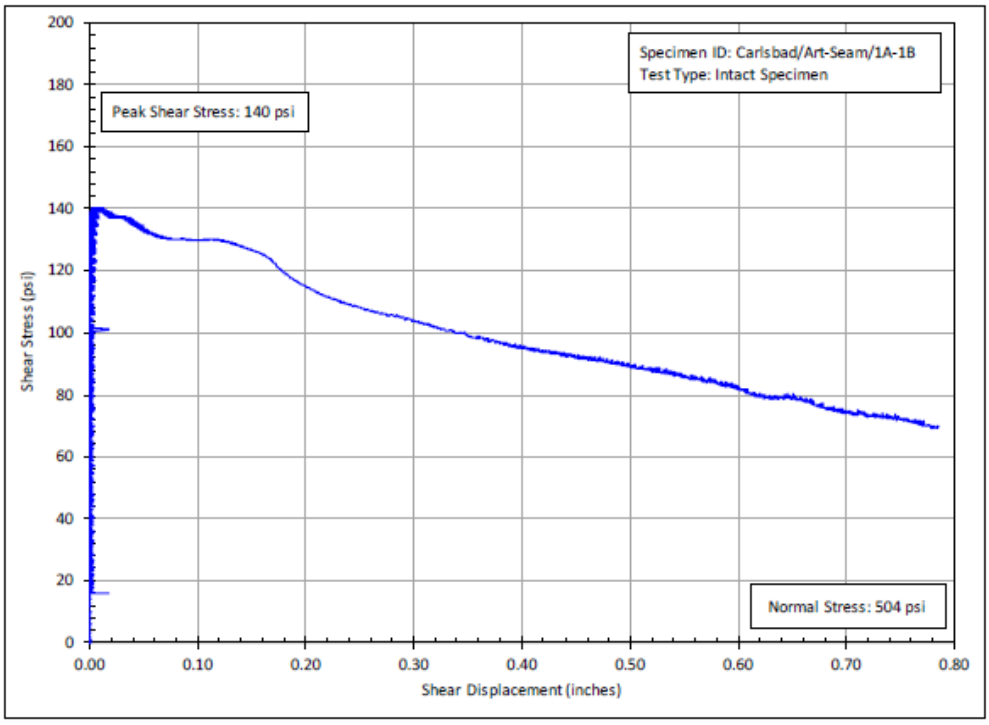

Figure B-2. Plot of Shear Stress Versus Shear Displacement for Intact Specimen Carlsbad/Art-Seam/1A-1B.

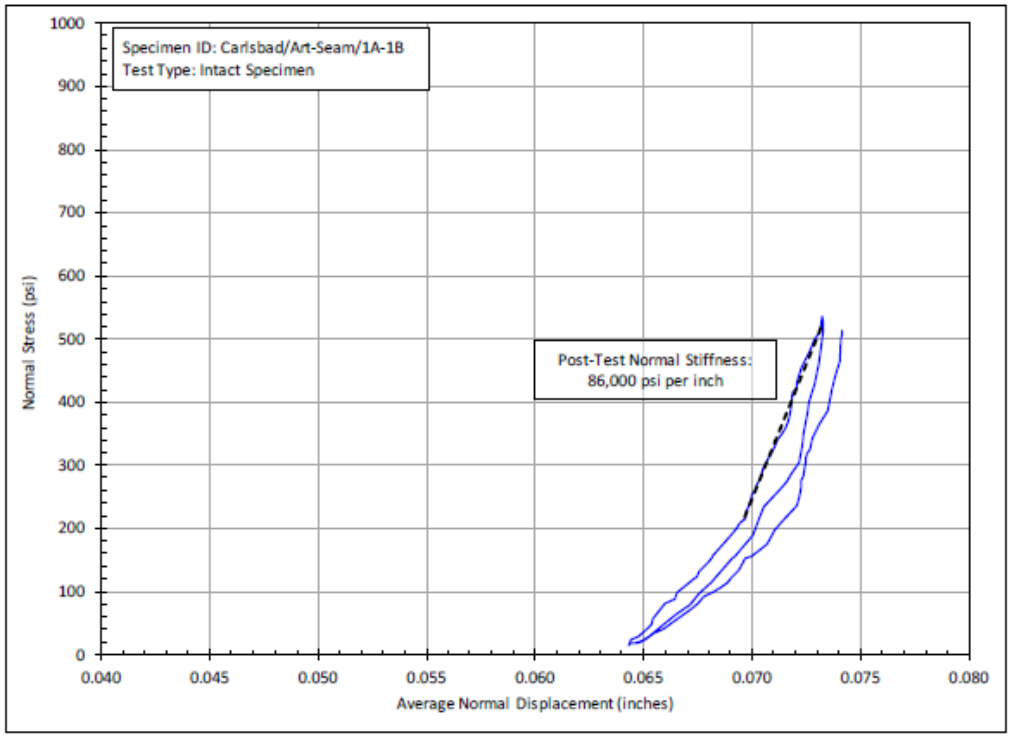

Figure B-3. Posttest Normal Stiffness Fit for Intact Specimen Carlsbad/Art-Seam/1A-1B.

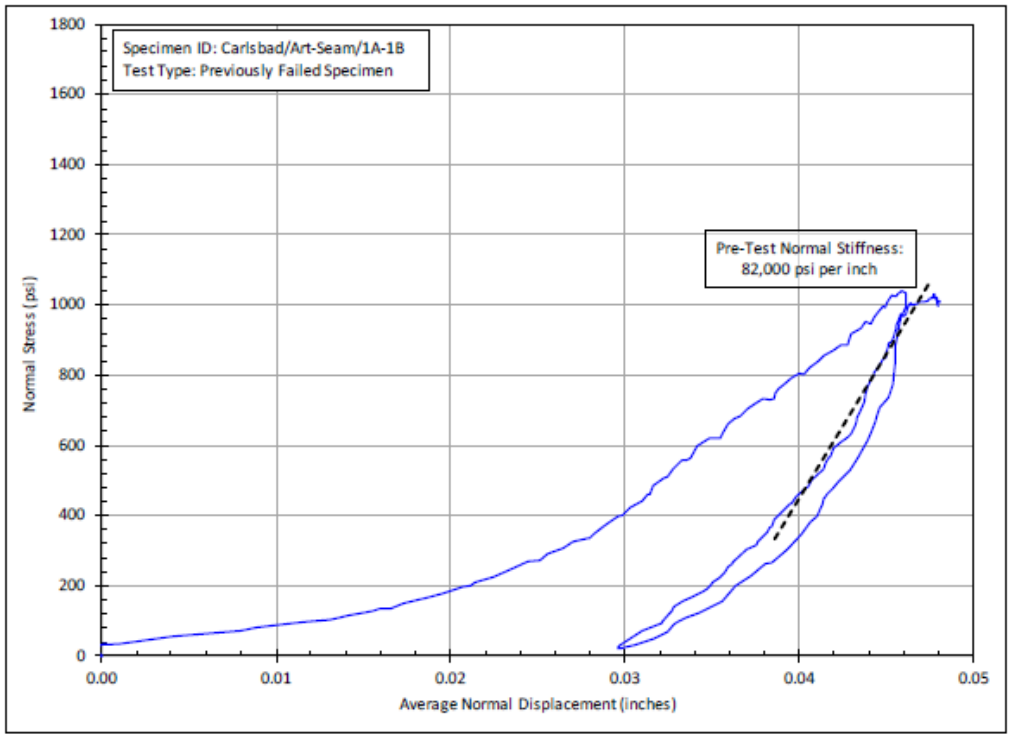

Figure B-4. Pretest Normal Stiffness Fit for Previously Tested Specimen Carlsbad/Art-Seam/1A-1B.

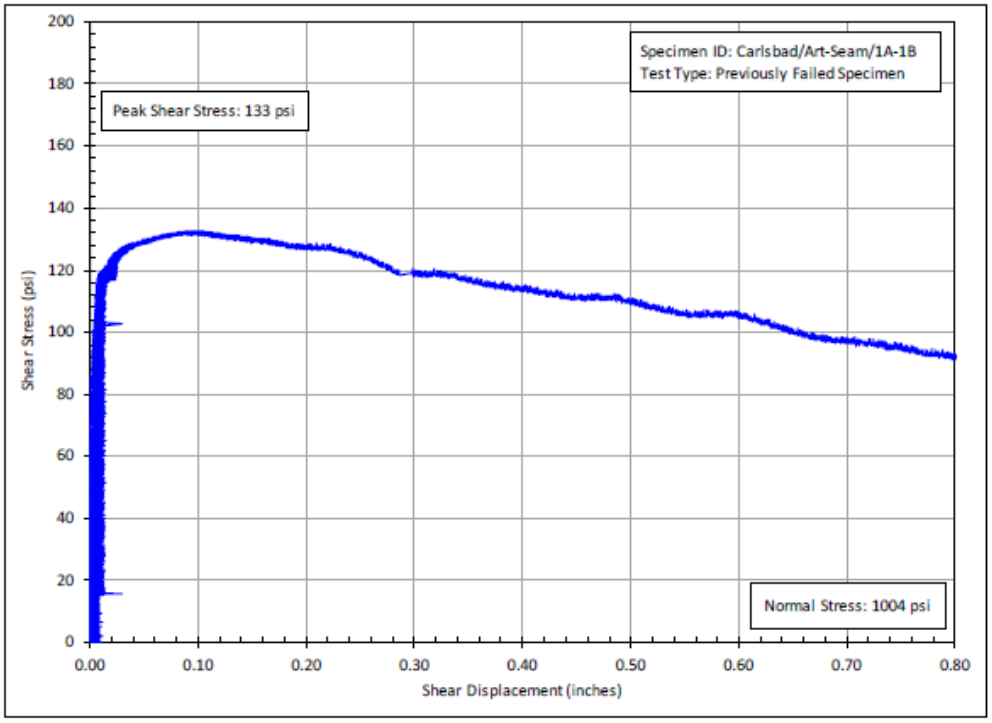

Figure B-5. Plot of Shear Stress Versus Shear Displacement for Previously Tested Specimen Carlsbad/Art-Seam/1A-1B.

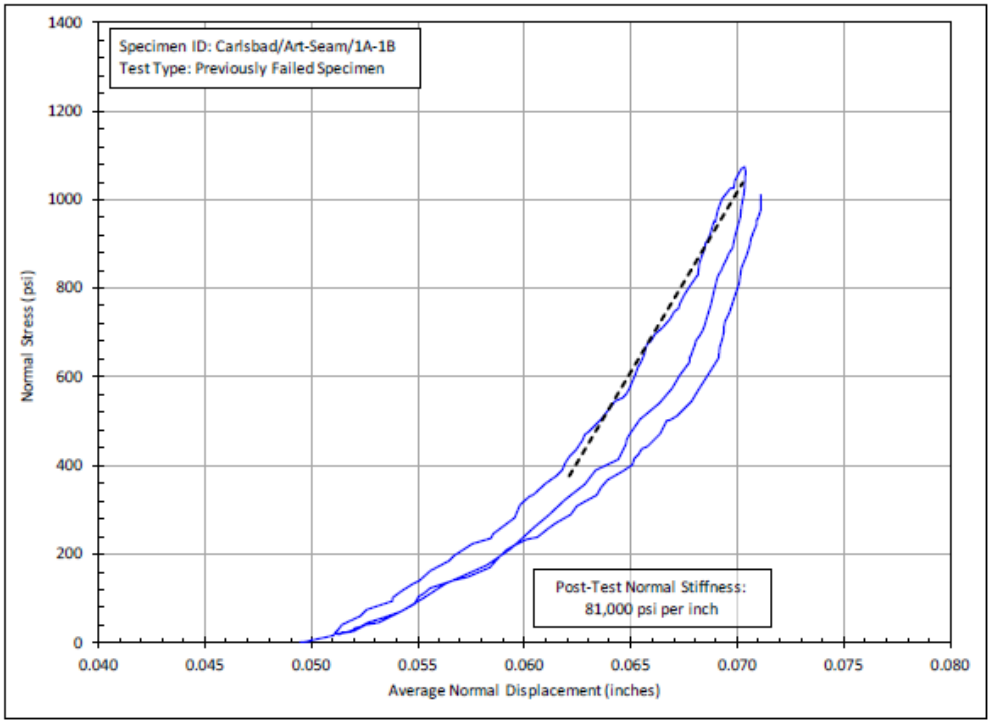

Figure B-6. Posttest Normal Stiffness Fit for Previously Tested Specimen Carlsbad/Art-Seam/1A-1B.

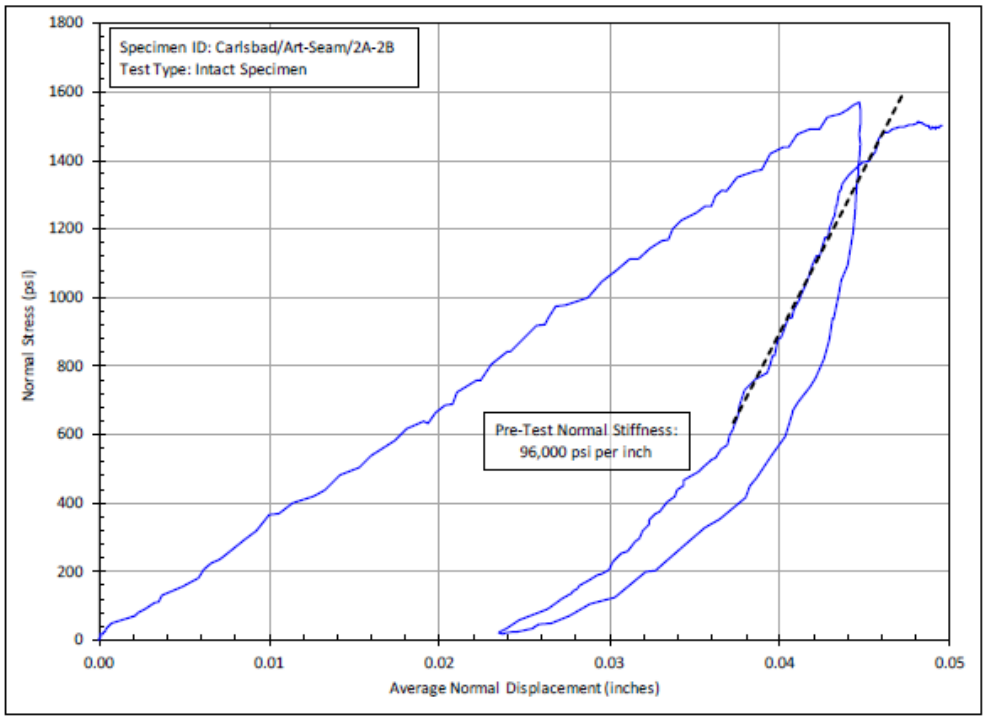

Figure B-7. Pretest Normal Stiffness Fit for Intact Specimen Carlsbad/Art-Seam/2A-2B.

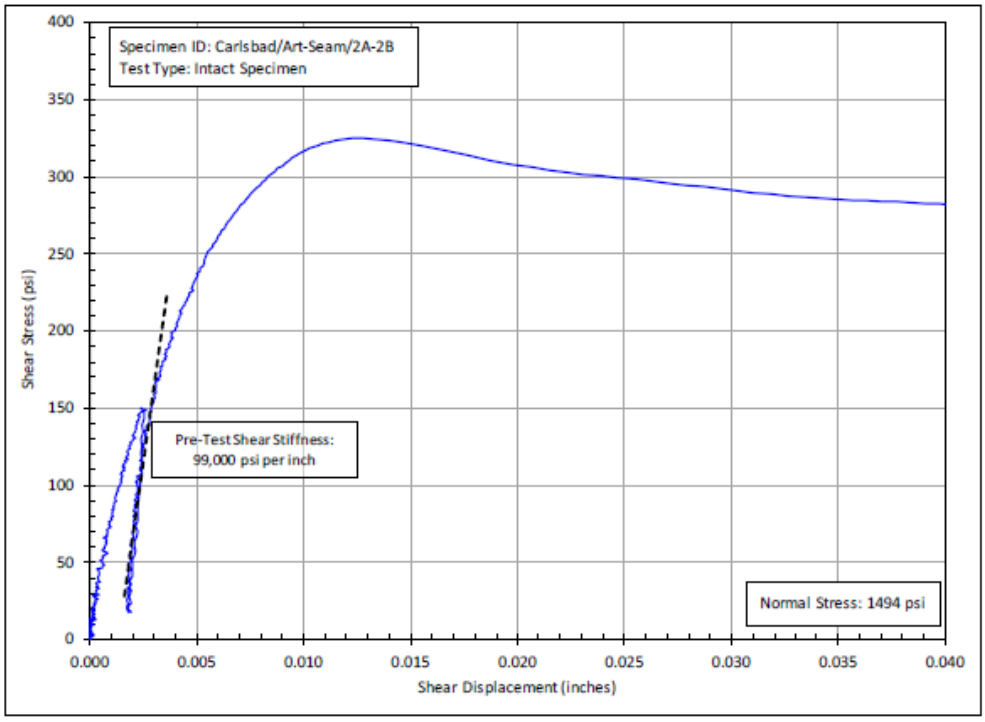

Figure B-8. Pretest Shear Stiffness Fit for Intact Specimen Carlsbad/Art-Seam/2A-2B.

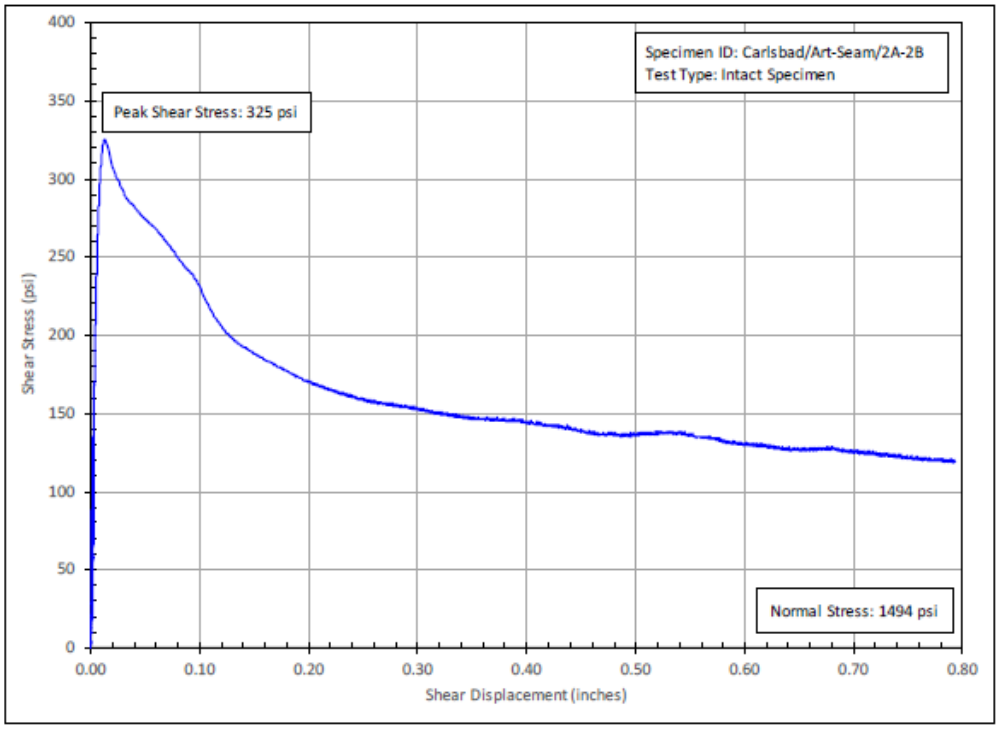

Figure B-9. Plot of Shear Stress Versus Shear Displacement for Intact Specimen Carlsbad/Art-Seam/2A-2B.

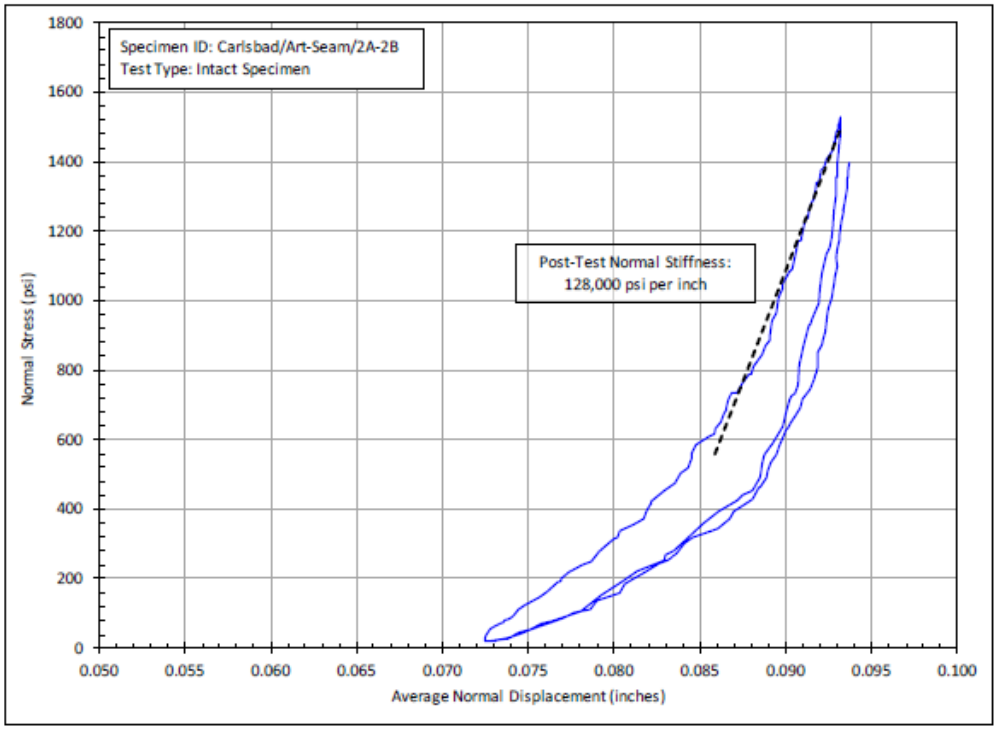

Figure B-10. Posttest Normal Stiffness Fit for Intact Specimen Carlsbad/Art-Seam/2A-2B.

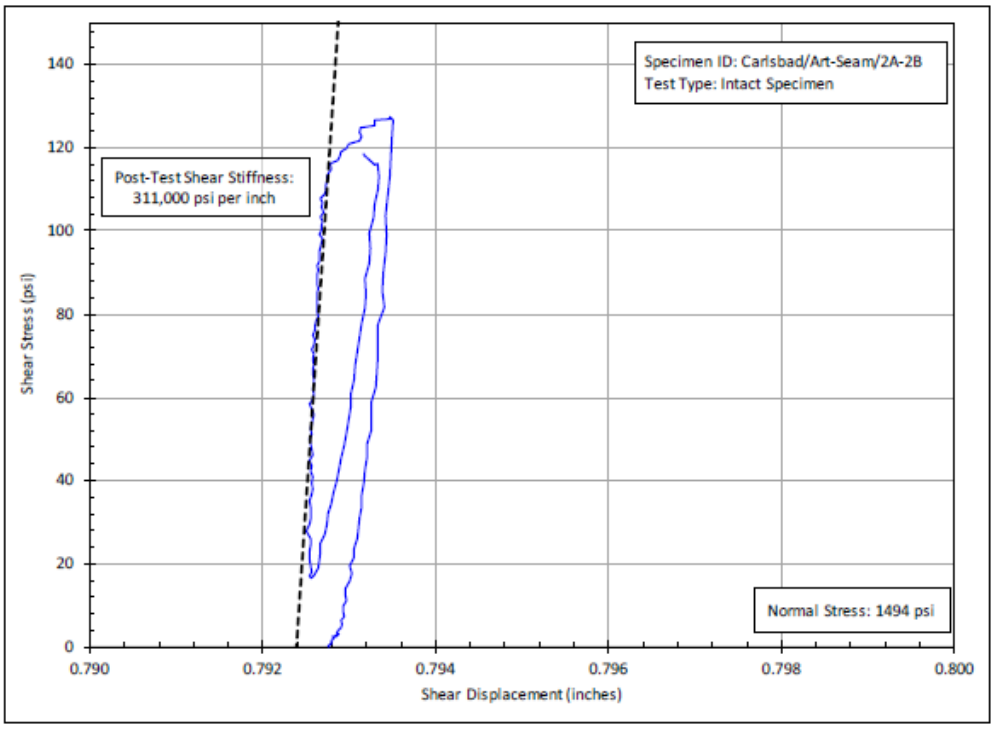

Figure B-11. Posttest Shear Stiffness Fit for Intact Specimen Carlsbad/Art-Seam/2A-2B.

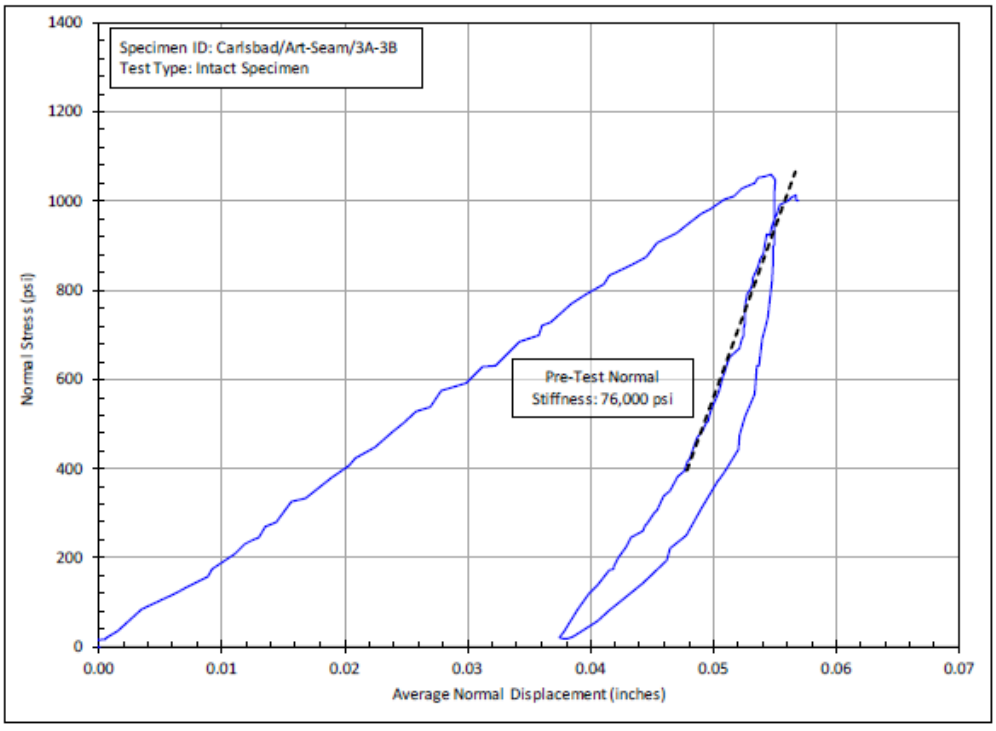

Figure B-12. Pretest Normal Stiffness Fit for Intact Specimen Carlsbad/Art-Seam/3A-3B.

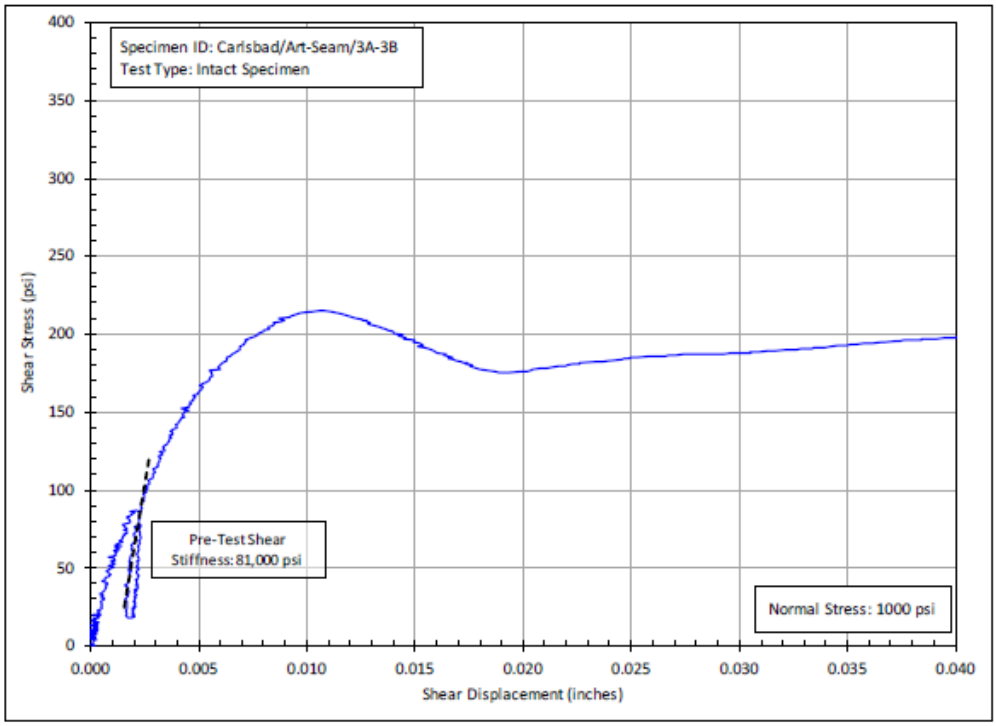

Figure B-13. Pretest Shear Stiffness Fit for Intact Specimen Carlsbad/Art-Seam/3A-3B

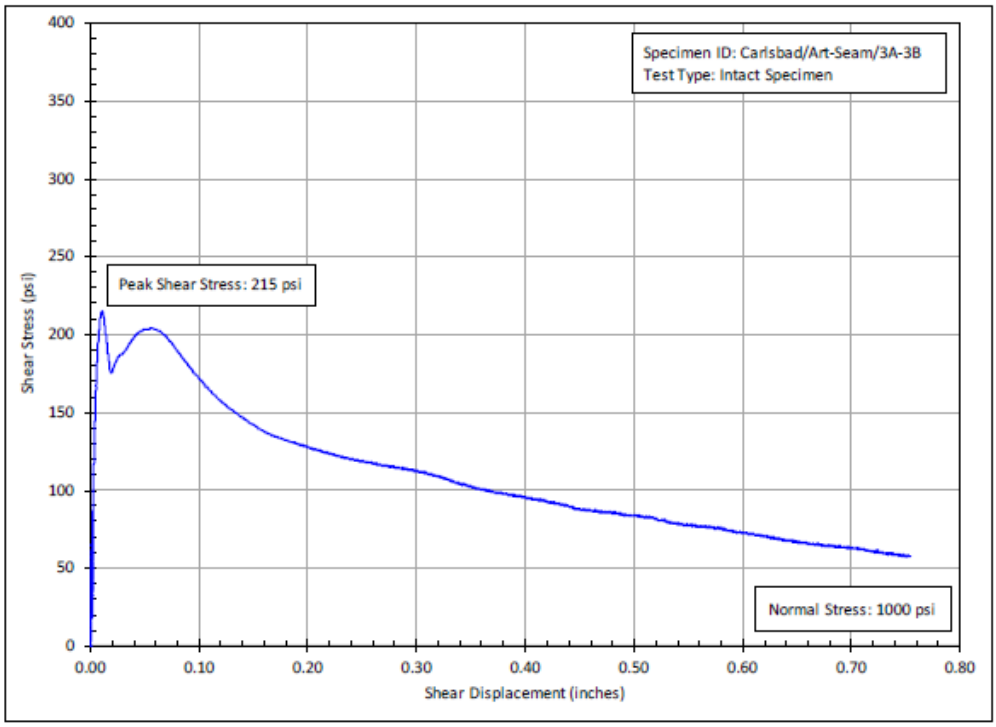

Figure B-14. Plot of Shear Stress Versus Shear Displacement for Intact Specimen Carlsbad/Art-Seam/3A-3B.

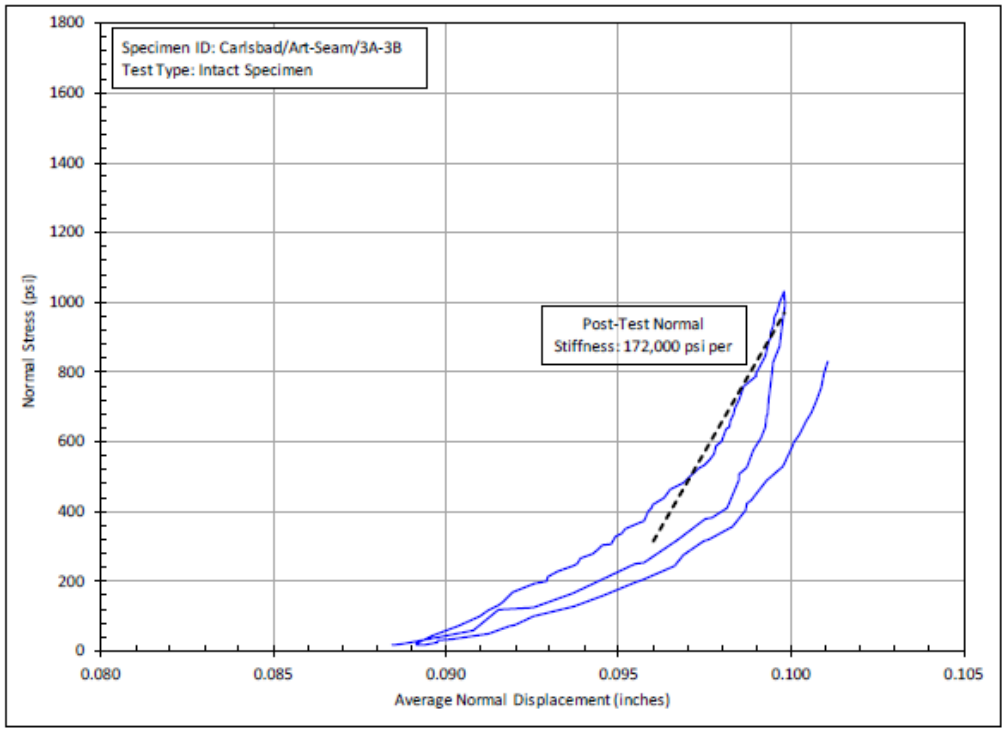

Figure B-15. Posttest Normal Stiffness Fit for Intact Specimen Carlsbad/Art-Seam/3A-3B.

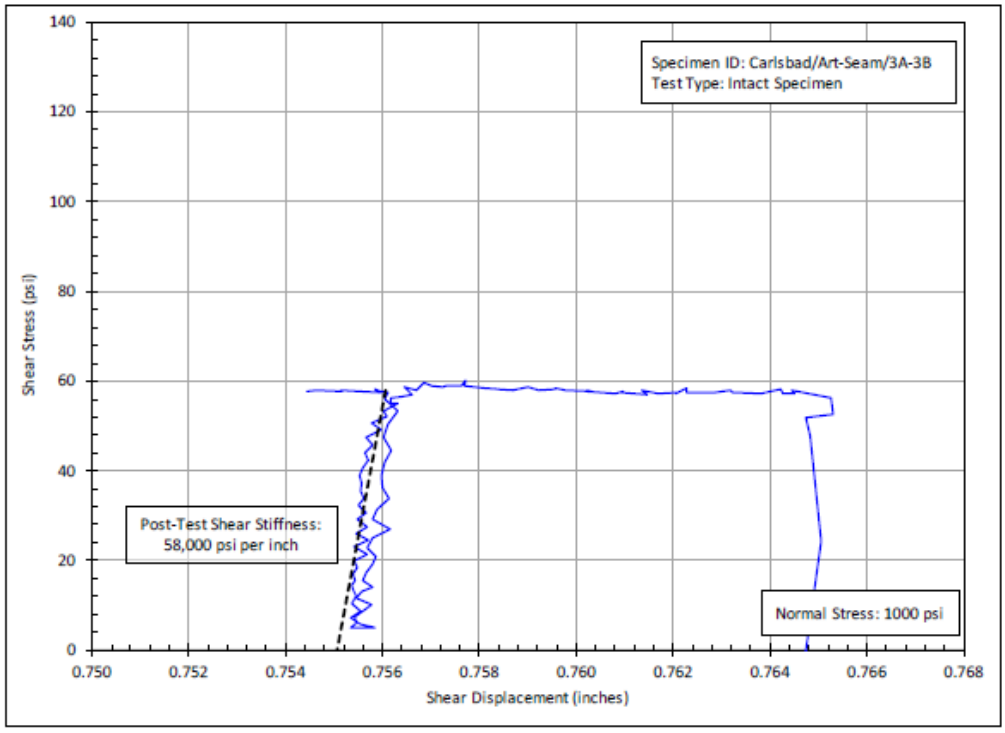

Figure B-16. Posttest Shear Stiffness Fit for Intact Specimen Carlsbad/Art-Seam/3A-3B.

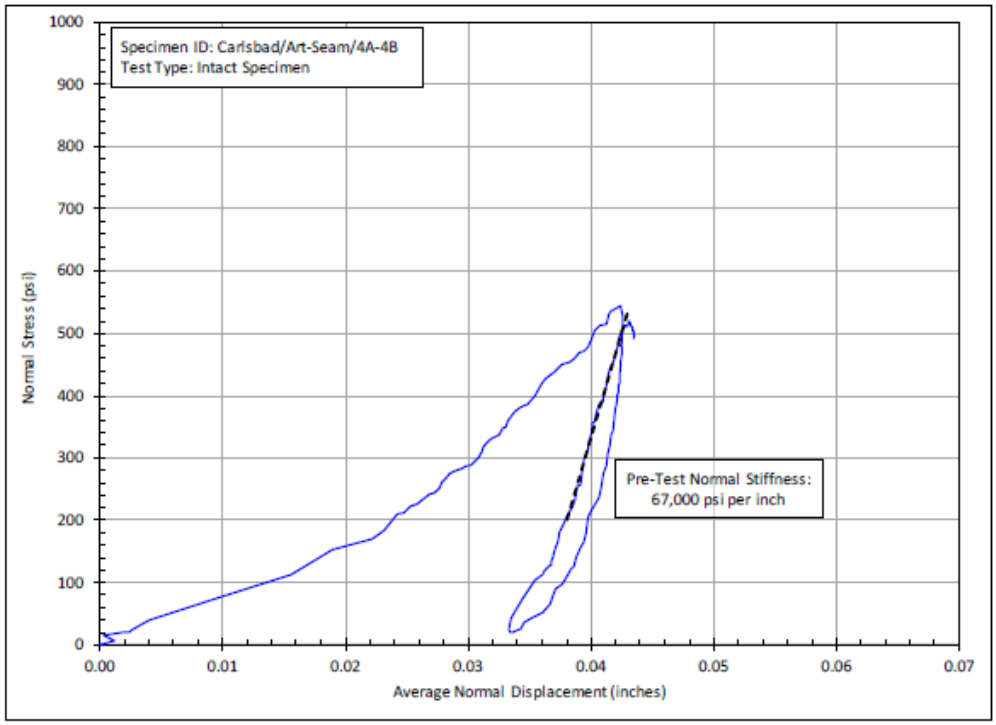

Figure B-17. Pretest Normal Stiffness Fit for Intact Specimen Carlsbad/Art-Seam/4A-4B.

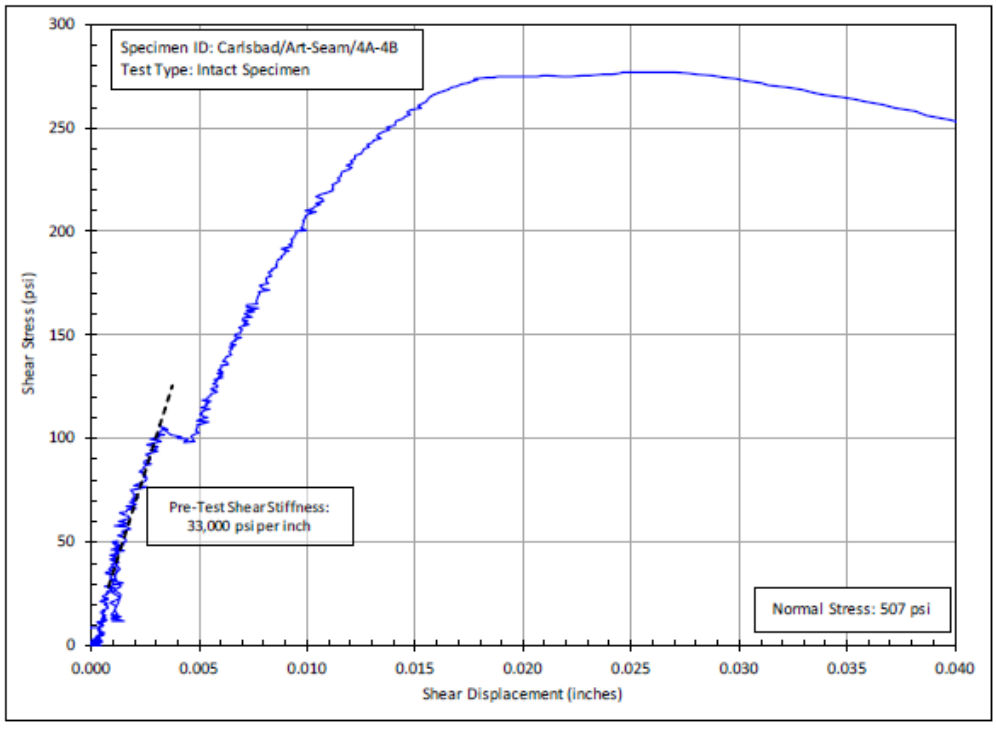

Figure B-18. Pretest Shear Stiffness Fit for Intact Specimen Carlsbad/Art-Seam/4A-4B.

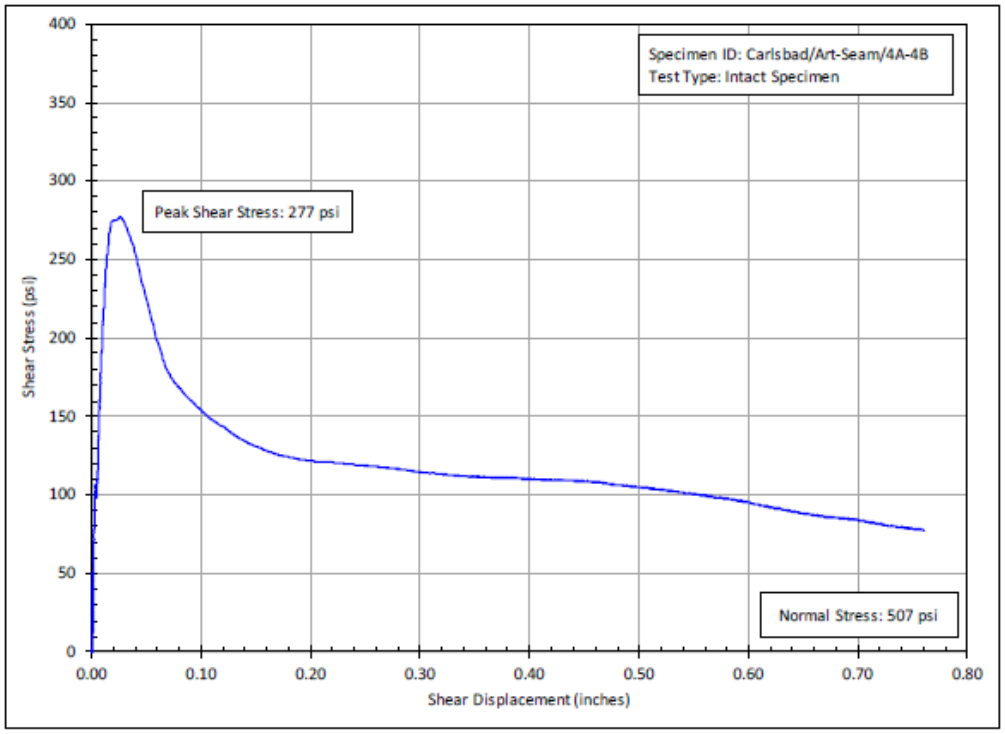

Figure B-19. Plot of Shear Stress Versus Shear Displacement for Intact Specimen Carlsbad/Art-Seam/4A-4B.

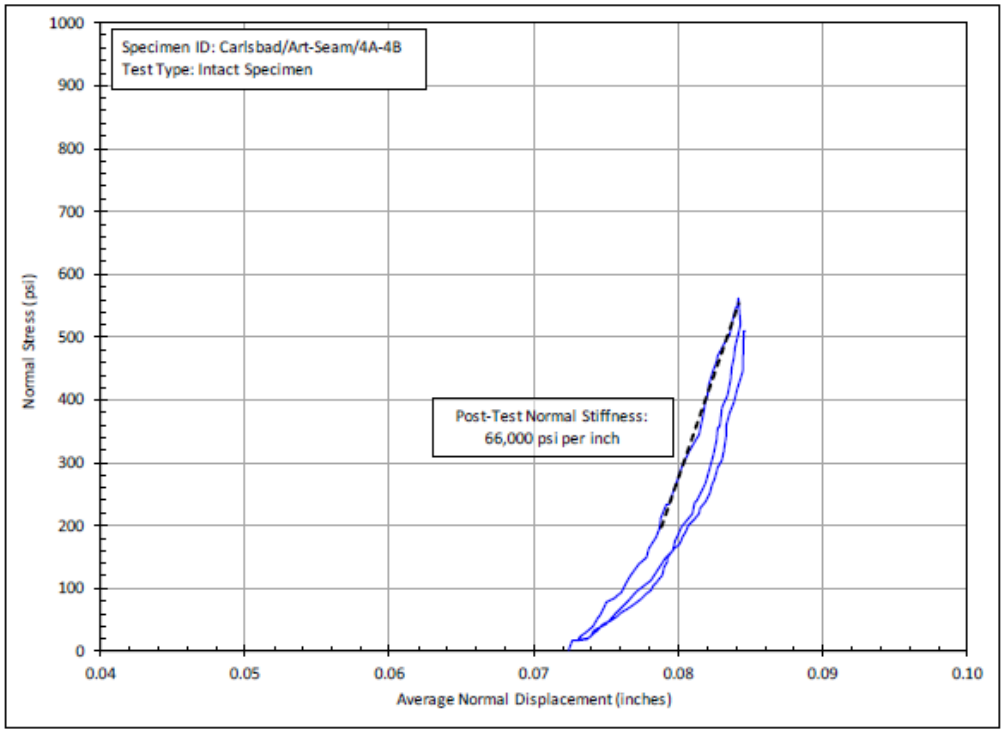

Figure B-20. Posttest Normal Stiffness Fit for Intact Specimen Carlsbad/Art-Seam/4A-4B.

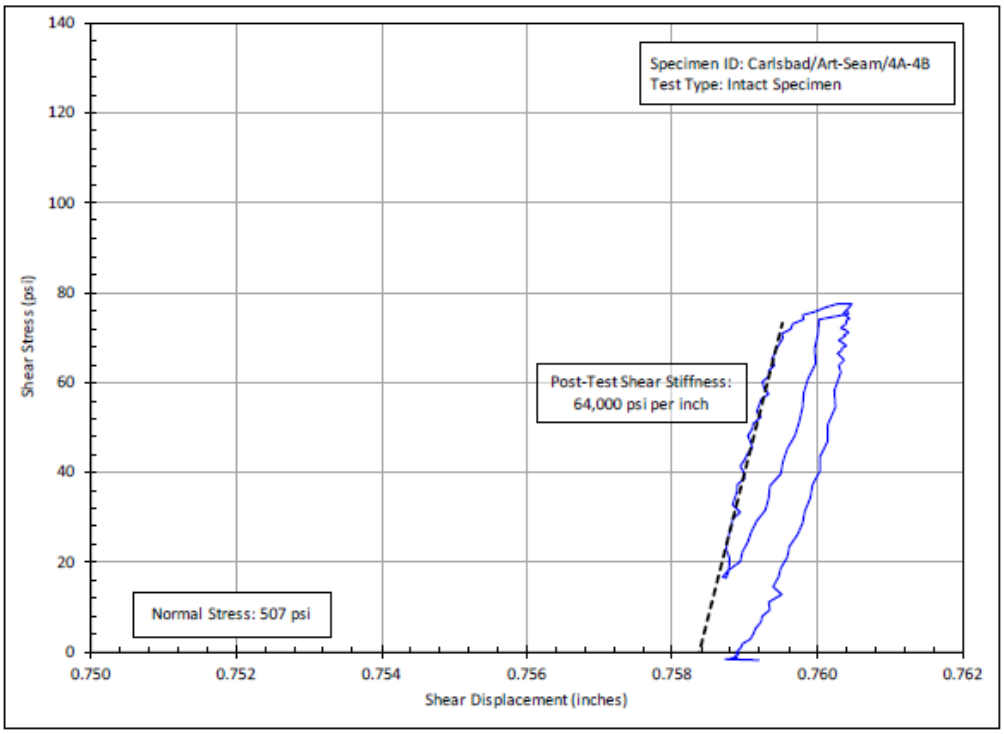

Figure B-21. Posttest Shear Stiffness Fit for Intact Specimen Carlsbad/Art-Seam/4A-4B.

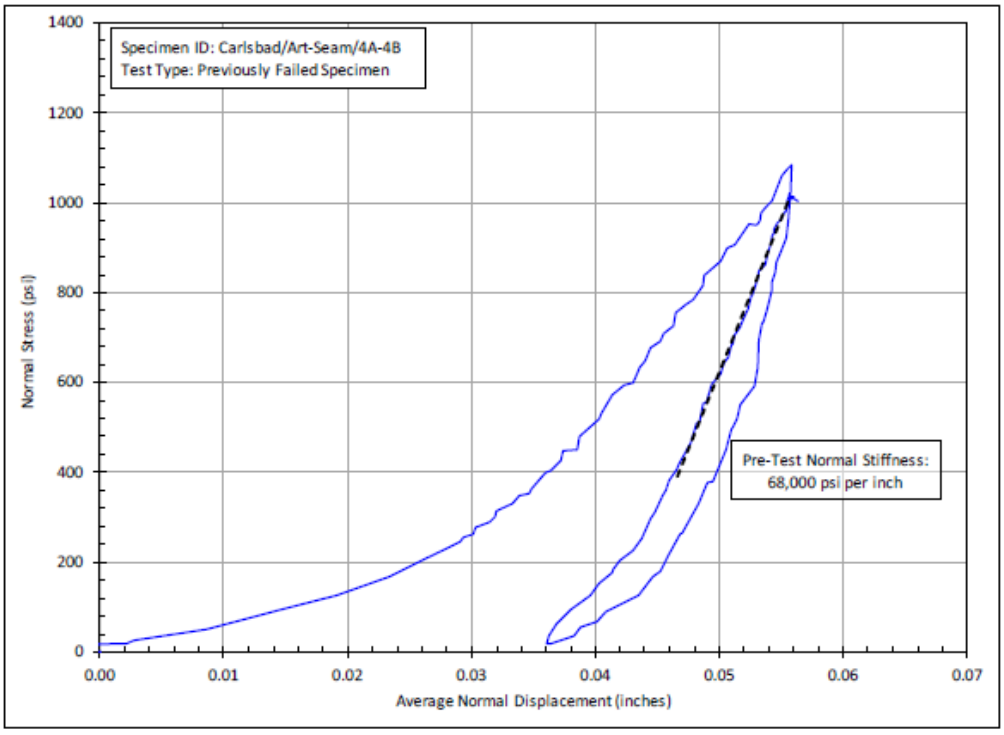

Figure B-22. Pretest Normal Stiffness Fit for Previously Tested Specimen Carlsbad/Art-Seam/4A-4B.

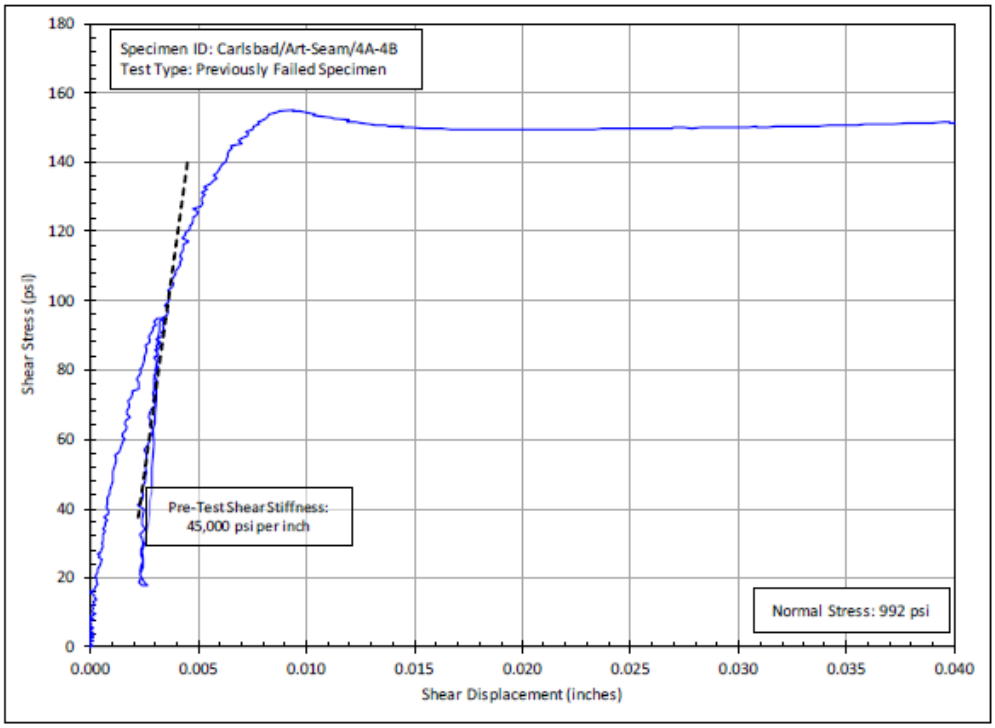

Figure B-23. Pretest Shear Stiffness Fit for Previously Tested Specimen Carlsbad/Art-Seam/4A-4B.

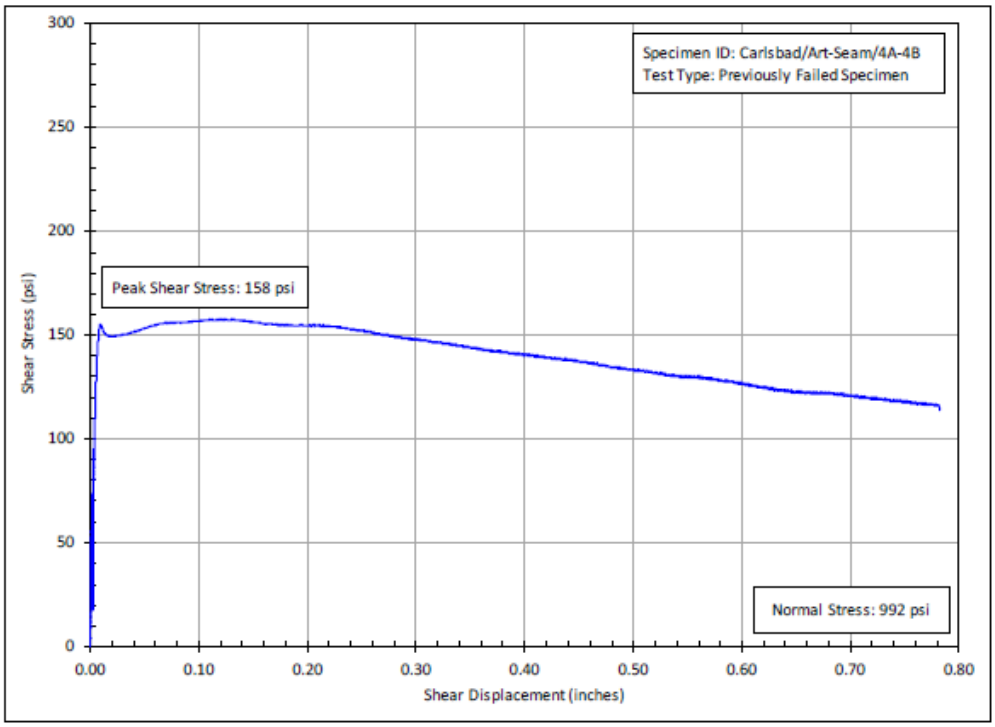

Figure B-24. Plot of Shear Stress Versus Shear Displacement for Previously Tested Specimen Carlsbad/Art-Seam/4A-4B.

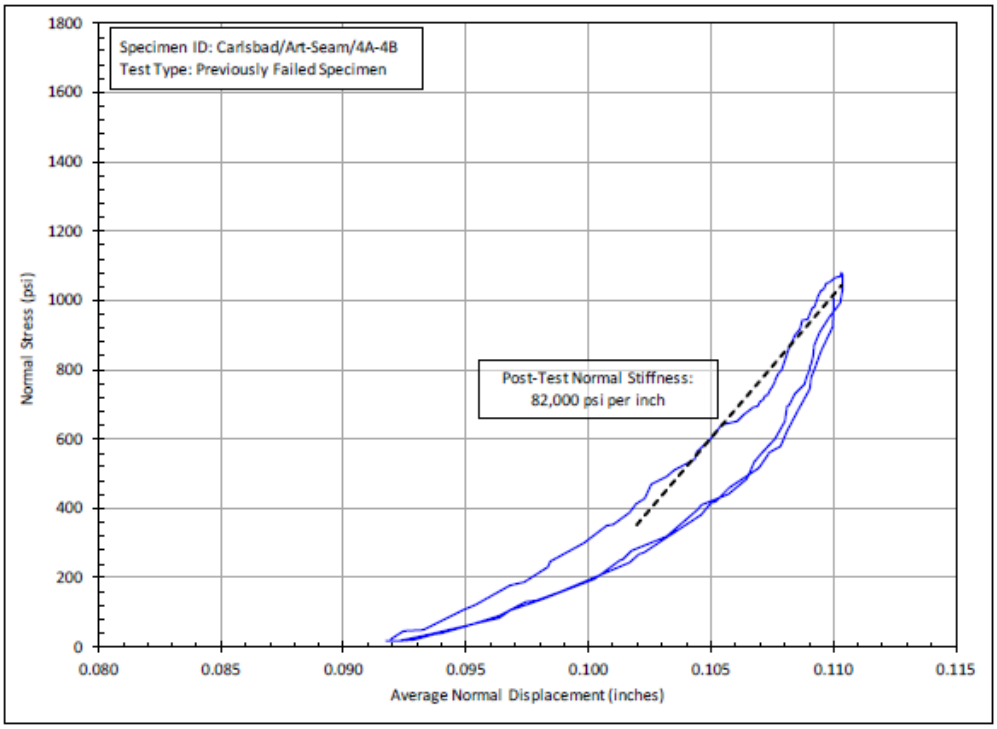

Figure B-25. Posttest Normal Stiffness Fit for Previously Tested Specimen Carlsbad/Art-Seam/4A-4B.

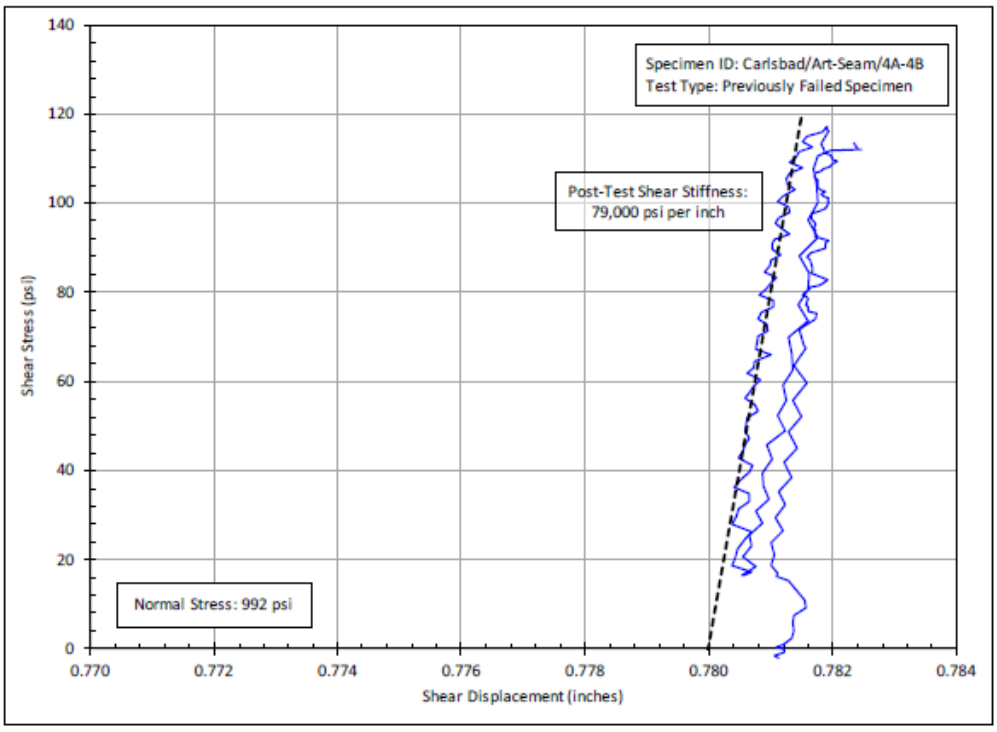

Figure B-26. Posttest Shear Stiffness Fit for Previously Tested Specimen Carlsbad/Art-Seam/4A-4B.

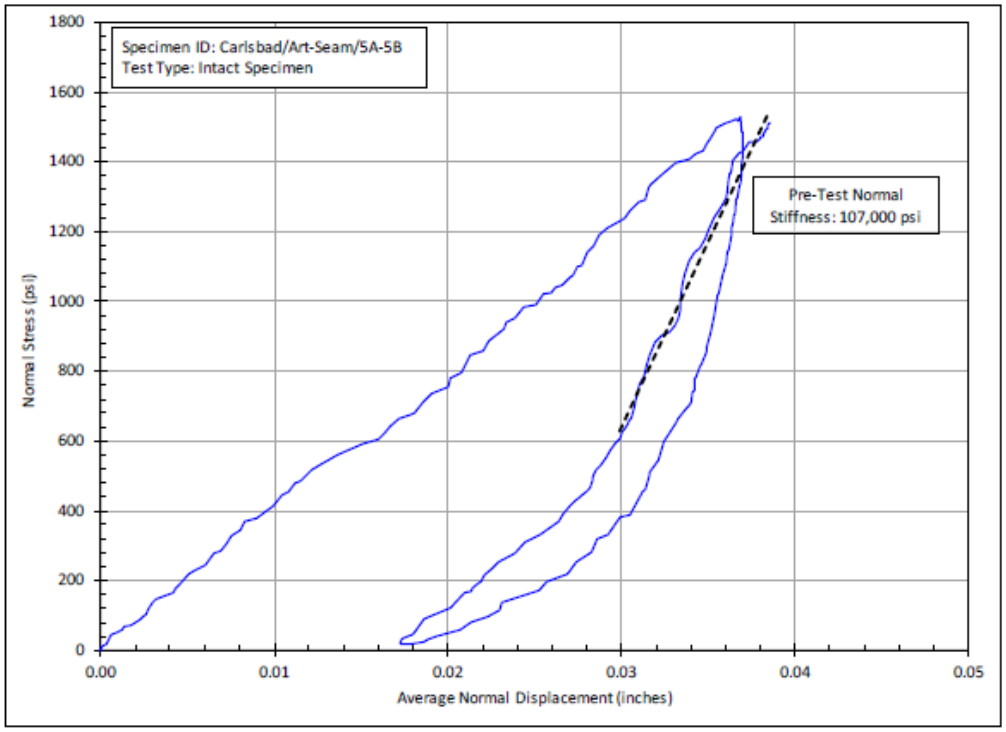

Figure B-27. Pretest Normal Stiffness Fit for Intact Specimen Carlsbad/Art-Seam/5A-5B.

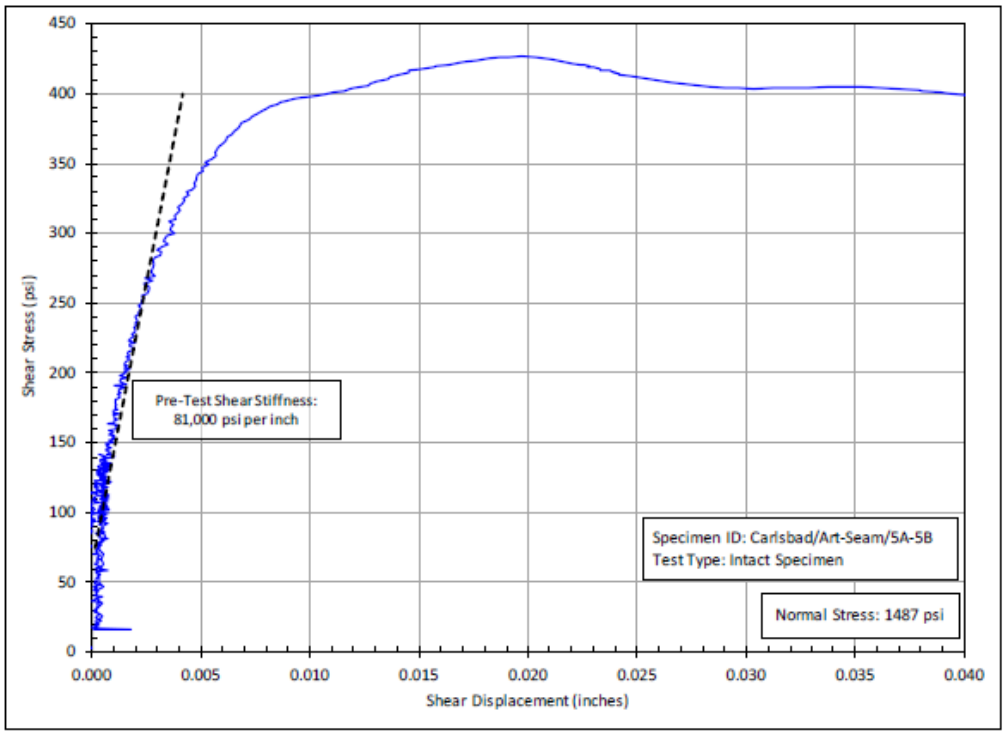

Figure B-28. Pretest Shear Stiffness Fit for Intact Specimen Carlsbad/Art-Seam/5A-5B.

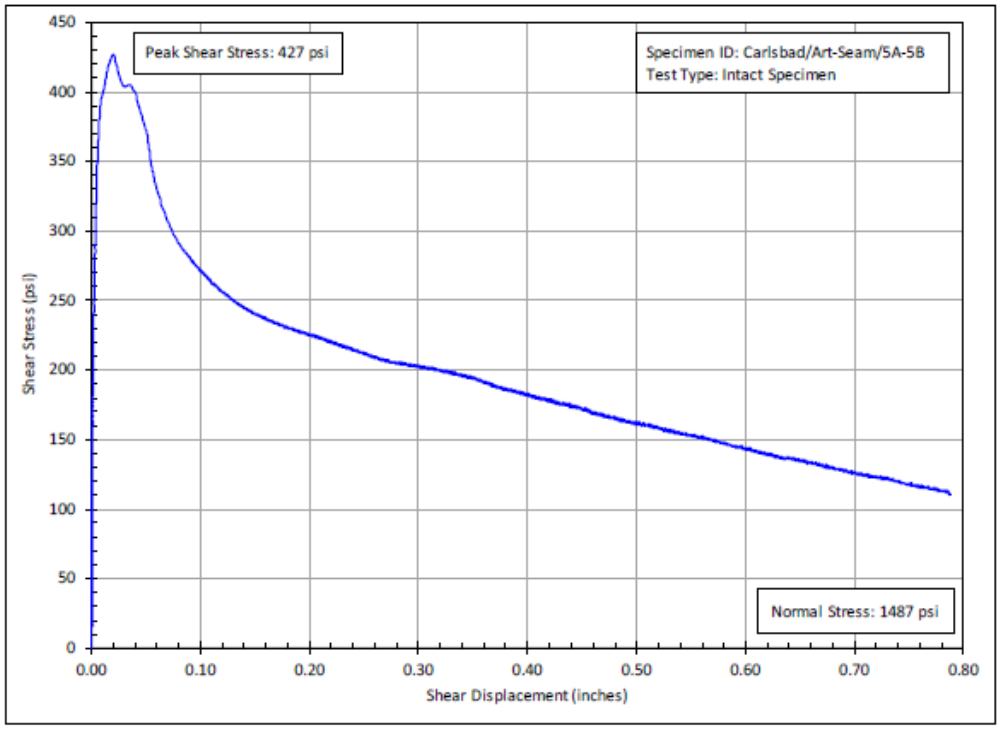

Figure B-29. Plot of Shear Stress Versus Shear Displacement for Intact Specimen Carlsbad/Art-Seam/5A-5B.

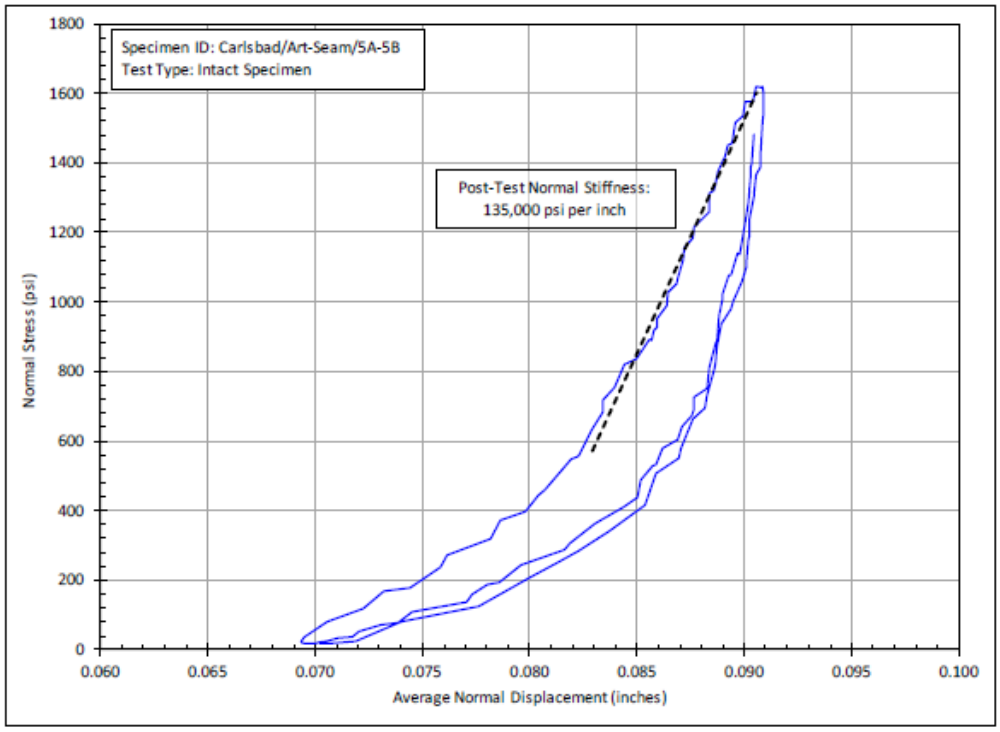

Figure B-30. Posttest Normal Stiffness Fit for Intact Specimen Carlsbad/Art-Seam/5A-5B.

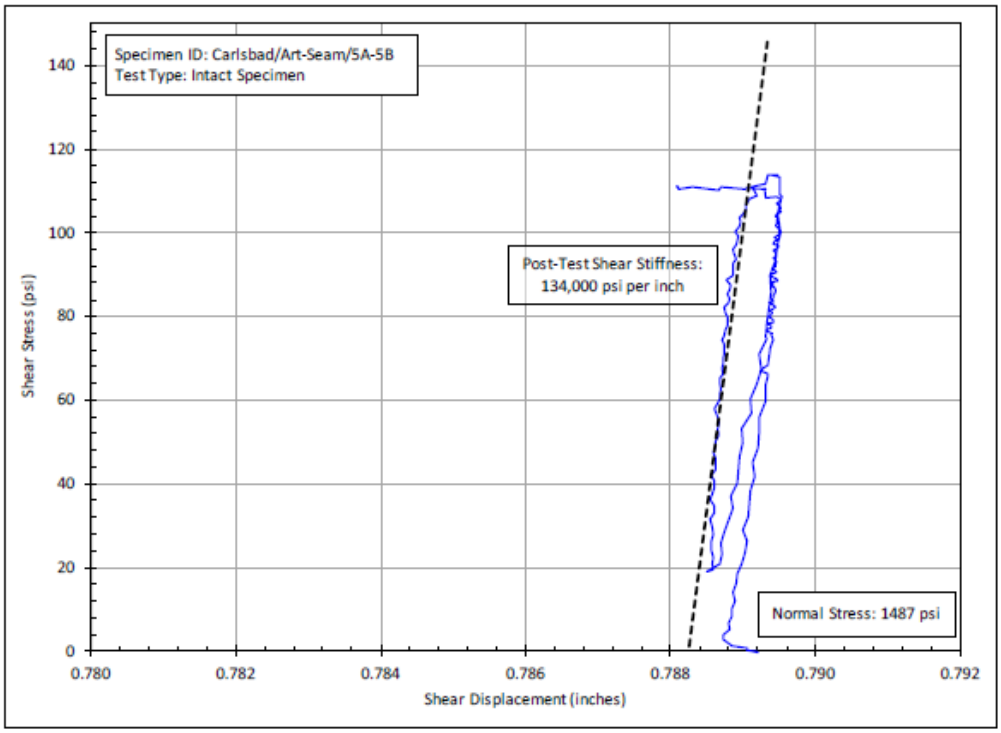

Figure B-31. Posttest Shear Stiffness Fit for Intact Specimen Carlsbad/Art-Seam/5A-5B.

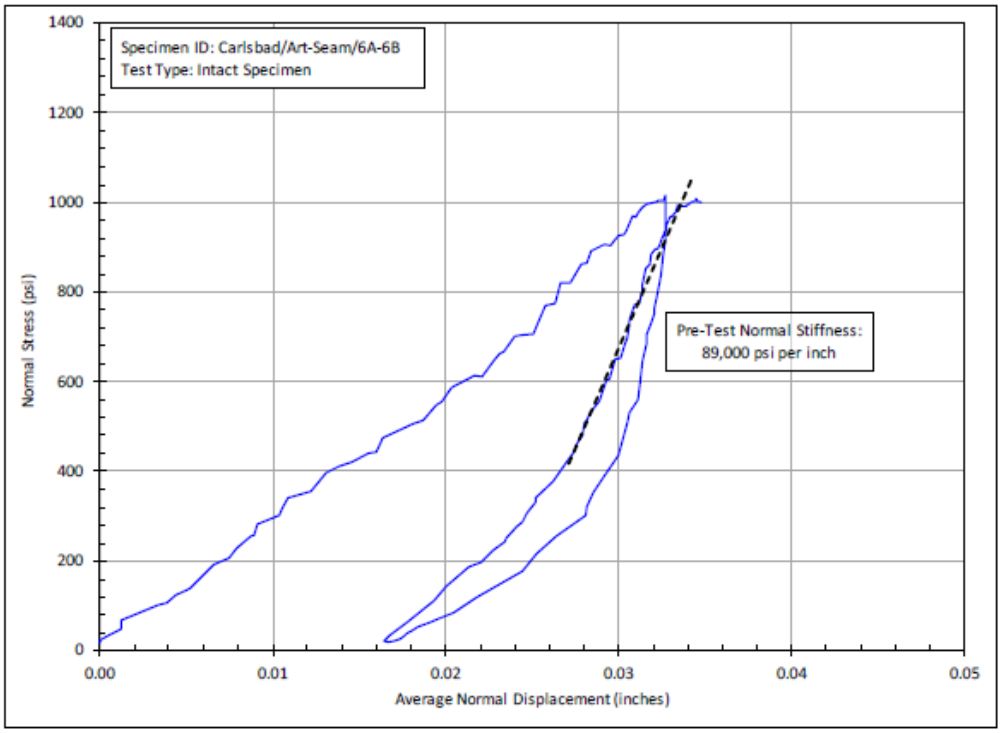

Figure B-32. Pretest Normal Stiffness Fit for Intact Specimen Carlsbad/Art-Seam/6A-6B.

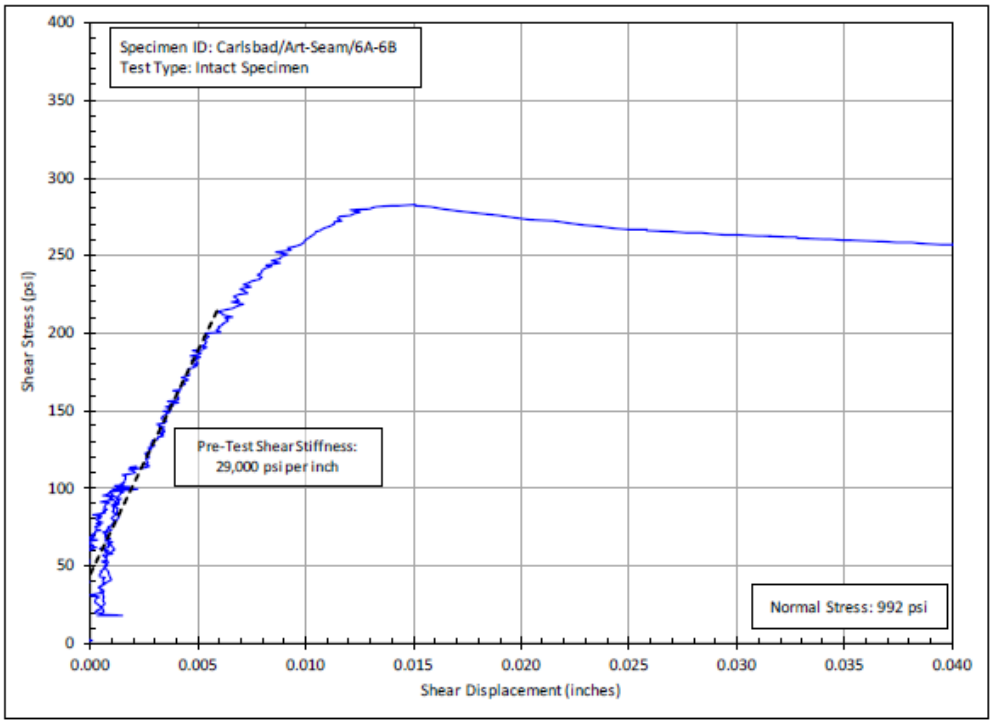

Figure B-33. Pretest Shear Stiffness Fit for Intact Specimen Carlsbad/Art-Seam/6A-6B.

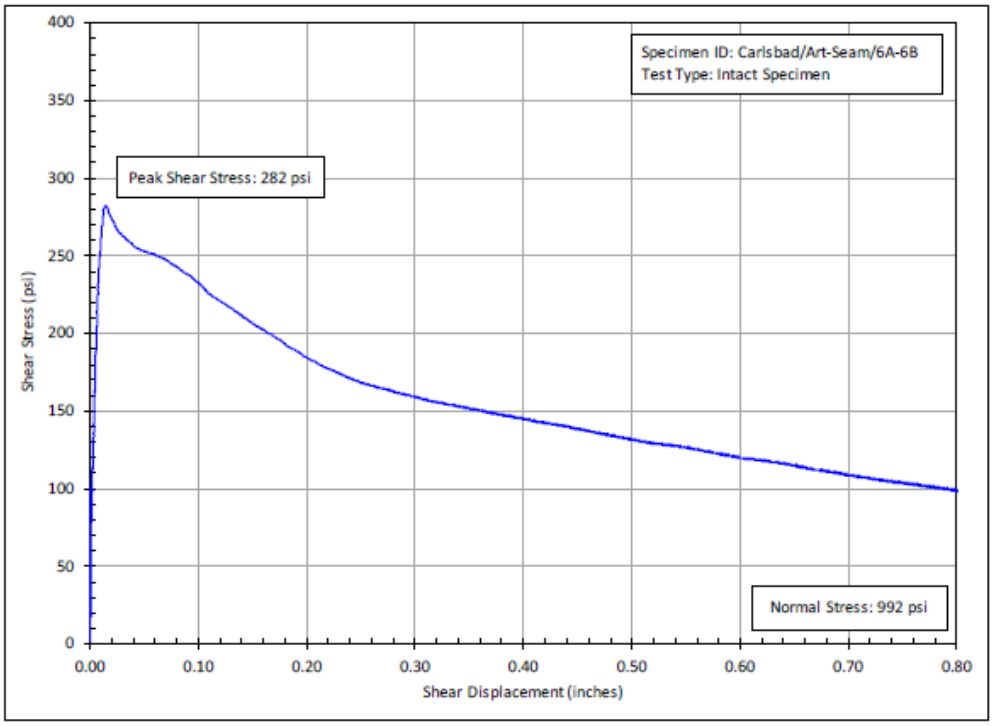

Figure B-34. Plot of Shear Stress Versus Shear Displacement for Intact Specimen Carlsbad/Art-Seam/6A-6B.

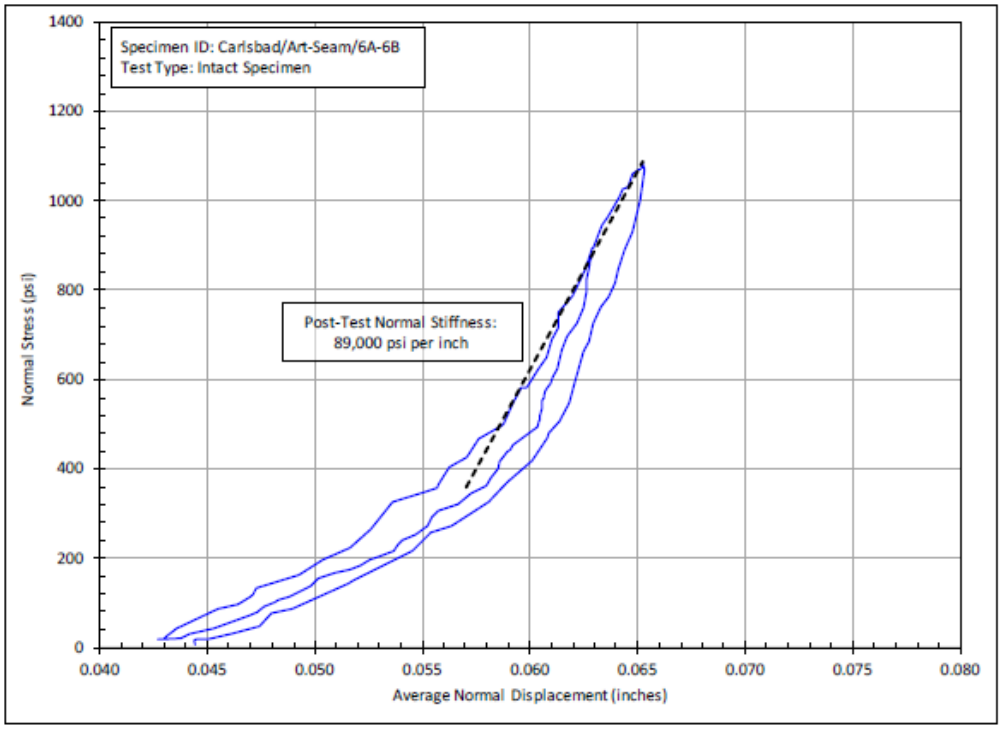

Figure B-35. Posttest Normal Stiffness Fit for Intact Specimen Carlsbad/Art-Seam/6A-6B.

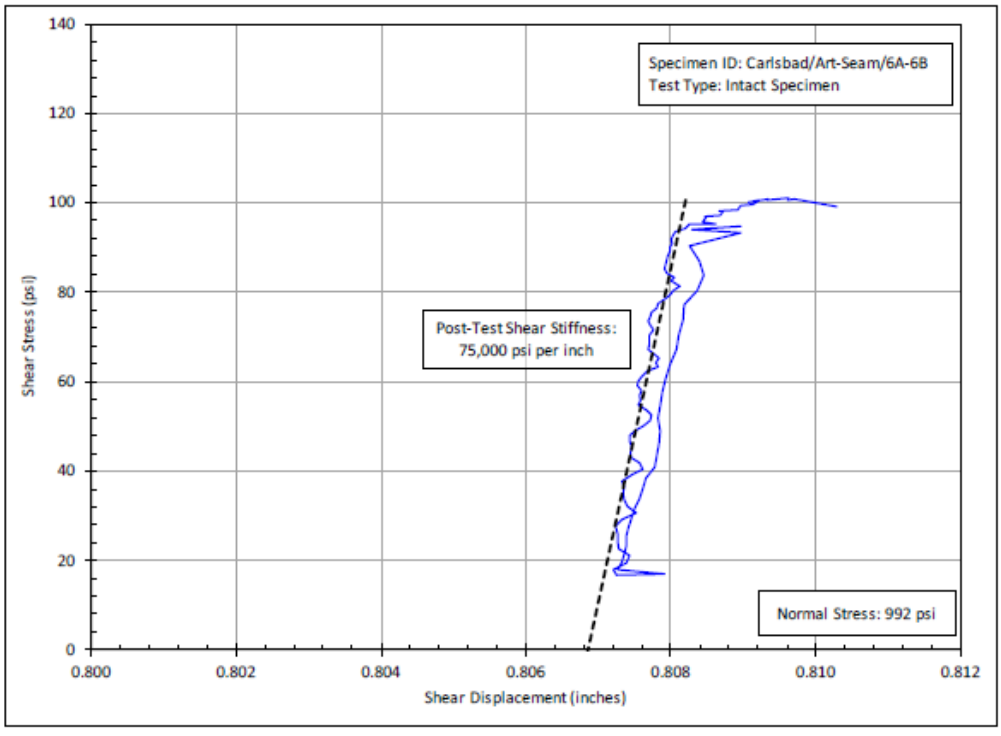

Figure B-36. Posttest Shear Stiffness Fit for Intact Specimen Carlsbad/Art-Seam/6A-6B.

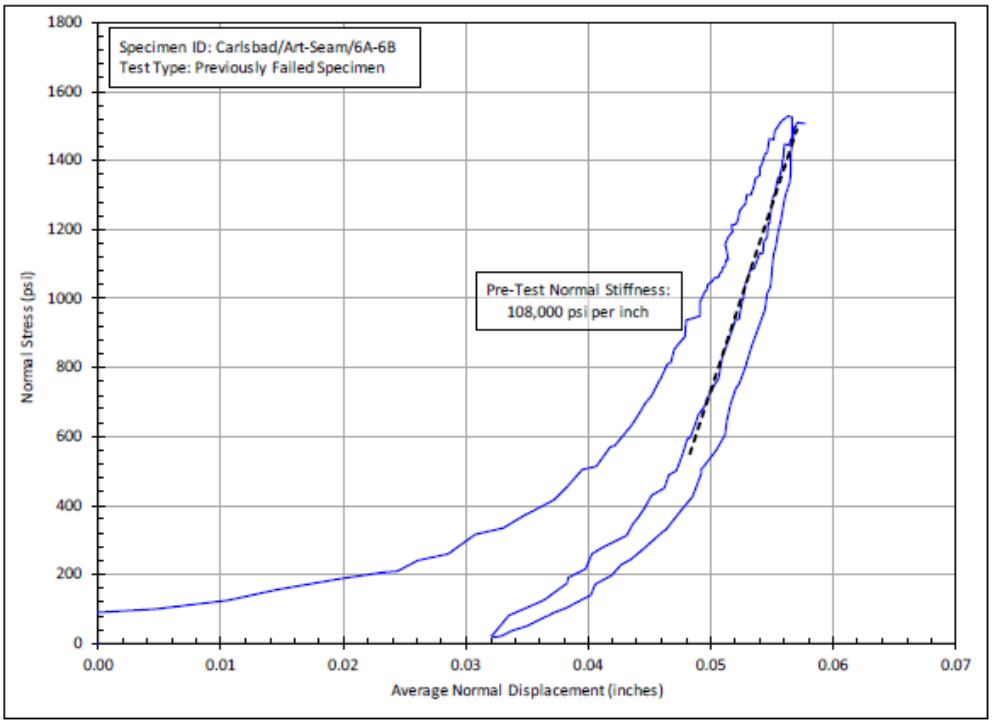

Figure B-37. Pretest Normal Stiffness Fit for Previously Tested Specimen Carlsbad/Art-Seam/6A-6B.

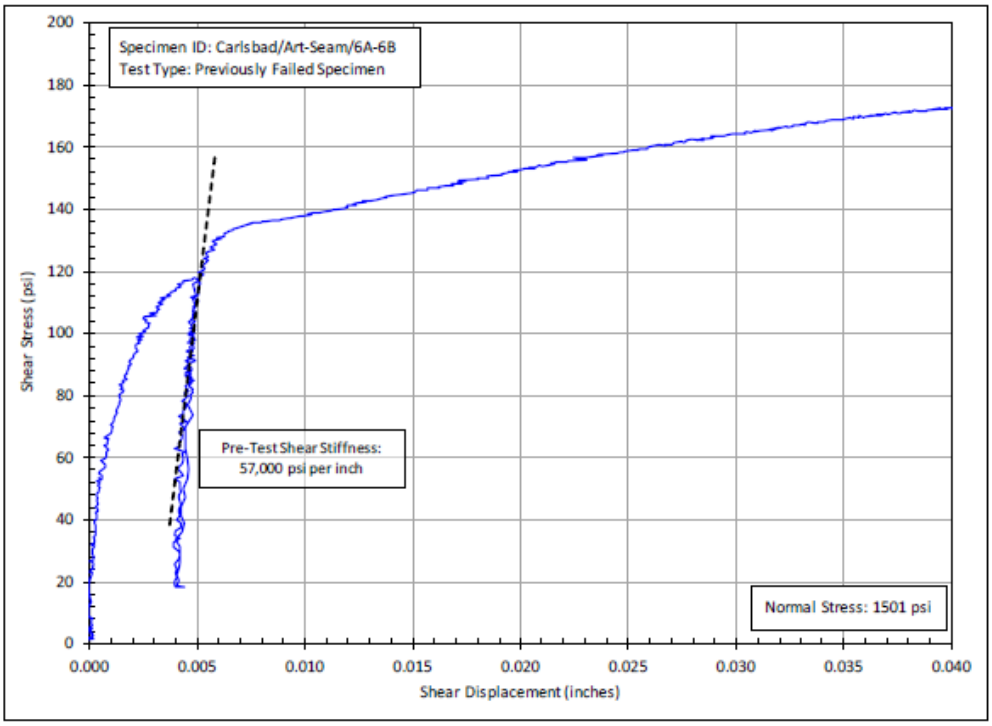

Figure B-38. Pretest Shear Stiffness Fit for Previously Tested Specimen Carlsbad/Art-Seam/6A-6B.

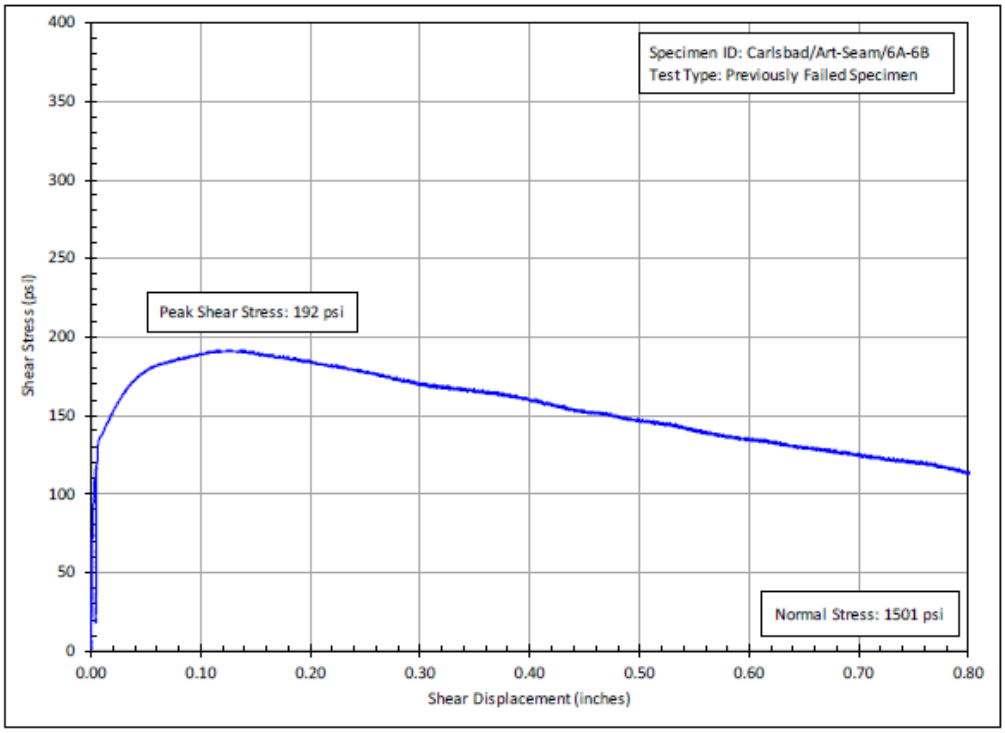

Figure B-39. Plot of Shear Stress Versus Shear Displacement for Previously Tested Specimen Carlsbad/Art-Seam/6A-6B.

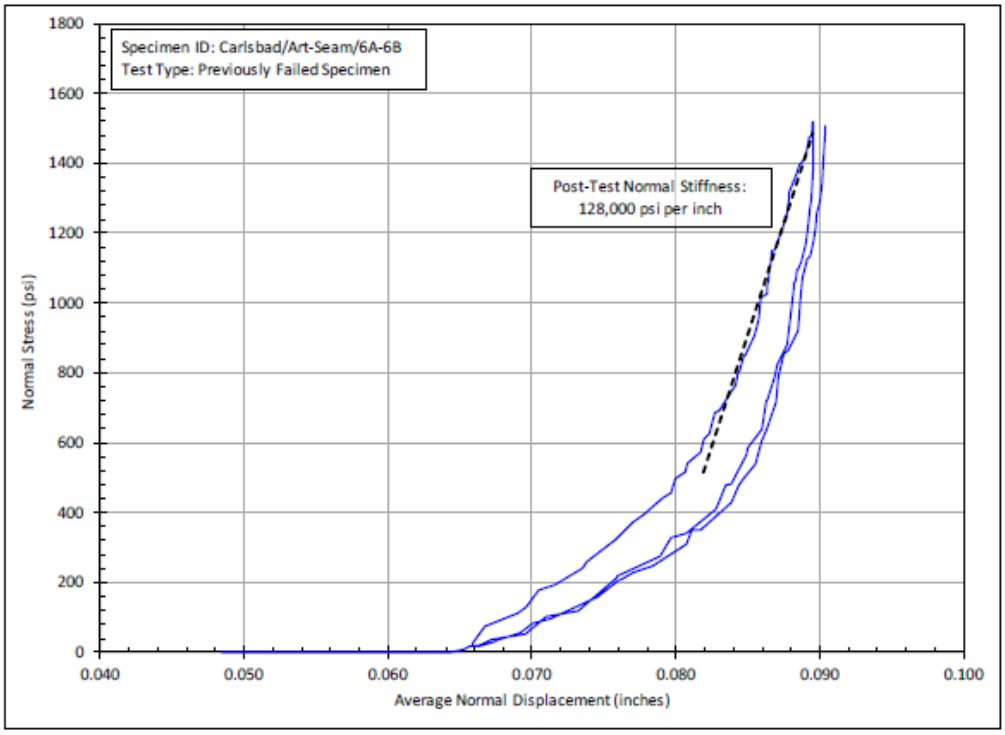

Figure B-40. Posttest Normal Stiffness Fit for Previously Tested Specimen Carlsbad/Art-Seam/6A-6B.

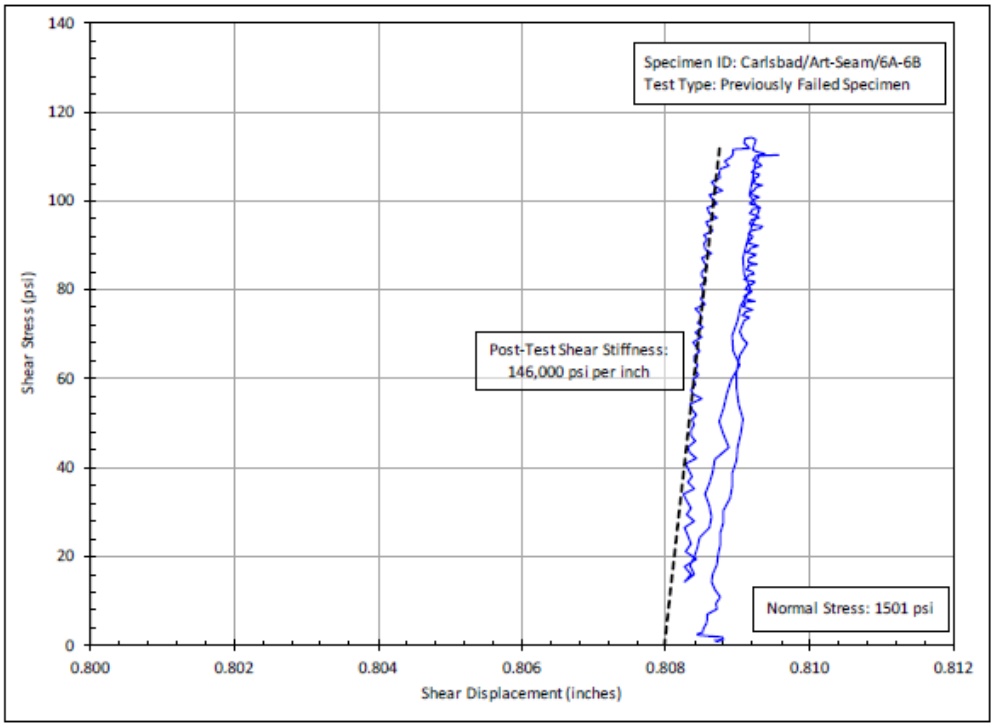

Figure B-41. Posttest Shear Stiffness Fit for Previously Tested Specimen Carlsbad/Art-Seam/6A-6B.

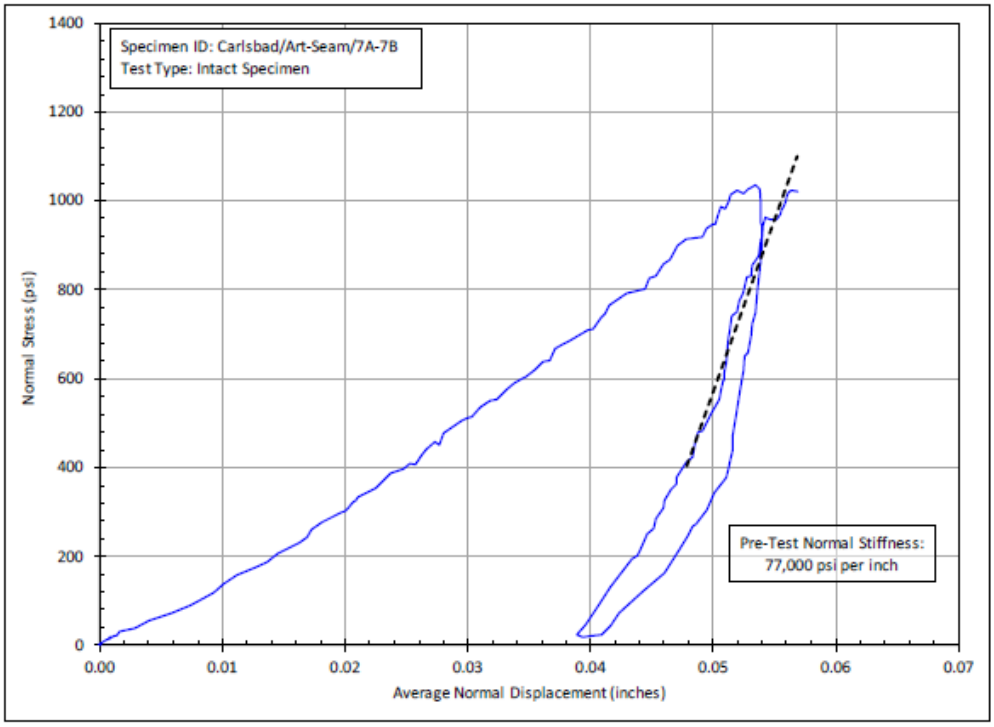

Figure B-42. Pretest Normal Stiffness Fit for Intact Specimen Carlsbad/Art-Seam/7A-7B.

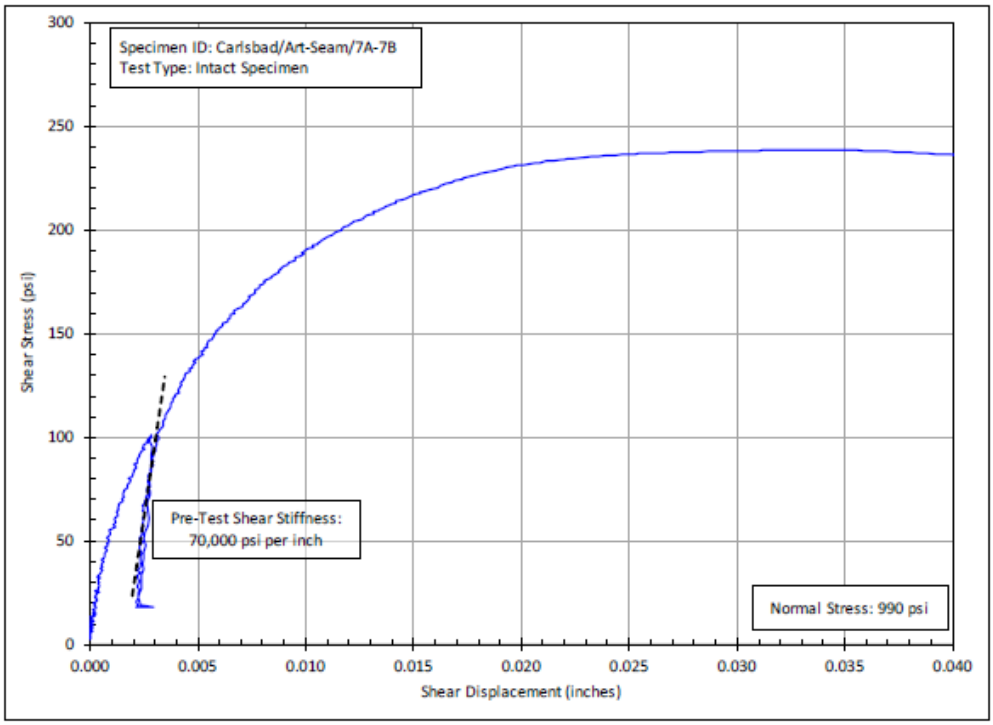

Figure B-43. Pretest Shear Stiffness Fit for Intact Specimen Carlsbad/Art-Seam/7A-7B.

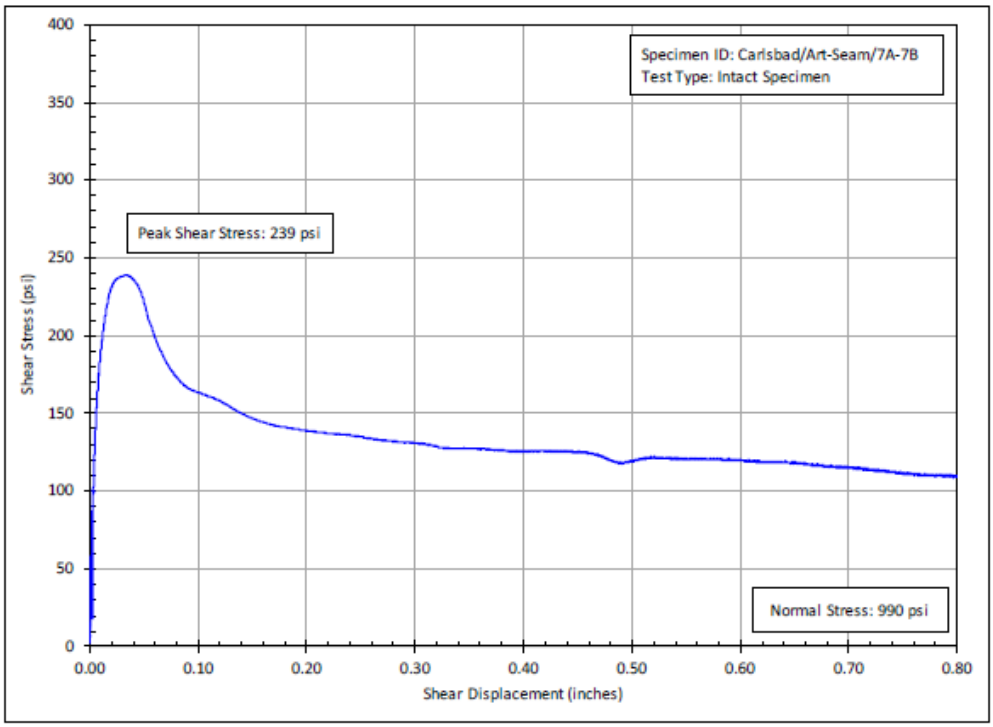

Figure B-44. Plot of Shear Stress Versus Shear Displacement for Intact Specimen Carlsbad/Art-Seam/7A-7B.

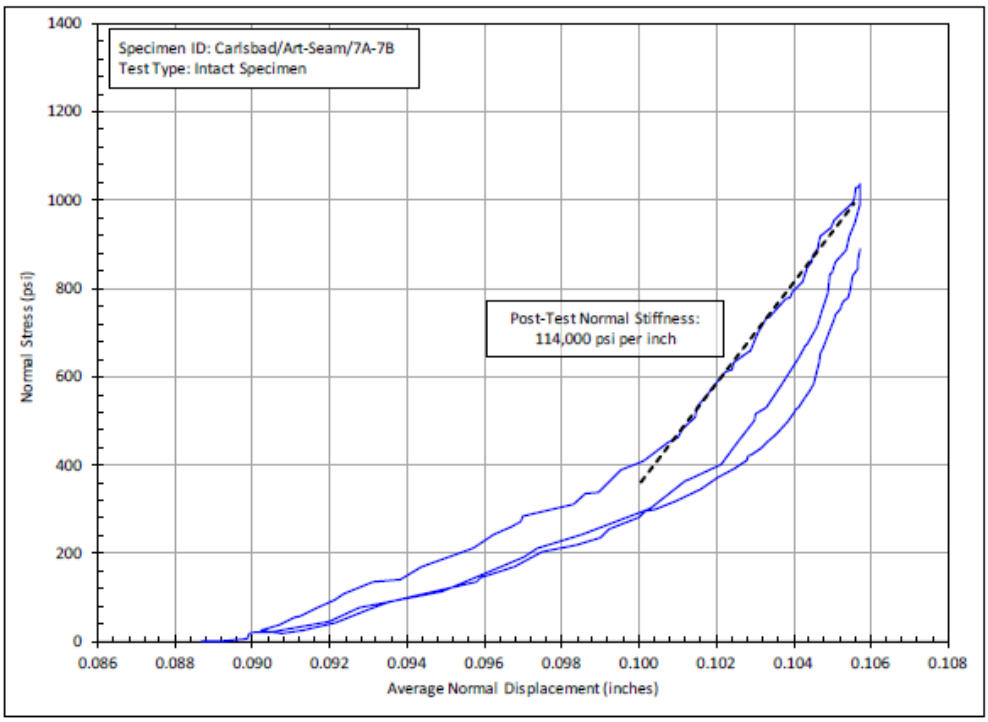

Figure B-45. Posttest Normal Stiffness Fit for Intact Specimen Carlsbad/Art-Seam/7A-7B.

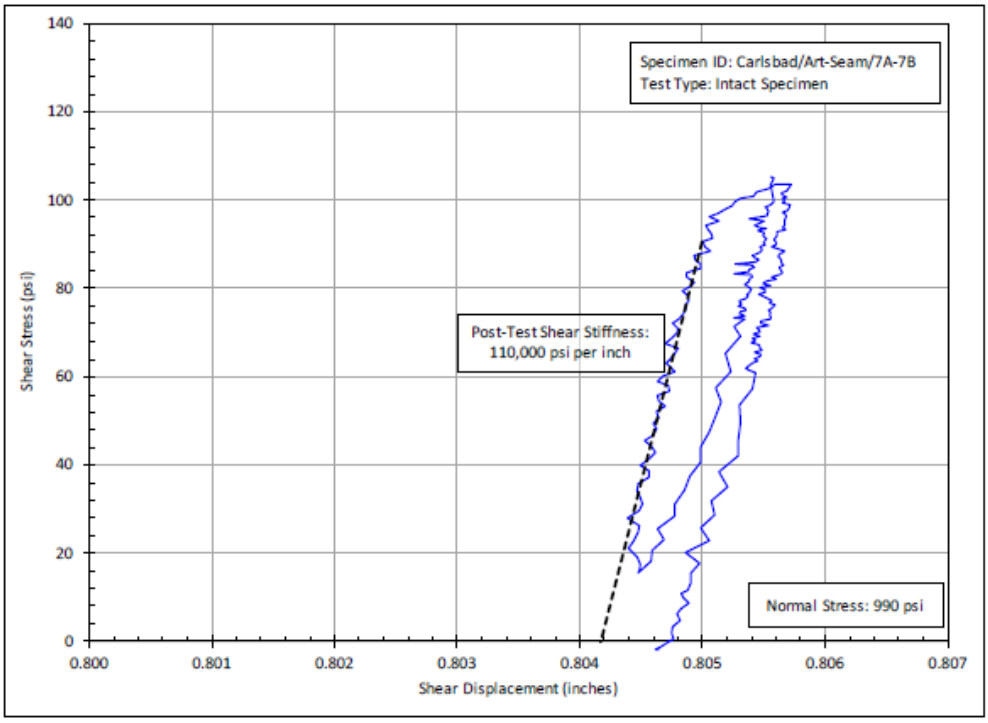

Figure B-46. Posttest Shear Stiffness Fit for Intact Specimen Carlsbad/Art-Seam/7A-7B.

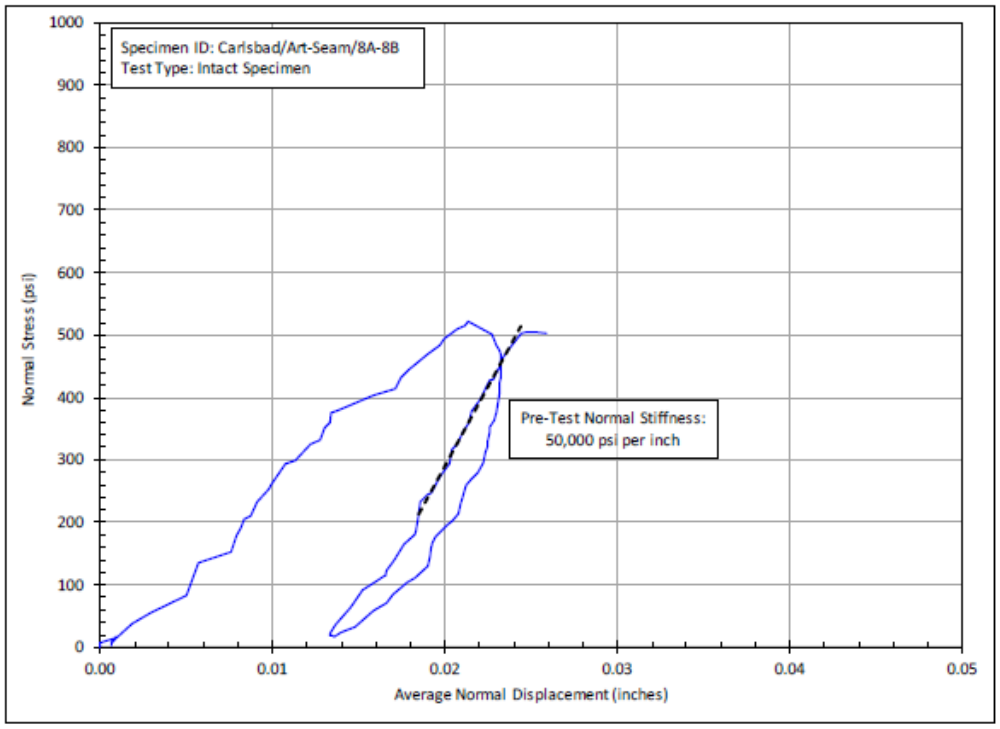

Figure B-47. Pretest Normal Stiffness Fit for Intact Specimen Carlsbad/Art-Seam/8A-8B.

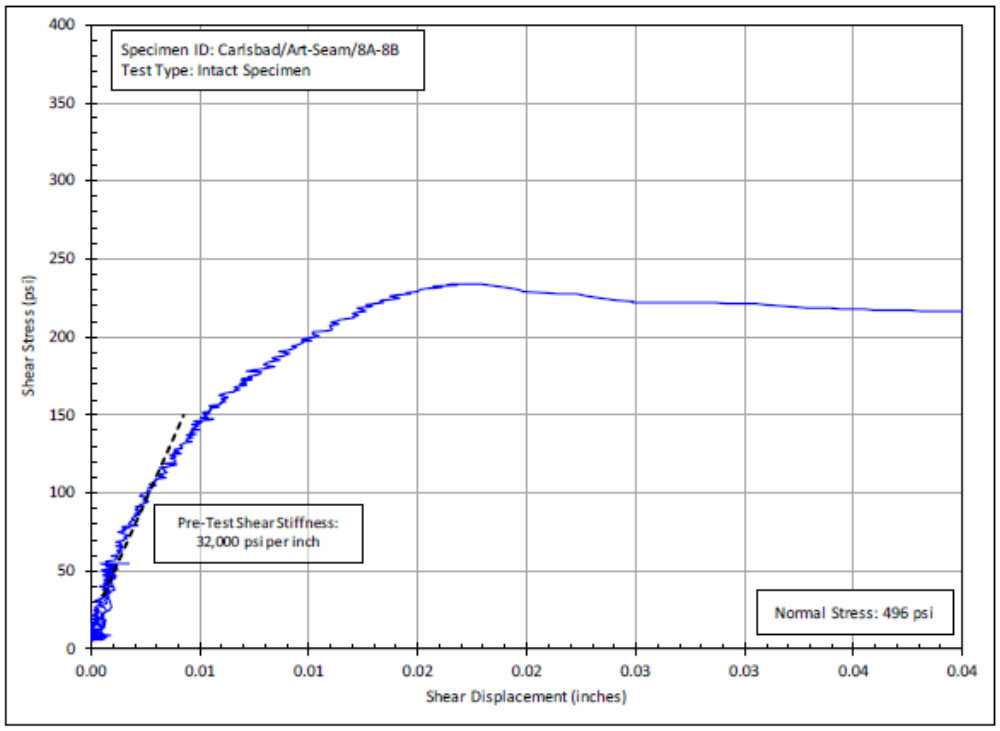

Figure B-48. Plot of Shear Stress Versus Shear Displacement for Intact Specimen Carlsbad/Art-Seam/8A-8B.

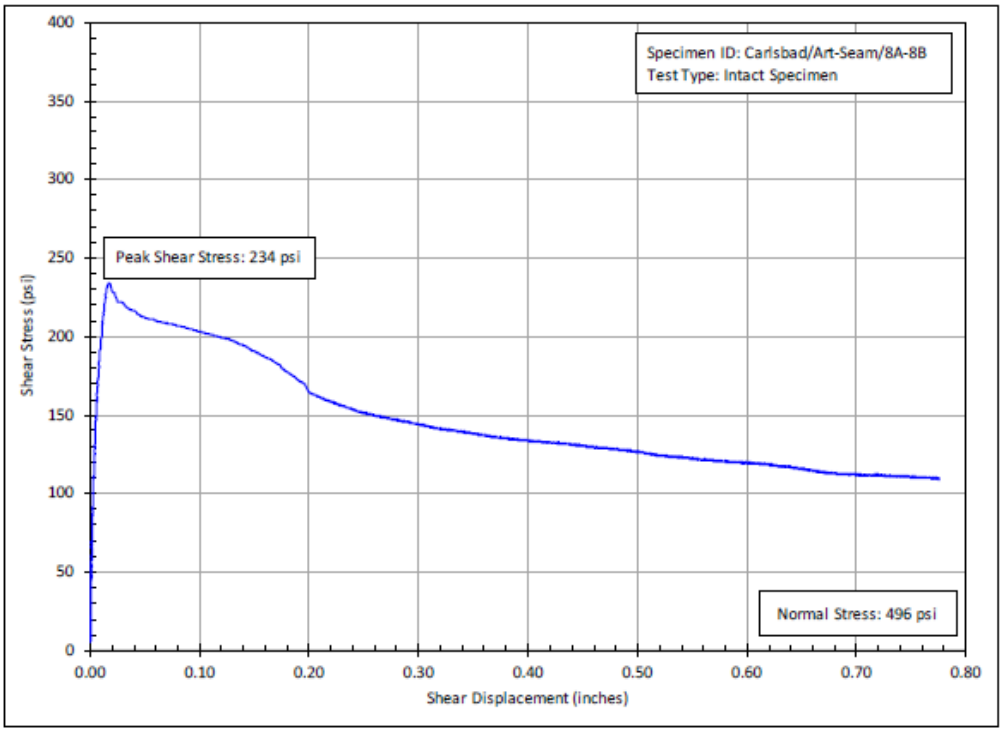

Figure B-49. Plot of Shear Stress Versus Shear Displacement for Intact Specimen Carlsbad/Art-Seam/8A-8B.

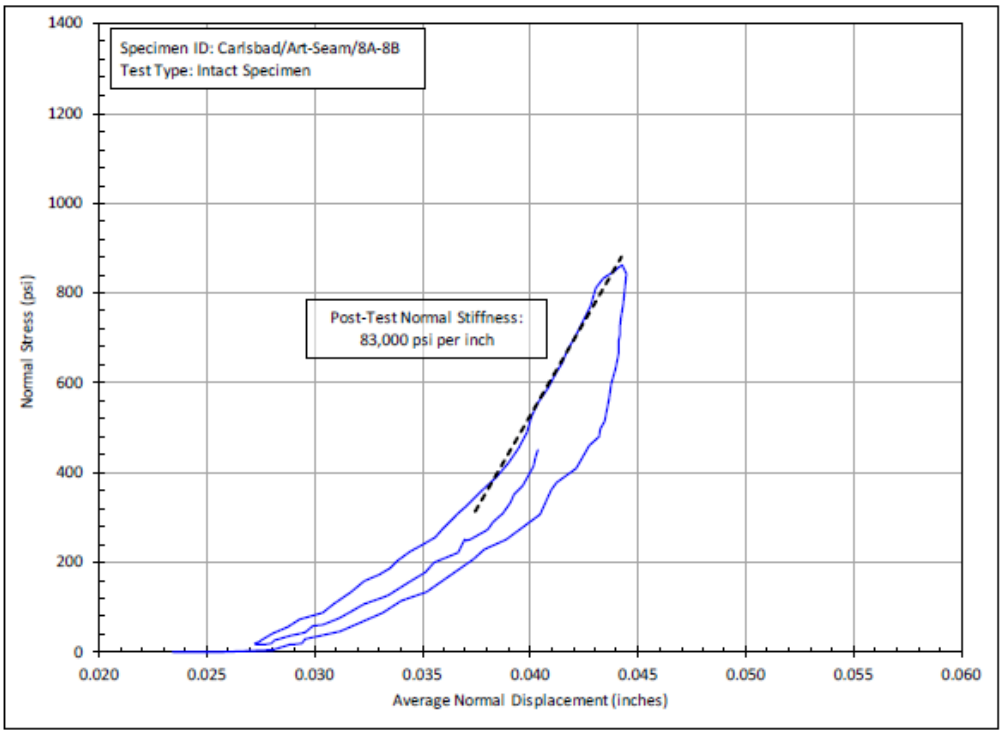

Figure B-50. Posttest Normal Stiffness Fit for Intact Specimen Carlsbad/Art-Seam/8A-8B.

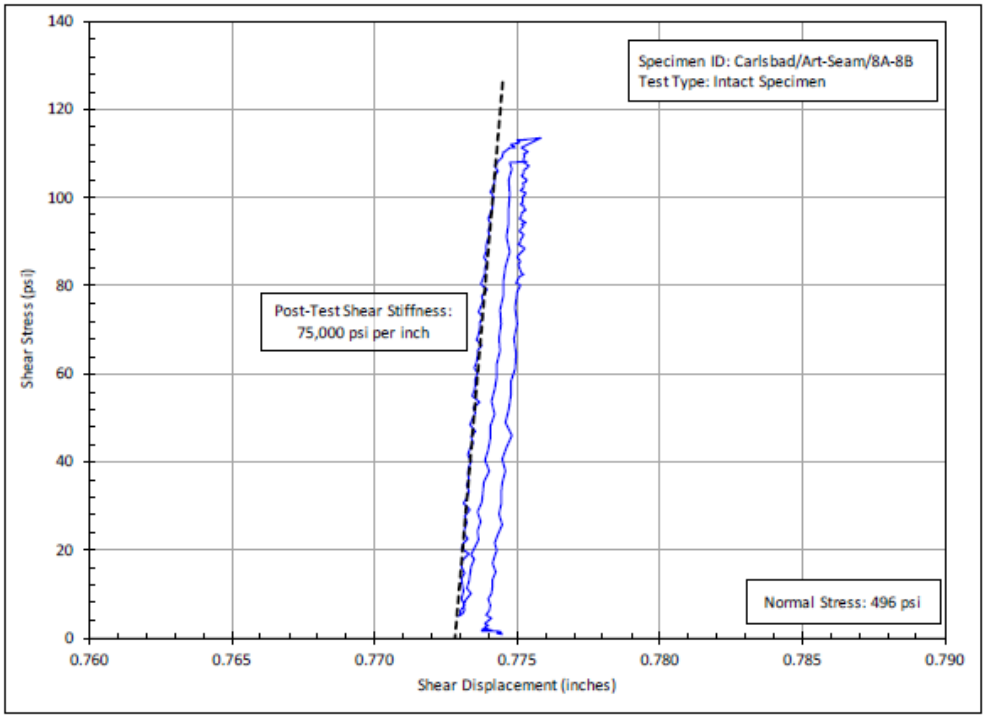

Figure B-51. Posttest Shear Stiffness Fit for Intact Specimen Carlsbad/Art-Seam/8A-8B.

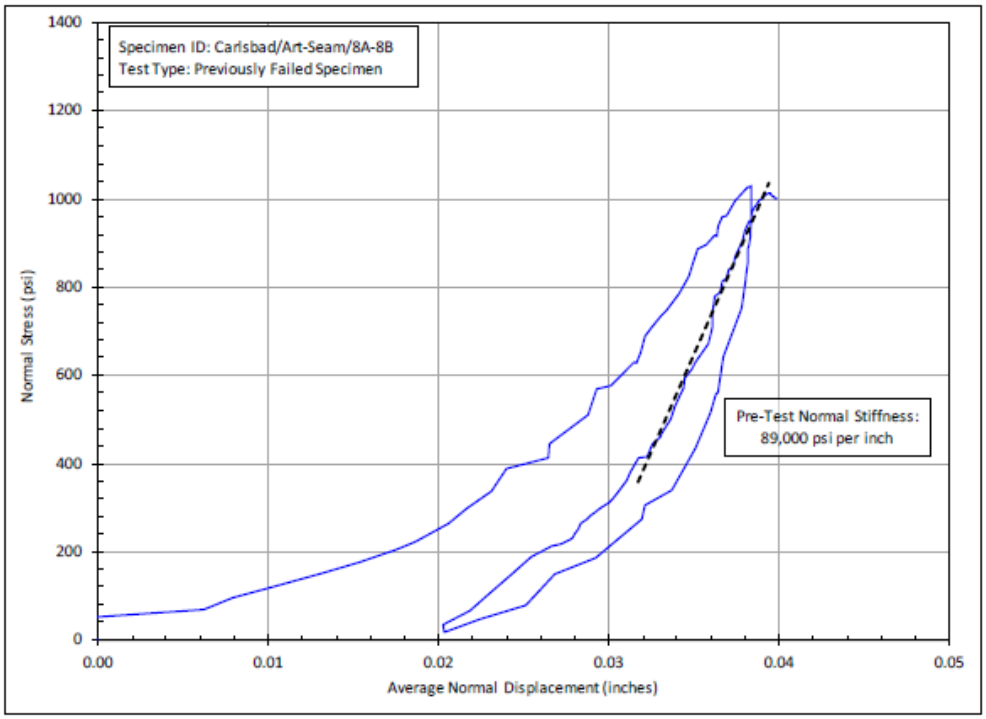

Figure B-52. Pretest Normal Stiffness Fit for Previously Tested Specimen Carlsbad/Art-Seam/8A-8B.

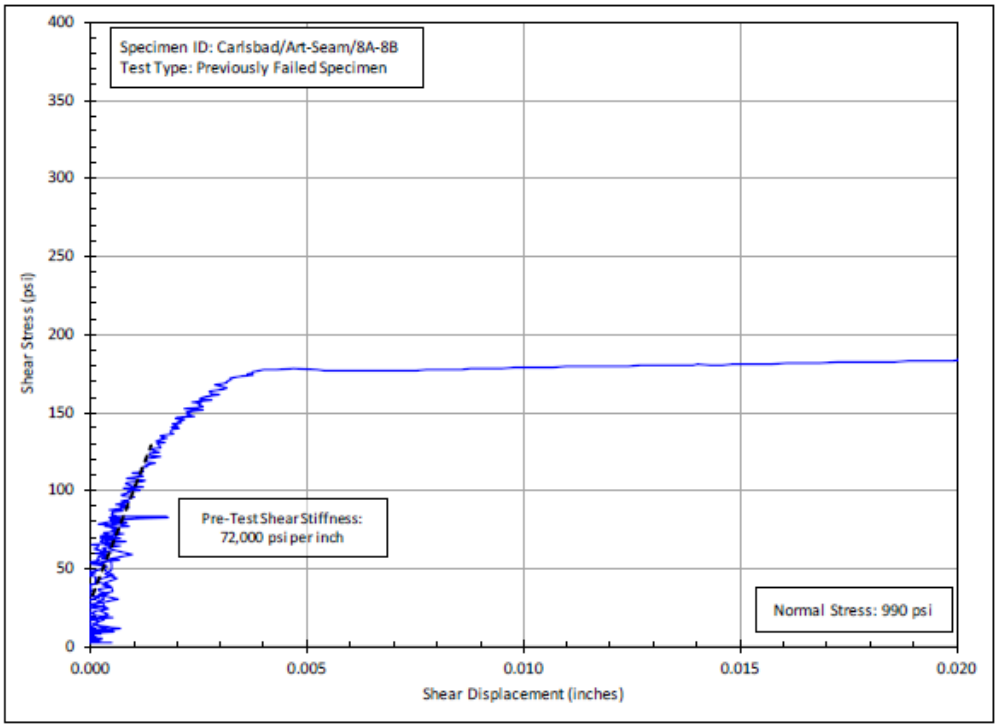

Figure B-53. Pretest Shear Stiffness Fit for Previously Tested Specimen Carlsbad/Art-Seam/8A-8B.

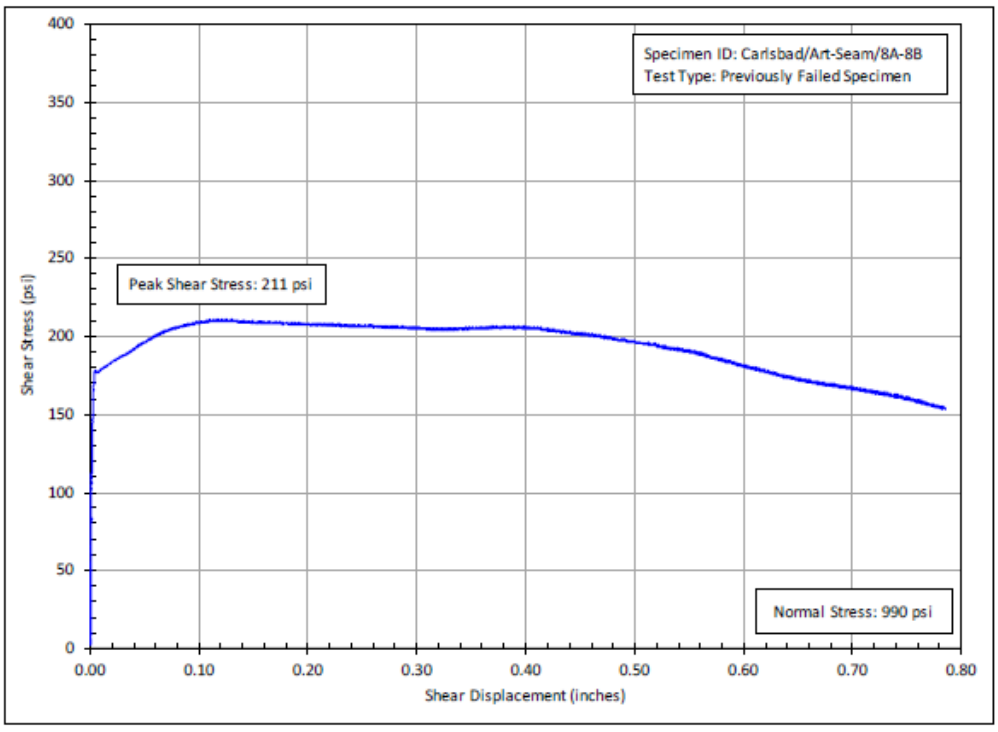

Figure B-54. Plot Of Shear Stress Versus Shear Displacement for Previously Tested Specimen Carlsbad/Art-Seam/8A-8B.

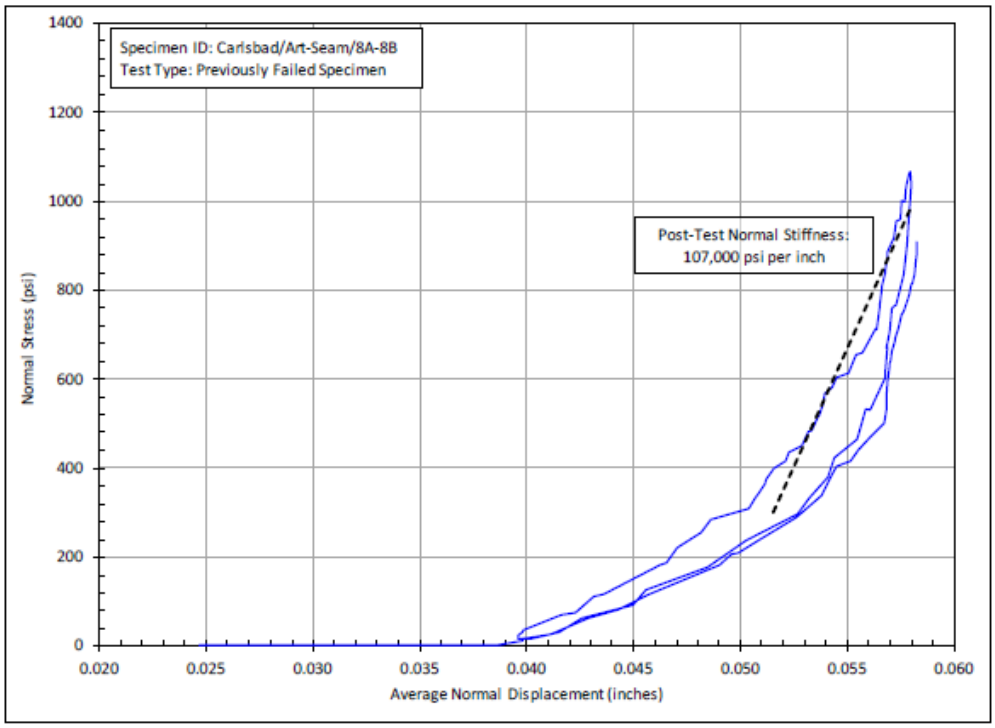

Figure B-55. Posttest Normal Stiffness Fit for Previously Tested Specimen Carlsbad/Art-Seam/8A-8B.

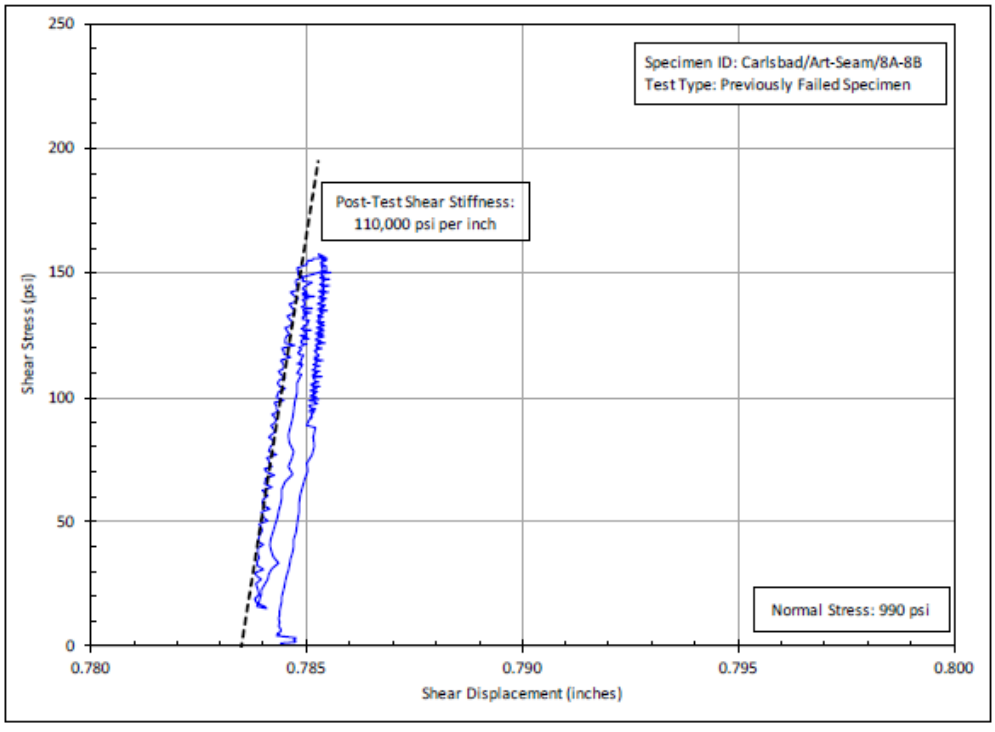

Figure B-56. Posttest Shear Stiffness Fit for Previously Tested Specimen Carlsbad/Art-Seam/8A-8B.

DISTRIBUTION

Hardcopy—Internal

Number of Copies	Name	Org.	Mailstop
1	WIPP Library	8880	1395
1	S. Sobolik	8862	0751

Hardcopy—External

Name	Company Name, Email Address
Stuart Buchholz	RESPEC, 3824 Jet Drive, Rapid City, SD 57703; stuart.buchholz@respec.com
Evan Keffeler	RESPEC, 3824 Jet Drive, Rapid City, SD 57703, evan.keffeler@respec.com
Russ Patterson	U.S. Dept. of Energy WIPP Management Office, 4021 National Parks Highway, Carlsbad, NM 88220, russ.patterson@cbfo.doe.gov
George Basabilvazo	U.S. Dept. of Energy WIPP Management Office, 4021 National Parks Highway, Carlsbad, NM 88220, george.basabilvazo@cbfo.doe.gov
Andreas Hampel	Grünberger Straße 56, 55129 Mainz, Germany, hampel@hampel-consulting.de
Mike Gross	mike_gross@earthlink.net
Gordan Gjerapic	ggjerapic@gmail.com

Email—Internal

Name	Org.	Sandia Email Address
Technical Library	9536	libref@sandia.gov
M. Neilsen	1558	mkneils@sandia.gov
C. Herrick	8864	cgherri@sandia.gov
M. Lee	8864	mylee@sandia.gov
K. Kuhlman	8844	klkuhlm@sandia.gov
R. Jensen	8864	rpjense@sandia.gov
D. Conley	8862	dconley@sandia.gov
E. Matteo	8842	enmatte@sandia.gov
B. Reedlunn	1558	breedlu@sandia.gov
C. Vignes	1558	cvignes@sandia.gov
J. Koester	1554	jkoeste@sandia.gov
J. Bean	1554	jebean@sandia.gov

Name	Org.	Sandia Email Address
S. Bauer	8866	sjbauer@sandia.gov
M. Rascon	8880	mdrasco@sandia.gov
P. Shoemaker	8880	peshoem@sandia.gov
S. Wagner	8881	swagner@sandia.gov

This page left blank

This page left blank

Sandia National Laboratories is a multimission laboratory managed and operated by National Technology & Engineering Solutions of Sandia LLC, a wholly owned subsidiary of Honeywell International Inc. for the U.S. Department of Energy's National Nuclear Security Administration under contract DE-NA0003525. This research is funded by WIPP programs administered by the Office of Environmental Management (EM) of the U.S. Department of Energy.